THE STABILIZATION OF A TWO AXES GIMBAL OF A ROLL STABILIZED MISSILE

A THESIS SUBMITTED TO
THE GRADUATE SCHOOL OF NATURAL AND APPLIED SCIENCES
OF
MIDDLE EAST TECHNICAL UNIVERSITY

BY

ÖZGÜR HASTÜRK

IN PARTIAL FULFILLMENT OF THE REQUIREMENTS
FOR
THE DEGREE OF MASTER OF SCIENCE
IN
ELECTRICAL AND ELECTRONICS ENGINEERING

SEPTEMBER 2011

Approval of the Thesis:

THE STABILIZATION OF A TWO AXES GIMBAL OF A ROLL STABILIZED MISSILE

submitted by **ÖZGÜR HASTÜRK** in partial fulfillment of the requirements for the degree of **Master of Science in Electrical and Electronics Engineering Department, Middle East Technical University** by,

Prof. Dr. Canan Özgen _____
Dean, Graduate School of **Natural and Applied Sciences**

Prof. Dr. İsmet Erkmen _____
Head of Department, **Electrical and Electronics Engineering**

Prof. Dr. Aydan M. Erkmen _____
Supervisor, **Electrical and Electronics Eng. Dept., METU**

Examining Committee Members:

Prof. Dr. Erol Kocaoğlan _____
Electrical and Electronics Engineering Dept., METU

Prof. Dr. Aydan M. Erkmen _____
Electrical and Electronics Engineering Dept., METU

Prof. Dr. Yücel Ercan _____
Mechanical Engineering Dept., TOBB ETU

Assist. Prof. Dr. Afşar Saranlı _____
Electrical and Electronics Engineering Dept., METU

Assoc. Prof. Dr. Tayfun Çimen _____
ROKETSAN

Date: September 13, 2011

I hereby declare that all information in this document has been obtained and presented in accordance with academic rules and ethical conduct. I also declare that, as required by these rules and conduct, I have fully cited and referenced all material and results that are not original to this work.

Name, Last name: Özgür Hastürk

Signature :

ABSTRACT

THE STABILIZATION OF A TWO AXES GIMBAL OF A ROLL STABILIZED MISSILE

Hastürk, Özgür

M.Sc., Department of Electrical and Electronics Engineering

Supervisor: Prof. Dr. Aydan M. Erkmen

September 2011, 146 pages

Nowadays, high portion of tactical missiles use gimbaled seeker. For accurate target tracking, the platform where the gimbal is mounted must be stabilized with respect to the motion of the missile body. Line of sight stabilization is critical for fast and precise tracking and alignment. Although, conventional PID framework solves many stabilization problems, it is reported that many PID feedback loops are poorly tuned. In this thesis, recently introduced robot control method, proxy based sliding mode control, is adopted for the line of sight (LOS) stabilization. Before selecting the proposed method, adaptive neural network sliding mode control and fuzzy control are also implemented for comparative purposes. Experimental and simulation results show a satisfactory response of the proxy based sliding mode controller.

Keywords: Line of sight stabilization; two axis gimbal system; Unscented Kalman Filter (UKF); PID control; proxy based sliding mode control.

ÖZ

YUVARLANMA KONTROLLÜ BİR FÜZE İÇİN İKİ EKSENDE GİMBAL KARARLILIĞININ SAĞLANMASI

Hastürk, Özgür

Yüksek Lisans, Elektrik ve Elektronik Mühendisliği Bölümü

Tez Yöneticisi: Prof. Dr. Aydan M. Erkmen

Eylül 2011, 146 sayfa

Günümüzde taktik füzelerin büyük bir kısmında gimballi arayıcı başlık teknolojisi kullanılmaktadır. Kusursuz bir şekilde hedef izlenmesi için, gimbalin bağlandığı platform, füzenin gövde hareketinden bağımsız olarak stabilize edilmelidir. Görüş açısının kararlığının sağlanması, hızlı ve kesin hedef izlenmesi ile hedefe yönelim için kritik bir unsurdur. PID kontrolcü eskiden beri bir çok stabilizasyon problemlerinde kullanılsa da PID kontrolcülerinin büyük bir kısmını zayıf olarak ayarlandığı bildirilmiştir. Bu tezde son zamanlarda robot kontrol için oluşturulmuş vekil tabanlı kayan kipli denetim, görüş hattı kararlılığının sağlanması problemine uyarlanarak kullanılmıştır. Bu yöntemi seçmeden önce bu probleme çözüm olabilecek bulanık mantık ve sinir ağları ile kayan kipli denetim de mukayese amaçlı olarak uygulanmıştır. Donanım testleri ve simulasyonlar vekil tabanlı kayan kipli denetimin memnun edici sonuçları göstermektedir.

Anahtar kelimeler: Görüş açısı stabilizasyonu; iki eksenli gimbal sistemi; Unscented Kalman Filter; PID kontrol; vekil tabanlı kayan kipli denetim.

To My Dear Family

ACKNOWLEDGEMENTS

I wish to express my deepest gratitude to my supervisor Prof. Dr. Aydan M. Erkmen for her helpful criticism, never ending guidance, patience, advice and support in the progress and preparation of this thesis.

I would like to express my thanks my colleagues in ROKETSAN especially Assoc. Prof. Dr. Tayfun ÇİMEN for his support.

I appreciate the support and facilities provided by ROKETSAN for the completion of this thesis, especially in the application of experimental studies that would otherwise be impossible.

Finally, I would like to thank Burcu for her support and my dear family for their help and support not only during my thesis preparation but also throughout my life.

TABLE OF CONTENTS

LIST OF TABLES

TABLES

LIST OF FIGURES

FIGURES

NOMENCLATURE

θ_a	Azimuth angle
θ_e	Elevation angle
θ_m	Angular position of the missile body centerline
ε	Angle between missile target line and the gimbal axis
λ,	Angle between centerline of the payload and inertial reference line
V_m	Missile velocity vector
θ_D	Pitch angle of the gimbal with respect to inertial frame
δ	Error between actual pitch angle and desired angle of the missile
T_f	Friction torque
T_e	External torque
T_s	Breakaway torque
σ_{stiff}	Stiffness parameter
T_c	Coulomb friction level
σ_1	Micro-displacement damping coefficient
v	Velocity between the two contact surface
z	Internal friction state
k_t	Torque constant of DC Motor
R	Resistance of DC Motor
L	Inductance of DC Motor
k_b	Back emf constant of DC Motor
J	Inertia of the elevation motor with gimbal
b	Viscous friction
J_{Ix}	Moment of inertia of inner gimbal about the X axis
J_{Iy}	Moment of inertia of inner gimbal about the Y axis
J_{Iz}	Moment of inertia of inner gimbal about the Z axis

J_{Px}	Moment of inertia of the payload about the X axis
J_{Py}	Moment of inertia of the payload about the Y axis
J_{Pz}	Moment of inertia of the payload about the Z axis
J_{Oz}	Moment of inertia of the outer gimbal about the Z axis
m	Total mass of payload + inner gimbal
l	Eccentricity (unbalance)
N_θ, N_φ	Generalized forces (torques)
σ	Sliding manifold
V	Positive definite Lyapunov function
$T_{\theta p}$	Control torque applied on the proxy
T_θ	Counter torque between proxy and inner gimbal
U	Control gain that varies at each step
k	Time step
S	Sliding surface
q_p	Position and velocity of the proxy
$\dot{q_p}$	Velocity of the proxy
q_d	Desired position of the inner gimbal
$\dot{q_d}$	Desired velocity of the inner gimbal
K_p	Proportional gain
K_d	Derivative gain
K_i	Integral gain
I_p	Inertia of the proxy
I_{xz}	Product of inertia

CHAPTER 1

INTRODUCTION

State-of-art missile systems use electro-optical (EO) and infrared (IR) guidance systems because of excellent lethality of the records and ease of operation [1]. Missile systems locking upon a target through its seeker have to point it out at all times, thus needing the optical sightline between the seeker and the target to be critically stabilized under vibrations caused by imprecisely estimated missile dynamics and aerodynamically conditions. Therefore, high precision servo performance in order to provide a stabilized target image and high disturbance rejection to maintain the line of sight to a target are required.

Today, the majority of the modern-day tactical missile systems use a gimbaled seeker. In this type of seeker, an inertial sensor is generally used to stabilize the optical sightline between the seeker and target with gimbal rings, which tries to render the pointing vector insensitive to missile body motion, enabling the precise tracking of the target [2]. However, these sensory systems have to work on platforms that are highly maneuverable and where angular vibration is large in comparison with the spatial resolution of the sensor. In addition, the electro-optical sensors tend to have a limited field of view to provide good spatial resolution so stabilization of the optical sightline on such a tactical missile requires fast and precise tracking of the line of sight especially at the end game portion of the flight, because, weak performance of the stabilized

seeker leads to large miss distances and low probability of the mission success [3].

Moreover, missile dynamics and the aerodynamical conditions cannot be precisely estimated, resulting in uncertain base motion of the electro-optical payload which must be compensated and stabilized for high quality target image. Consequently, the stabilization of the gimbal system is a complicated task to be executed under uncertain disturbance due to not only the uncertainties and nonlinearities of the controlled system and but also due to changes of the operation environment.

Previously, gimbal stabilization was realized by use of mechanical gyroscopes and, the controller structures of these systems have been basically proportional + integral + derivative (PID) based controllers. Although, the PID framework solves many control problems and is sufficiently flexible to incorporate additional capabilities, it is reported that many PID feedback loops are poorly tuned and known to lack adaptivity and robustness against changes in the operation environment [4]. Therefore, these types of classical controllers have been found not to satisfy high performance criteria for camera stabilization on guided missiles. To achieve robust controllers, adaptation of PID controllers can be enhanced with the ability of gain scheduling; however, such controllers still hardly handle nonlinearity and changes in the operation environment [4].

In summary, line of sight (LOS) stabilization is crucial work for an electro-optical system on a moving platform such as the one incorporating an infrared missile seeker and the control tasks needed for the stabilization of the line of sight are very hard due to the challenges such as a stabilization precision of one pixel under various disturbances and the requirements of the modern day battlefields which are fast response and excellent dynamic performance with

zero steady state error. The nonlinearities and the uncertainties involved in the plant and the frequent large disturbance originating from the operating conditions complicate the control mission.

Two axis gimbal systems are used for a wide range of applications and many researchers focused on control of these systems. However, large portion of their studies address the position control problem and focus on either very basic mathematical models originated from DC motors or on linearized system models used to derive the control algorithm. The main subject in this thesis being stabilization of a two axis unbalanced nonlinear gimbal model is not studied extensively in the literature, although some studies represented include identification and estimation of system parameters. Our general aim is to develop control algorithms in order to yield a better dynamic performance for the gimbal axes. Hence, the main motivation of this thesis is to develop and propose control algorithm for the stabilization of a two axis gimbal system of a roll stabilized missile, which can overcome nonlinearities, uncertainties and change in operating conditions and minimize the error due to uncertain base motion.

1.1 Problem Definition and Characteristics

Two axis gimbal system is utilized in many kinds of air vehicle and usually consists of a target tracker, pitch/yaw gimbals and separate armature controlled DC drive motors having each of their shafts equipped with encoder for measuring angular displacement for the pitch and yaw gimbals. In addition, rate sensors are used to detect the vector motion and digital image processing technology enables the compensation of the jittering in the image sequence. The stabilization loop plays a vital role in searching and tracking the

target in the pitch and yaw planes. Thus, the two axis gimbaled platform must accomplish a fast and accurate reaction to the given input while remaining stabilized during the target tracking. It is well known that the tracking performance of the missile highly depend upon the stabilization performance that is able to isolate the target tracker from various disturbances induced by the missile motion and vibration [5].

The overall objective of the gimbal control system is to follow a desired trajectory produced in real time by the missile signal processing unit as rapidly as required and with minimum steady state error [6]. The desired trajectory is generated using the electro-optical payload output with selected guidance law by the missile signal processing unit. Therefore, at every output, the gimbal system has to pursue the given input within the predefined error tolerances.

Closed loop controller performance requirements are generally determined by taking into account the operating characteristics of the electro optic payload and the demand by the guidance law. Settling time of the line of sight stabilized control is very short generally in milliseconds. However, such systems usually work in atrocious condition because of the uncertainties and vibrations during operation and what is requested of even in these rugged conditions are fast dynamic response and high stabilization precision with adaptability and robustness vis-à-vis model parameter changes.

The two axis gimbal system used in seeker head on missiles requires very accurate stabilization in the order of micro radians because small angular deviations result in huge position errors when a target on a few kilometers away is being tracked. The general trend for the stabilization accuracy requires a stabilization degree lower than ½ pixel instantaneous angle of view field within the frame of the camera [7]. Within this framework, the rate sensor or

gyroscope, as the key component of motion vector detection, directly determines the accuracy of the motor vector, while deciding at the same time, the compensation precision of subsequent shifts and rotations. Consequently, it is necessary to analyze whether the gyroscope accuracy can meet our requirements.

In our system, an IR (infrared) camera with 0.00174 deg instantaneous field of view is used. Therefore according to the ½ pixel stabilization, at least 150 μrad stabilization accuracy is required. For achieving such very tight stabilization errors, high grade gyroscopes or accelerometers as an extra sensor can be used. However, using high grade gyroscope results in extra costs because the two axes DTG (Dynamically Tuned Gyroscope) or FOG (Fiber Optic Gyroscope) is four times as expensive as the MEMS gyroscope. Using such additional sensors not only induces extra cost but also increases substantially the complexity in the algorithm. Moreover, mounting of the accelerometers needs mechanical interface, which decreases the already limited space in the missile seeker. Therefore, within the aim of this thesis, we propose a control algorithm for two axis gimbal stabilization without the usage of additional sensors, minimizing the cost and complexity using good feedback elements and mechanical part, utilizing a high quality rate sensor while keeping in mind the prices and complexity of the elements.

1.2 Objective and Goals of the Study

The line of sight stabilization of a two axis gimbal system of a roll stabilized missile is a complicated task because of the uncertainties and nonlinearities of the controlled system and due to changes of the operation environment.

Disturbance frequency and amplitude generates uncertain base motion leading to inestimable missile motion.

In addition, the uncertain response of the feedback element, the manufacturing tolerances, nonlinearities due to system dynamic and friction owing to low velocities introduce nonlinearity and uncertainty in the system. The objective of this study is to design a controller, which handles these unpredictable changes both in the controlled plant and in the operating environment to track a target as fast as required with a minimum steady state error even under the effect of disturbances due to uncertainty in the base motion.

In the direction of this objective, the goals of the proposed method are summarized. The line of sight control task requires the minimization of the transient and steady state control between the given input and the actual output. Manufacturing tolerance, unbalance, friction and uncertainty in the sensor noise affect the controller performance therefore compensation or estimation algorithms will be used to handle problems introduced by the aforementioned complexities.

In addition, our proposed control algorithm is designed for a two axis gimbal system for a roll stabilized missile which is digitally controlled. Therefore, the most important requirement is the real-time implementation of proposed controller. As a result, the controller has to require minimum memory and hardware complexity as much as possible.

The overall system requirements can be summarized as follows:

- The diameter of the gimbaled system is 160 mm.
- The mass of the gimbaled system shall be less than 2 kg.

- The gimbal shall move at least ±20 deg in both axes.
- The gimbal shall have minimum 100 deg/s slew rate.
- The length of the gimbaled system shall be less than 250 cm.
- The angular position of the azimuth and elevation gimbal shall be measured with a resolution 0.005 deg.
- The settling time of the controller shall be less than 40 ms in both axes.
- Stabilization error shall be less than 0.4 deg/s.
- The standard deviation of the stabilization accuracy shall be less than 150 μrad under a base disturbance whose frequency ranges from 1-10 Hz and its peak to peak amplitude between 2 and 8 deg.
- The controller shall run with a sampling time 0.0001 sec.

Here, the gimbaled system refers to the gimbal mechanics, actuators, payload and the feedback elements. The drive and controller electronics is not included.

1.3 Methodology

In the previous subsection, some important physical and performance properties required for the two axis gimbal system are listed and physical requirements are highly related to the mechanical design. However, the stabilization performance depends not only on the mechanical assembly but also the actuator, rate sensor and the control algorithm itself. Since the rate sensor noise, unbalance and friction introduce nonlinearity and uncertainty, the designed controller must handle these unpredictable changes. While positioning of the gimbal axes can be achieved with high resolution angular encoder and high quality DC motor without using sophisticated control algorithms, the problem of high performance stabilization cannot be

accomplished only using high grade sensors and classical controllers due to the lack of adaptivity and robustness against changes in the operation environment of the conventional controllers. Therefore, it is important to utilize a special algorithm for the compensation of a specific problem. To reduce the uncertainty in the rate sensor response, a suitable filtering technique should be used and it is very important to find a control methodology to alleviate the influence of friction in controlled system in order to have satisfactory stabilization performance. Some gravity or unbalance compensation method should be added if the unbalance of the gimbal system is not modeled. In our work, Unscented Kalman Filter (UKF) is used to estimate the state of the rate sensor because of its superior accuracy in the nonlinear filtering problem. Extended Kalman Bucy Filter (EKBF) is utilized to improve the stabilization accuracy by compensating the effect of friction.

In order to achieve the required stabilization objective, many kind of controller architecture can be used. If the conventional PID or variants is not used, fuzzy logic, neural network and sliding mode controller will be the candidate for the solution of the stabilization of the nonlinear gimbal problem. Therefore, in this thesis, a comparative study between these controllers is conducted before selecting proposed architecture for a controller as introduced in this thesis. Fuzzy control, sliding mode control and neural networks are implemented to solve gimbal stabilization problem in this thesis work. The chattering phenomena in sliding mode still exist even though some precautions are taken. Although, fuzzy control provides more satisfactory results than sliding mode control with adaptive linear neural network, the results obtained using fuzzy control in simulations cannot reach the desired stabilization accuracy. Since, the settling time of the line of sight stabilized control is very short, Windrow-Hoff delta rule with ADALINE is used instead of the back propagation algorithm with multilayer feed forward networks in order to refrain from

intensive calculation. In addition, back propagation algorithm takes longer than the desired step time. However, in general, each of the control technique implemented has some disadvantages either at the design stage as in fuzzy control or at the real time application stage, therefore, another control algorithm that is simple as well as powerful in order to implement in real time and handle nonlinearities and uncertainties is required and studies in this thesis work show that these controller does not permit us to reach the desired objective mentioned before.

In the literature, a recently introduced controller, proxy based sliding mode control, for the robot motion control is established. This method is an alternative discrete time representation of a class of sliding mode control and also as an extension of PID control and it is capable of producing overdamped resuming motion from large errors. In this method, the small scale response can be set as fast as conventional PID while the large scale response can be adjusted arbitrarily. Therefore, in order to perform the line of sight (LOS) stabilization control objective, a proxy based sliding mode controller is used. Using such a controller, error between the speed command from the user which is the guidance processor in the missile system and the feedback signal from the angular rate sensor device is minimized based on the voltage signal of actuation system.

To handle the uncertainty in the rate sensor response, a suitable filtering technique is incorporated for the estimation of the actual states of the rate sensor. The friction in the system is identified using an observer designed to estimate the parameters of dynamic system and provide the required compensation to enhance the controller performance.

1.4 Contributions of the Thesis

In the literature, several stabilization controllers are proposed in order to have better stabilization accuracies. Most of them either uses the traditional controlling methods or uses the acceleration feedback. However, traditional controlling methods cannot meet the demands of high speed, high accuracy and strong robustness. Although, successful results are obtained with angular acceleration assisted stabilization, the use of extra accelerometers increase both the cost of the system and the complexity of the control algorithm, and sensors must be mounted rigidly to have a correct calculation of angular accelerations. In addition, there exist quite a few publications with more advanced control techniques such as neural network and fuzzy logic focusing on the gimbal stabilization and majority of them address the tracking problem and treat only friction as nonlinearity.

To achieve the defined goal, a modified version of the recently introduced control technique is implemented. The proxy based sliding mode control is proposed for the joint space control for industrial robots. This task space control is limited to 1-D, which can be used for independent joint angle control. Although, multidimensional PBSMC for task-space position control is empirically demonstrated, the joint-space stabilization implementation is not available. In this thesis work, the proxy based sliding mode control is adopted for the independent gimbal axis stabilization. The tracking performance and disturbance rejection capability of the proxy based sliding mode control is compared with that of conventional PID control and sensitivity of the PBSMC to system parameters such as unbalance, friction and inertia is examined.

The model based and non-model based friction compensation techniques are compared and a non-model based friction compensation technique which is Extended Kalman Bucy Filter (EKBF) because of the superior friction cancellation performance compared to model-based methods is used.

In order to estimate the states of the rate sensor, several filtering techniques are investigated and Unscented Kalman Filter (UKF) is selected for the optimal estimation of the actual states of the rate sensor.

1.5 Outline of the Thesis

In this first chapter of the thesis, definition and characteristics of the problem, the motivation of this study, objective and goals of the study and contributions to the literature are given.

In the second chapter, a literature survey and mathematical background about stabilization, line of sight systems and control algorithms used in the literature are presented.

The rest of this thesis is organized as follows: Chapter three explains the design of early developed controller for comparative purpose together with the mathematical modeling of the line of sight system. Chapter five introduces our hardware prototype on which we implement the developed stabilization methodology based on proxy based sliding mode introduced in Chapter four. Chapter five also discusses the demonstrative results of our approach on the actual hardware. Chapter six presents simulation results that analyze the sensitivity of the method to parameter changes while the last chapter provides concluding remarks.

CHAPTER 2

LITERATURE SURVEY

The most important trends nowadays in missile technology are the development of smart ammunition which has huge advantage over the conventional one. Smart ammunition is a new type of weapon bearing possible independent target detection and tracking capabilities. The development of such ammunition systems became possible with the target recognition systems which generally use stabilized gimbal platforms [8]. Line of sight (LOS) stabilization plays a key role for the overall tracking performance of these platforms, when locked upon a target. Such seeker stabilization mechanism when in pursuit of a target requires the compensation of disturbances arising from various parts of the tracking system such as those from the servomechanism, the electronics and the optics [9]. Moreover, target dynamics may generally be quite unpredictable. Therefore, the precise stabilized line of sight from the seeker to target is a vital issue in designing smart ammunition.

In the literature, there exist two different methods for inertial stabilization of pointing vector defining the line of sight. The conventional technique is the direct LOS stabilization and it uses rate sensors to sense the rate disturbances on the LOS axes. In direct LOS stabilization, the rate sensors are often mounted on the inner gimbal axis as depicted in Figure 2.1. Since the rate disturbances are measured directly by rate sensors, the stabilization technique is defined as direct LOS stabilization and this method is generally recommended for the precise pointing applications [19]. Since direct LOS

stabilization requires only two axis rate sensors mounted on the inner gimbal, this stabilization method is simple to implement. The only drawbacks of direct LOS stabilization is that it requires not only larger inner gimbal volume to mount the sensors on but also vibration resistant sensors because of the exposal of the high angular rates during flight as well as during launch [17].

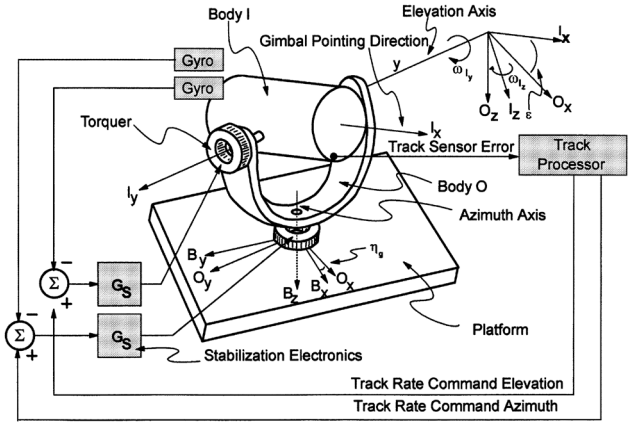

Figure 2.1 : Two axis gimbal configuration in direct LOS stabilization [19]

The other stabilization technique, indirect LOS stabilization, employs a rate sensor which is mounted on the gimbal base. Since the disturbance is rather measured about the missile body instead of the inner gimbal, this method is known as indirect LOS stabilization. In this type of LOS stabilization, it is required to transform the missile angular disturbance in terms of the LOS axes.

Thus, in indirect LOS stabilization, disturbances are not directly measured in the LOS coordinate system, which needs a transformation that generally degrades stabilization performances [17][19]. This method can be seen as a suitable technique for a two axis gimbal stabilization of a roll stabilized missile because of the built-in three axis inertial measurement unit located as

close as possible to the center of mass so that the coordinate transformation does not induce high errors. However, this method is more complex that the direct method because indirect method requires measured missile disturbance transformation about the LOS, and the transformation of the disturbance depends highly upon the gimbal geometry, encoder resolution mounted on the gimbal rings and the disturbance transformation sampling rate.

2.1 Missile Seeker Technology

Today's modern missiles which are fire-and-forget missiles have to be able to track and destroy targets without the interference of an operator. Their unmanned mission is realized using an onboard infrared (IR) imaging system with an onboard tracking system. The operator comes into play initially for identifying the target using the imaging system of the Command Launch Unit (CLU). CLU usually has a higher performance IR imaging system contrary to missile onboard IR imaging system because the operator require high resolution image of the target in order to classify it as friend or foe before launching the missile. Then, the onboard imaging system comes into play for staying focused on the identified target as the target moves or as the angle of attack changes.

Nowadays, missile seeker technology is classified either as strap down or gimbaled according to where the electro-optical payload is mounted upon. In strap down seeker configuration, the payload is rigidly fixed to the missile body, resulting in simplification of the sensor electronics. On the other hand, in gimbaled seeker configuration, seeker is installed on the platform which is stabilized by the gimbal system with complex electronics such as servo motors and rate sensors [11][12].

The strap down seeker has a simple mechanical design, but, a gimbaled system requires complex mechanical structures for its gimbals, pickoffs and low-friction platform connections. In addition, the strap down seeker does not require rate sensor which is the core element in the gimbaled seekers. Therefore, the lack of tactical grade rate gyro and mechanical gimbals in strap down systems provides a low cost solution for target tracking. This is the main advantage of the strap down seeker solution over the gimbaled system.

Strap down seeker technology have strongly benefited from the advance of computer technologies, being built upon electronics, optics, and solid state technology with less moving parts than gimbaled systems, however, two fundamental problems are encountered when strap down seeker guidance is considered instead of the conventional gimbaled seeker guidance. First, conventional gimbaled seeker continuously monitors the error angles to reduce the harmful effect of the seeker gain errors. On the other hand, strap down system must accomplish electronically what the gimbaled seeker does mechanically. Second, the complexity of the strap down guidance algorithms is increased because it is necessary to monitor the changes in the rotating body coordinate system. Usually, this requires precise computation of the inertial to body transformation matrix which sensor errors degrade the accuracy of the computation [10].

In general, strap down seekers provide reduced weight and low cost over traditional gimbaled seekers. However, the main disadvantage of the strap down seekers is to offer limited field of regard (FOR). It is not possible to have a 20 deg FOR without using gimbal mechanism is strap down seekers. Therefore, it is mandatory to use gimbal to reach to requirement. Therefore, gimbaled seekers and gimbal stabilization is explained in the following subsections.

2.2 Gimbaled Seekers

A typical gimbaled seeker illustrated in Figure 2.2 mainly consists of an imaging system, gimbal system and signal processing unit. The imaging system can be either day vision such as charge-coupled device (CCD) camera or night vision camera using Forward Looking Infrared (FLIR). In both cases, the number of pixels and frame rates determine the tracking behavior. Cameras with high frame rates are usually used for high maneuvering targets.

The gimbal system, in most cases, is a two axes pitch over yaw configuration. Mechanical aspects such as orthogonality, wobble and sensors features (resolution of the rotary position sensor and gyro noise) define the quality of the gimbal system. In the majority of cases, the gimbal mechanics is designed with the constraint that the geometrical center of the payload coincides with the intersection of the gimbal axes to minimize the effect of the interaction of the instantaneous gimbal angle. However, if the payload is not located at the intersection of the gimbal axes, optical parallax which is the apparent displacement in the apparent position of an object viewed along two different lines of sight occurs. In such a case, angle dependent compensations are necessary.

The stabilization equipment or rate sensor is capable of sensing inertial movements. According to these movements, it generates electrical signal which is used by the stabilization controllers.

Signal processing usually occurs in the target tracker and the controller. The target tracker receives its input from the imaging system and calculates the location of the target area in the camera field of view. Then, the tracking error

vector in azimuth and elevation axis is calculated and sent to the controller electronics. The controller is activated after receiving the tracking error. These electronic circuits serve as closed loop servomechanism control of the gimbal line of sight.

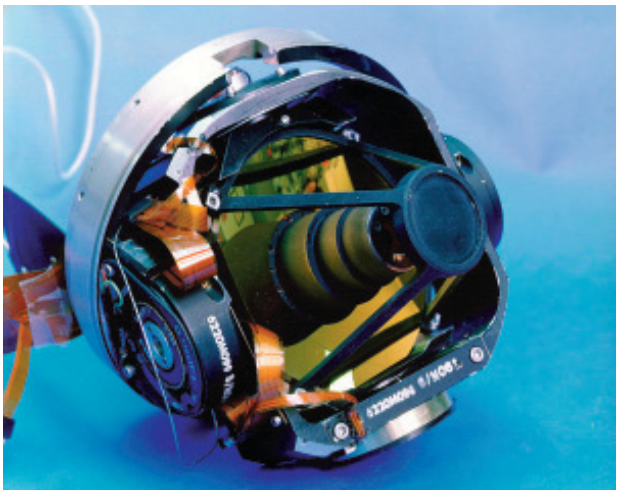

Figure 2.2 : Systems Development Future Missile Technology Integration Gimbal [13]

2.3 Gimbal Stabilization

The gimbal is a pivoted support which allows the rotation of the imaging system about the elevation and the azimuth axis. Figure 2.3 shows a typical configuration of gimbal system. In this configuration, azimuth angle (θ_a) and elevation angle (θ_e) of the payload with respect to base is controlled with a two axis gimbal mechanism. The X –axis of the payload indicates the line of sight (LOS).

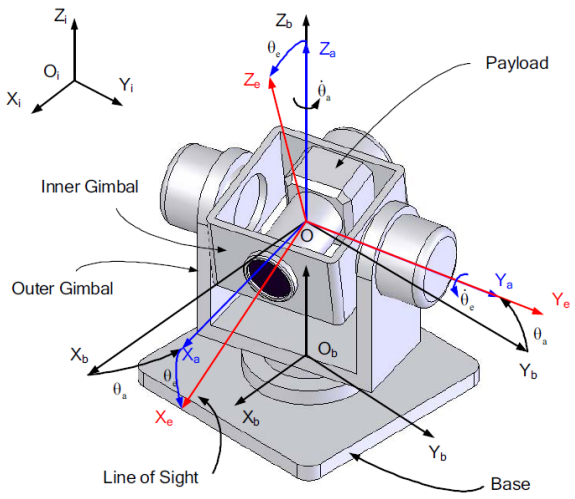

Figure 2.3 : Typical gimbal system configuration [14]

Figure 2.4 shows a typical missile seeker angular geometry. In this figure, θ_m is the angular position of the missile body centerline (pitch angle of the missile) and θ_h is the gimbal angle represented by the angle between gimbal axis and the missile body. In this figure, θ_h can be expresses as pitch angle of the gimbal, therefore θ_e in Figure 2.3 is equal to θ_h in Figure 2.4, ε is the angle between missile target line and the gimbal axis. This angle is annihilated by gimbal controller in order to keep the target in the center of the sensor field of view [15]. λ, is the angle between centerline of the payload and some arbitrary inertial reference line. V_m is the missile velocity vector and θ_D is pitch angle of the gimbal with respect to inertial frame. δ is the difference between the actual pitch angle and the desired angle of the missile.

In order to track the target accurately, the platform where the gimbal is mounted on, must be stabilized with respect to the motion of the missile body because the LOS stabilization plays a key role in the overall target tracking performance. The stabilization mechanism must compensate for the disturbances arising from various parts of the overall system and from the

environment. These disturbances alter the LOS if the base of the gimbal is moved. A noisy instrument can generate acoustical noise which is transferred through the atmosphere or missile ground. An external effect such as wind gust induces disturbing torque which is a common type of disturbances and requires high bandwidth controller for compensation. Internal sources of disturbances which are mainly due to tolerances in the mechanical component are bearing friction, mechanical gearing noises, unbalance of the gimbals, effects of wobble and axes orthogonality [9]. For example, unbalance and gimbal geometry throughout the flight induces a disturbance torque as an unbalanced moment and the presence of unbalanced moment results in reduction of motor torques, which causes the decrease in tracking accuracy due to the position errors. To eliminate the unbalanced moments, extra masses are mounted on to the gimbal at specific locations for shifting the center of mass to the intersection of the gimbal axes [16].

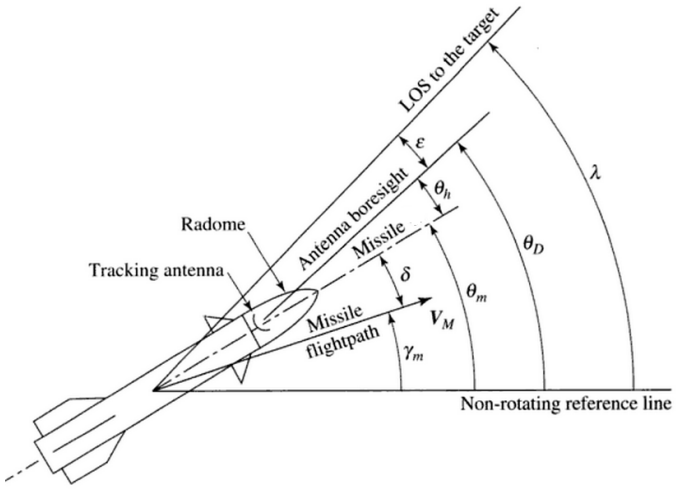

Figure 2.4 : Typical missile seeker angular geometry [15]

Hitting the target is requested, which leads to very tight error tolerances. To stay within these tolerances, the minimization of the effects of the disturbances both in the mechanical design stage and in the control electronics design is crucial. For instance, in order to avoid backlash, the general trend for the actuator is the use direct drive DC motors in hardware design. In addition, using direct drive system increases the overall efficiency because of the absence of the gearboxes. However, one disadvantage of the direct driven systems is the sensitivity to disturbance since removal of the gearboxes also removes the resistance against those disturbances.

Other than avoiding disturbance prone designs, uncertainties cause also an adverse issue in stabilization. There are many parameters which are not exactly known or measurable in gimbal systems. In mechanical assembly, the unbalance degree cannot be measured directly. Therefore, it is almost impossible to accurately determine the location of each gimbal, which makes estimation necessary. In addition, the inertia of gimbal rings which affect the angular rate of the gimbals cannot be measured individually without an experimental setup. The general trend for the estimation of the mass moment of inertia and the location of the center of mass for each gimbal is to measure them with a computer aided drawing (CAD) program. However, this process requires precise model of the system with harness design and the material properties of the all manufactured parts. In CAD programs, a material such as aluminum or steel is applied to a part or assembly, then, the values of inertia and unbalance are obtained. However, there are quite a lot of uncertainties in this process even though a precise CAD model is available, because the properties of the material used in the manufacturing can deviate from the original material type. For instance, in CAD system, the density of the aluminum is taken as 2700 kg/m^3, however, the density of the aluminum used in manufacturing can be 2709 kg/m^3.

Manufacturing tolerances and friction characteristics of the mechanical assembly also induces an unforeseen disturbance on the system which the stabilization controller must handle. In order to improve the accuracy of the overall performance of the system, accurate rate information is required in the stabilization loop. However, the uncertainty in the sensor output induces jitter to the system which is reduced by selecting gyroscopes with lower noise. Nevertheless, selecting such higher grade gyroscopes increases the cost of the seeker. Another approach is to suppress measurement noise by a suitable filtering technique.

In our gimbaled platform, there is quite a small level of unbalance which is measured inside the CAD model. The cable connection induces also compliance because cabling is not perfect. There is not any problem associated with the backlash because of the using direct drive motors. Our prototype includes a rate sensor with significant noise characteristics, which results in uncertainty in the measurement. In addition, the analog data from the rate sensor is taken with one meter cable therefore the filtering of the sensor noise is inevitable.

In most of the gimbal stabilization controllers, classical PID based controllers are utilized. In spite of PID's long history and widespread usage, PID controllers exhibit poor performances when the system is nonlinear [4] [21]. There are several improvement techniques to enhance the performance of PID controllers in nonlinear systems. Changing the controller parameters either by gain scheduling or adaptively modifying them based on the performance are well-known techniques. Improving measurement with more precise feedback element and cascading multiple PID controllers are other common performance enhancement approaches in the usage of PID controllers.

It is well known that the integral terms in PID controller accumulates significant errors when a large change in set point occurs, which causes excess overshooting [22]. If very stiff controller is selected, the controller generates very high controller output when the desired position is far from the actual position, which usually results in overshoots and oscillations. It is not very straightforward to eliminate such behaviors from PID-controller gimbal. Although, some torque limiters can be used to eliminate such unwanted behavior, they deteriorate the stabilization accuracy.

In order to deal with problems related with integral terms, a self-adjusting integral action with dual speed loop is proposed for LOS stabilization problem [23]. The inner loop is used to reject the friction while the outer loop is used for the disturbance from the carrier. The experimental results in this referred work illustrate that this time optimal self tuning method can achieve higher precision and perfect control performance within the linear region of the process, however, the dual loop stabilization controller in the literature, requires DC tachometer for inner loop and rate sensor for outer loop as in Figure 2.5 however, our system does not have an built-in tachometer for each axis. Although, the required information for the speed loop can be obtained by differentiation of the absolute encoder information, this process both requires computation and adds extra noises on the system. In addition, this type of dual controller cannot handle the vibration produced by the moving platform, therefore, serious disturbance degrades the stabilization.

In addition to the PID framework, in order to realize zero steady-state error of angular velocity when facing disturbances from the moving platform, a PI-II (proportional-integral-double integral) control scheme is proposed as an improved control technique for LOS stabilization [20]. Although, the proposed PI-II controller has the advantages of fast response, less angular oscillatory

and zero steady-state error, this method depends highly on the precision of system model. However, the two axis gimbal model derived in this thesis is not precise because of nonlinearities and uncertainties so PI-II controller cannot be selected as a stabilization controller.

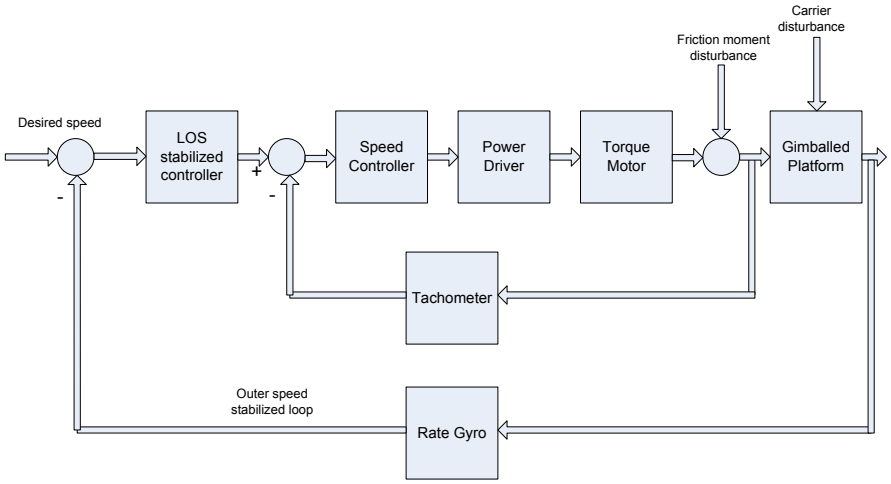

Figure 2.5 : Block diagram of dual speed loop cascade stabilized control (Adapted from [23])

One of the alternatives to PID control is Linear Quadratic Gaussian control with Loop Transfer Recovery (LQG/LTR) control. LQG/LTR theory, developed from LQG optimal control theory, is a very effective design tool for linear multivariable feedback systems, where loop shapes of optimal full-state regulators or filters are approximated at plant inputs or outputs via certain specific choices of free parameters [21][24]. However, uncertain system parameters must be identified and the magnitude of uncertainty should be known or estimated because LQG/LTR system may exhibit worse robustness qualities than the original LQG system [25]. Moreover, this type of controller

is a linear controller so the controlled system must be linearized to eradicate the nonlinearity.

Yet another proposed solution for the stabilization of the gimbal system is H_∞ robust control approach [29]. It addresses the problem which is to design a linear dynamic output feedback controller such that closed loop system is stable and achieves a prescribed level of disturbance attenuation. [26]. However, the linearized state space model is used while designing the controller because this is also a linear control design methodology that does not allow us to apply this methodology to our problem.

In addition to these control techniques, many researchers have worked on stabilization of the gimbal with more advanced approaches such as fuzzy logic and neural network control.

Fuzzy control has been considered as an alternative to traditional control problem, which can cope with complicated, ill defined and poorly mathematically understood processes by augmentation of the operator's knowledge. It incorporates the human's rule based control knowledge into the controller directly without relying on the system model. The behavior of a fuzzy control is easily understood by a human expert, as knowledge is expressed by means of intuitive, linguistic rules. In contrast to the traditional linear or nonlinear control techniques, fuzzy logic is widely used to solve problems with uncertainties and nonlinearities without a mathematical model. In addition, fuzzy control provides a certain level of intelligence to the conventional PID controllers providing them with a self-tuning ability and online adaptation to nonlinearity, time varyingness and uncertainties. Therefore, fuzzy logic seems to be good choice for the gimbal stabilization problem. Although, set point velocity tracking results represented in Chapter 3

are good enough, however, the fundamental problem is derivation of the required control rules that the success of the fuzzy control depends highly upon [27][30]. In addition, it is difficult to estimate type of the membership function.

In conventional controllers, a mathematical expression can determine the stability characteristics of the controller throughout the entire operation envelope. With a fuzzy system, the analysis of the structural properties of the control systems including the stability analysis and the sensitivity analysis with respect to parametric variations of the controlled plant is another major problem [28]. Since mechatronics applications require the analysis of these properties because of good steady-state and dynamic performance requirements, fuzzy control can be used if the global stability of the controller is studied well. That is the reason why fuzzy logic is not selected as the stabilization controller in this thesis.

Neural networks have been utilized in nonlinear systems due to its ability to learn and handle nonlinearities and uncertainties present in the control system. The most useful property of neural networks is their ability to approximate arbitrary linear or nonlinear mapping through learning. However, gradient-based back propagation learning algorithms and real-time recurrent learning are found to be the major drawbacks of the neural network [31]. Gradient based back propagation algorithm is simple and requires smaller amount of storage, however, it converges very slowly and the learning parameter which is experimentally assigned affects heavily the learning performance [32]. The real time recurrent learning (RTRL) algorithm is a gradient-following learning algorithm for fully connected recurrent neural networks. This learning algorithm requires a high computational burden in the training phase [33].

Choosing the architecture of a neural network for a particular problem usually requires some prior knowledge of the problem complexity and usually involves trials and errors. The network topology, however, directly affects two most important factors of neural network training; generalization and training time. In addition, convergence can be very slow, and training errors are not always guaranteed to be reduced with previously defined tolerances [34].

In addition, fuzzy logic controllers and neural network controllers are in general too complicated to be implemented in real time. Although, an industrial PC are used to demonstrate the control effect, the proposed control algorithm must run on missile signal processing unit which are usually a Digital Signal Processor (DSP) running at 100 Mhz and this requirements confines the control algorithm to be selected.

In our work, fuzzy control and neural networks are both implemented because fuzzy control helps the conventional PID controllers to have a self-tuning ability and online adaptation to nonlinearity and neural networks can learn and handle nonlinearities and uncertainties present in the control system. In neural controller, adaptive linear network with least mean square learning method is used because back propagation algorithm takes longer than the required step time which is 0.0001 sec. Although, fuzzy controller provides more satisfactory results than neural network, it still cannot be selected as gimbal stabilization controller.

Sliding mode control or variable structure systems is one of the popular control strategies and powerful control technology to deal with the nonlinear uncertain systems [35]. It is often used to cope with any worst-case scenario resulting from parametric perturbations with lower and upper bound, external disturbances and slip-stick friction etc. In addition, it provides robustness to

the system and does not generally require precise mathematical model of the system dynamics to develop controller. However, the robustness of the sliding control strongly depends on specified parameters in designing the sliding function [36]. Moreover, sliding mode imposes chattering on the system due to imperfect switching. Chattering results in extreme heating in electrical power circuits, high wear of moving mechanical parts and may excite high frequency nonlinear modes in the system dynamics. Chattering is also undesirable if control dynamics is costly which prohibits high control activity [37][38]. To reduce chattering, various compensation techniques have been proposed. Integral sliding mode and boundary layer approach are widely used solutions to the chattering problem. In our case, the control variable is costly and limited because of the power source in the missile, therefore, the proposed controller must use control in a frequency as low as possible, which makes chattering undesirable. In Chapter 4 of thesis, we have used classical sliding mode control where we demonstrate the elimination of chattering which could not be removed completely in our hardware system, so, classical sliding mode controller was found not to be a solution to the gimbal stabilization problem.

Proxy-based Sliding Mode Control (PBSMC), as introduced by Kikuuwe and Fujimoto in 2006 for robot control, combines accurate tracking and smooth response because of the separation of local and global dynamics [88][89]. PBSMC is defined as a modified version of sliding mode control adapted to discrete environment and, at the same time, as an extension of force-limited PID control [88][89]. The local dynamics, response to the small errors, is determined by the PID-type virtual couplings while the global dynamics, response to the large errors, is determined by the sliding mode controller. Therefore, this control technique is an alternative representation of a classical type sliding mode controller as well as an extension of PID control. In addition, the output of the controller is continuous, thus, there is not any

chattering problem. Furthermore, PBSMC does not result in overshoots and oscillations when unexpected environmental conditions and temporal power failures occur and the detailed derivation of the control law of PBSMC is given in Chapter 4. Initial introduction of the PBSMC is to control the industrial robots without any overshoots after a power failure occurs. PBSMC which is used in this thesis work is adopted for the gimbal stabilization problem. In addition, performance of the PBSMC is investigated by comparing it with the conventional PID controller using identical gains because PBSMC is introduced as an extension of PID control.

In summary, there are several control techniques which can be used in LOS stabilization. Controller in LOS stabilization should minimize the effect of the nonlinearities and uncertainties. In addition, the controller should provide good stability, robustness and consistent performance under the presence of uncertainties and external disturbances. However, each control technique mentioned in the previous paragraphs either addresses only a subset of required performance metrics without improvements or has difficulties to achieve the stability of the controller under uncertain operation condition. Moreover, some of the control technique require high computational burden, which makes it difficult to apply in real time environments. In expert control such as fuzzy control, the derivation of the control rules and study of stability are not straightforward. Sliding mode control, on the other hand, provides robustness to the system without perfect mathematical model where reduction of chattering seems to be a solution for the line of sight stabilization control of a two axis gimbal for a roll stabilized missile.

In the literature, the application of the sliding mode control to the nonlinear gimbal dynamics with unbalance is limited and most controllers designed for the stabilization assume that the angular rate measurement of the azimuth and

elevation gimbals is noise-free and exact. In addition, the high portion of the controllers existing in the literature does not have real-time experiment result. In our case; imbalance, cable restraint torques, gyro noise, residual motion from the missile acceleration, structural vibration are the main disturbance source which must be rejected.

In order to solve the gimbal stabilization problem, sliding mode control, fuzzy logic and neural networks can be implemented. Since these controller can address the problems mentioned in the previous paragraphs, a comparative study between these controllers is performed before selecting proposed architecture. Windrow-Hoff delta rule with ADALINE is used instead of the back propagation algorithm with multilayer feed forward networks in order to refrain from intensive calculation because LOS controller has a very short settling time. However, in this controller, the learning time is very long and increasing the learning coefficient results in overshoots in the response of the controller. In order to reduce the chattering effect existing in the sliding mode control, Windrow-Hoff delta rule with ADALINE is augmented in sliding mode. In this controller, some safety measures such as sign approximation are also taken. However, it is not possible to eliminate high-frequency oscillation even several assumption has been made. Although, fuzzy control offers more satisfactory result, the stabilization accuracy values stills are beyond the required values. In addition, the derivation of the control rules, selecting the interval of the membership functions and determining the types of the membership functions are quite difficult. Therefore, for the aim of having good stabilization performance in spite of these disturbance sources, PBSMC is used and results show a satisfactory performance.

2.4 Friction Modeling and Compensation

Friction is a natural phenomenon, which is complicated and not well understood and is universally present in the motion of bodies coming in contact [41]. The presence of friction imposes severe performance loss such as tracking lags, position errors, stick-slip motions, and limit cycles, for motion control systems [42][43]. Therefore, precise motion control requires the estimation and compensation of complex behavior due to friction evident in a variety of motion control system such as machine tool positioning and pointing and tracking in airborne navigation systems [44]. Hence, it is very important to find a control methodology to alleviate the influence of friction in motion control system. Several compensation methods are available in the literature for compensation of the friction effect. These methods can be classified into two groups: model based friction compensation and non-model based compensation.

Tribology, the science of the friction, has provided remarkable effects for explaining the atomic level of friction and forming the predictive model [46]. Based on the experimental data, friction is considered as a function of velocity and the classical friction model is described by the following equation.

$$T_f = T_C sign(\dot{\theta}) + b\dot{\theta} \tag{2.1}$$

where T_C is the Coulomb friction level, b is the viscous friction coefficient and

$$sign(\dot{\theta}) = \begin{cases} 1, \dot{\theta} > 0 \\ 0, \dot{\theta} = 0 \\ -1, \dot{\theta} < 0 \end{cases}. \tag{2.2}$$

Static friction can be added to explain the stick friction. In this case, friction torque is

$$T_{stick} = \begin{cases} T_e & ,|T_e| < T_s, \dot{\theta} = 0, \ddot{\theta} = 0 \\ T_s sign(T_e) & ,|T_e| > T, \dot{\theta} = 0, \ddot{\theta} \neq 0 \end{cases}. \tag{2.3}$$

Here, T_e is the external torque, and T_s is the breakaway torque, which is the limit between static friction and kinetic friction and these classical elements can be combined in different manner as in Figure 2.6 in order to explain to the friction.

However, tribological experiments conducted later have shown that this type of classic friction model in any form cannot explain the behavior of the friction in low velocity regime because the friction force which increases from the breakaway level to the Coulomb level is a function of velocity as in Figure 2.6 [46]. This continuous behavior of the friction is usually called as Stribeck effect and this effect is described in [48] as,

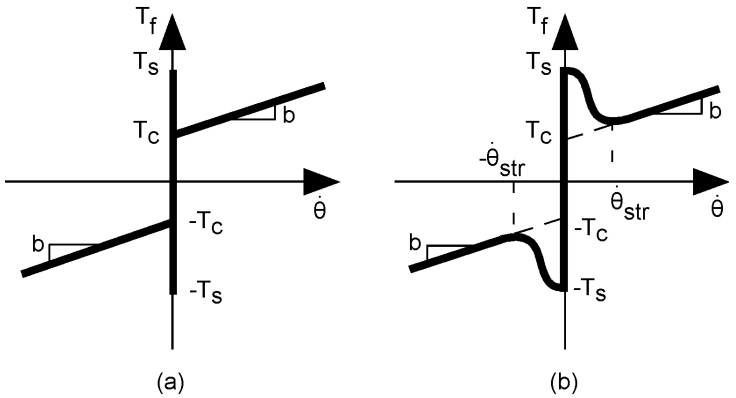

Figure 2.6 : (a) The classical friction model, (b) The General Kinetic Friction (GKF) model [48]

$$T_f = \begin{cases} T_f(\dot{\theta}) & ,\dot{\theta} \neq 0 \\ T_e & ,|T_e| < T_s, \dot{\theta} = 0, \ddot{\theta} = 0 \\ T_s sign(T_e) & ,|T_e| > T_s, \dot{\theta} = 0, \ddot{\theta} \neq 0 \end{cases}. \quad (2.4)$$

and there is large number of different parameterization of this model and one of them can be written as in [47],

$$T_f(\dot{\theta}) = \left[T_c - (T_s - T_c)\exp(-\left|\frac{\dot{\theta}}{\dot{\theta}_{str}}\right|^2) \right] sign(\dot{\theta}) + b\dot{\theta} \quad (2.5)$$

However, GKF cannot explain clearly the region of zero velocity, which is vital during the real time experiments [48].

In [49], Dahl explained friction by using the stress-strain property of materials. If an object is exposed to a small displacement, it returns to the original position while a large displacement results in a plastic deformation. According to this idea, the maximum stress before the plastic deformation is the stiction force and friction is not only functions of the velocity, but, it is also function of the displacement. The following empirical expression explains the Dahl friction model.

$$\frac{dT_f(x)}{dx} = \sigma_{stiff} \left| 1 - \frac{T_f}{T_c} sign(\dot{x}) \right|^n sign(1 - \frac{T_f}{T_c} sign(\dot{x})) \quad (2.6)$$

where σ_{stiff} is the stiffness parameter, where T_f=0, n is a positive number which is smaller than one for brittle materials and larger than one for ductile materials, while T_c is the Coulomb friction level. In general, the simplest case where *n=1* is used.

In [50], the comparison between the kinetic/viscous model and with the Dahl friction model is conducted and this referred work shows that adaptive friction compensation with Dahl model decreases the error significantly even in low velocity regime. Although, Dahl expression is able to represent pre-displacement and hysteresis as in Figure 2.7, it is unable the capture the Stribeck effect and the slip-stick motion. However, it is used for the derivation of the more advanced model because of the good approximation of the pre-sliding behavior [51].

Lugre model, based on the Dahl model, models the friction as the average deflection of the elastic springs as in Figure 2.8. Lugre uses the Dahl model with $n=1$ by introducing

$$z = \frac{T_f}{\sigma_0} \tag{2.7}$$

as a new state variable z which can be defined as the average brittle deflection.

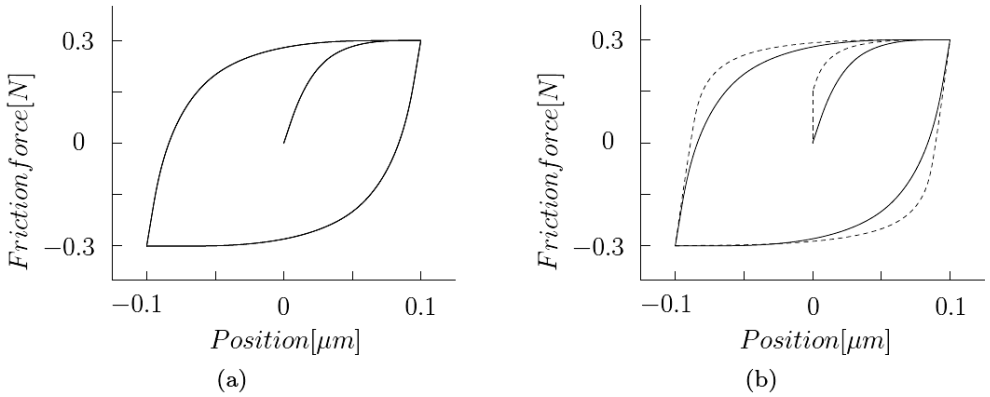

Figure 2.7 : Behaviors of (a) Dahl and (b) Lugre model for sinusoidal input with two different frequencies [51]

In addition, T_c is replaced by a velocity dependent function $g(v)$ and an additional damping term σ_1 associated with the micro-displacement is added. Then, Lugre model results in,

$$\dot{z} = v - \sigma_0 \frac{|v|}{g(v)} z \tag{2.8}$$

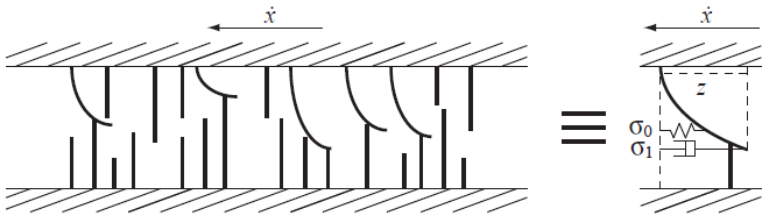

Figure 2.8 : Lugre model analogy [53]

$$T_f = \sigma_0 z + \sigma_1 \dot{z} + f(v). \tag{2.9}$$

Here, T_f is the friction force, v is the velocity between the two contact surface and z is the internal friction state.

Lugre friction model explains properly both presliding and sliding regimes; however, it still lacks the ability to describe hysteresis with nonlocal memory as illustrated in Figure 2.9 and simulations shows that Lugre model has an undesired position drift because Lugre model is velocity dependent [51]. In addition, friction compensation using Lugre model requires the assumption of σ_0 and σ_1[58]. Although these problems are solved with the introduction of Leuven model, however, Leuven model still have some numerical and implementation problems.

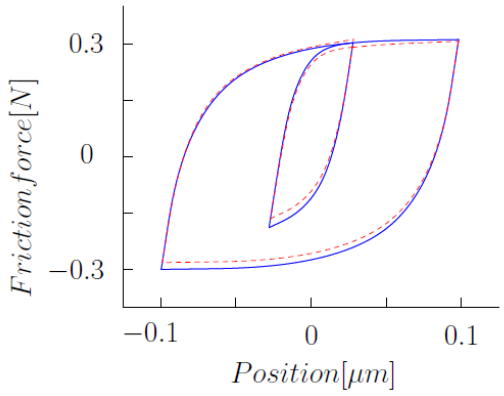

Figure 2.9 : A qualitative comparison between the predicted behavior of the Lugre model (dashed line) and reality (solid line) at velocity reversals [51].

In general , model based friction compensation techniques is successful if precise model of friction is present or parameters involved in the friction model can be easily determined. Although, many sophisticated model-based friction compensations have been proposed by researchers, both the selection of the appropriate friction model and its parameter identifications for a certain system are difficult in practical applications. Precise positioning applications where low velocities are present like gimbal stabilization require high stabilization performance and the results obtained with existing model based friction are not satisfactory especially low velocity region. Therefore, friction is still quite hard to model and is not yet completely understood even though several improvements are proposed by researchers.

The basic and most known unmodelled friction compensation is the changing of the controller gain. Conventional PD controllers are not able to provide satisfactory results because they cannot compensate the steady state error produced by friction. Although the errors may be reduced somehow using high gain PD controllers, system instability occurs due to the increasing system

stiffness. In addition, using high proportional and high derivative feedback requires strong actuator which increases cost. Adding integral action can compensate the steady state error; however, the generation of limit cycles at low or zero velocity is inevitable because of the slip-stick friction. This issue can be compensated with a dead band at velocity reversal; however, using dead band also introduces other problems like steady-state errors which decrease the performance. [50][52][54]. Another non-model based friction compensation is done by introducing dither to the controlled system [55]. Dither is a high frequency signal with amplitude greater than the maximum stick friction force. The focus here is to smooth the discontinuity behavior of friction at low velocity. This high frequency signal is incorporated into control signal and slip-stick friction is avoided because controlled system always has non zero velocity. However, introducing dither to control input is energy-consuming and parameters neglected in the system dynamics may be excited. This is unwanted for our system.

The more recent technique for the non-model based friction compensation is the utilizing the friction observer based on a filter or a local function estimator. The observer output is used to compensate friction by adding a force or torque to the control signal with a value equal and opposite to the instantaneous friction as illustrated in Figure 2.10.

Non model based observers do not require a structured model of friction and it is reported that they explain the friction characteristics even in the presence of humidity, wear and sudden load variation. In addition, non-model based friction compensation methods can capture the multiple sources of friction or nonlinearities adequately compared to the single structured friction model. In addition, in [57], it is shown that non-model-based methods have equal to

superior friction cancellation performance compared to adaptive or well-tuned model-based methods.

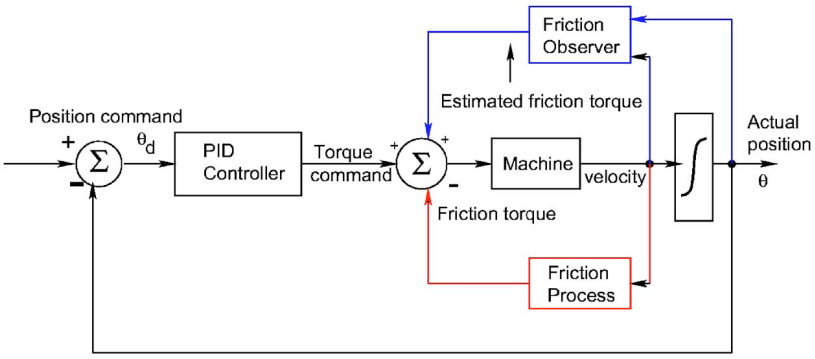

Figure 2.10 : Block diagram of a position control system with friction compensation [56]

To summarize, there are lots of friction models and techniques for the identification and compensation of friction. However, the majority of them require a perfect model of the controlled system. In addition, most of them assume that a precise measurement of relative speed is available. Moreover, the identification of friction characteristics using experimental data to decide the parameters involved in the friction models is valid only for the conditions under which the experiments are conducted.

For two axis gimbal system, it is not very easy to obtain a precise mathematical model and conducting experiment is not a smart solution for the identification of friction characteristics because of the changing friction characteristics due to load, humidity and temperature variations. In addition, the relative velocities of the gimbal rings are not accurate because of the angular position sensors mounted on the gimbal axes. Since non model friction compensation is capable of characterizing the multiple sources of

friction, this approach seems to be a good choice for the compensation in our thesis work.

Non-model based friction estimator is constructed in our work using an Extended Bucy Kalman Filter (EKBF) because it is reported in [44] that EKBF based friction compensator has provided more than fifty percent RMS tracking error reduction over a set of compensator including well-tuned PID, adaptive control using local function estimator, Dahl friction observer. In this technique, friction torque is treated as an unknown state variable and friction torque which is required for the compensation is estimated by measuring the motion along with the applied torque by knowing the system parameters such as moment of inertia and viscous friction. The absolute encoder provides measurement of the angular position for each axis and two axis gimbal system is modeled as a second order system for the friction estimation purpose only. For the inner gimbal, by neglecting the inductance, the state equations can be written as,

$$\begin{bmatrix} \ddot{\theta}_e \\ \dot{\theta}_e \end{bmatrix} = \begin{bmatrix} -\frac{k_t k_b}{RJ} - \frac{b}{J} & 0 \\ 1 & 0 \end{bmatrix} \begin{bmatrix} \dot{\theta}_e \\ \theta_e \end{bmatrix} + \begin{bmatrix} \frac{k_t}{RJ} \\ 0 \end{bmatrix} [V_{in}] + \begin{bmatrix} -\frac{1}{J} \\ 0 \end{bmatrix} [Tf] \qquad (2.10)$$

Here, k_t , R and k_b are the motor parameters while J is the inertia of the elevation motor with gimbal, and b is the viscous friction. EKBF optimally filters noise and estimates the friction torque with the angular position and the angular velocity of the gimbal and friction torque is modeled as a random walk of order n to describe the transient behavior of the friction. Actually, the friction torque term with its derivatives act as tuning parameter to model the friction.

$$\begin{bmatrix} \dot{T}_f \\ \ddot{T}_f \\ \dddot{T}_f \\ \vdots \\ T_f^{\,n} \end{bmatrix} = \begin{bmatrix} 0 & 1 & 0 & \cdots & 0 \\ 0 & 0 & 1 & \cdots & 0 \\ 0 & \cdots & 0 & 1 & 0 \\ \vdots & \vdots & \vdots & \vdots & \vdots \\ 0 & 0 & 0 & 0 & 0 \end{bmatrix} \begin{bmatrix} T_f \\ \dot{T}_f \\ \ddot{T}_f \\ \vdots \\ T_f^{\,n-1} \end{bmatrix} \tag{2.11}$$

(2.10) and (2.11) form the basis of a dynamic estimator to predict the augmented state which is

$$x = \begin{bmatrix} \dot{\theta}_e & \theta_e & T_f & \dot{T}_f & \ddot{T}_f & \dddot{T}_f & \cdots & \cdots & T_f^{\,n-1} \end{bmatrix} \tag{2.12}$$

EKBF propagates the augmented state equation along with the linearized matrix differential equation and updates the state estimate and covariance matrix by calculating an optimal filter gain and random walk equation is driven with the measurement residuals [45].

$$Q = \begin{bmatrix} Q_{\dot{\theta}_e} & Q_{\theta_e} & Q_{T_f} & Q_{\dot{T}_f} & Q_{\ddot{T}_f} & Q_{\dddot{T}_f} & \cdots & \cdots & Q_{T_f^{\,n-1}} \end{bmatrix} \tag{2.13}$$

In this technique, the filters gains can be computed once because the linearized state transition, control effect and the disturbance matrices are independent of the order of the random walk [44]. Therefore, only the state propagation and updating are required to implement in a real time environment. In this thesis, a second order random walk model is used and the compensation “as is” is not novelty.

2.5 Sensor State Estimation

Nowadays, MEMS (Micro Electronic Mechanical System) based sensor has been used extensively because of its remarkable advantages such as small volume and low cost. Such type sensors usually use vibrating element to sense the angular rate and the operating principle is based on the transfer of the energy between two vibrating modes caused by the Coriolis acceleration. However, these sensors have significant bias values because of the limitation of the today's manufacture technology. Although, static and dynamics errors can be compensated algebraically, mechanical imperfections also impose quadrature errors. Quadrature errors decrease the sensitivity of the gyroscope because they are mixed into the actual acceleration signal [60]. In addition, these sensors have stochastic error which cannot be estimated before and they can only be described by its statistical characteristic and diminished by using a filter [61].

MEMS gyroscope is very popular in most areas because of its outstanding advantage such as low profile, low cost and high reliability. However, MEMS gyroscope has significant bias and random error values because of the limitations in the manufacturing technology. Therefore, low cost MEMS gyroscopes are deficient in accuracy for a given working situation. In addition, periodic error terms are observed in the zero drift of the gyroscope in short operation time and high sampling rate and perfect real time compensation are required for efficient use of MEMS gyroscope [62].

In general, gyroscope errors can be classified into three groups which are static, dynamic and stochastic errors. The most important error is the stochastic one because it varies in a random manner. In the literature, a lot of materials are presented to improve the accuracy of MEMS gyroscopes. The

first compensation technique is to predict the inherent errors such as scale factor nonlinearity, zero point bias and asymmetry to increase the precision of the gyroscope output. However, estimation and correction of such errors cannot prevent occurrences of random noise and sampling errors. The other type of approach is to design a proper choice of filtering, which could restraint stochastic noise and sampling errors [63][64].

Kalman Filter (KF) is an effective and versatile procedure to combine noisy sensor outputs for estimating the state of a system with uncertain dynamics. Uncertain dynamics refers to unpredictable disturbance caused by host vehicle, environment and sensor parameters. In the literature, Kalman Filter is evaluated as an estimation algorithm rather than a filter. It uses knowledge of the deterministic and statistical properties of system parameters and measurements to find the optimal estimate based on available information. Kalman Filter is a Bayesian estimation technique requiring an initial set of estimates and deriving recursively the new values by updating its working estimates as a weighted average.

Although, Kalman Filtering seems to be an efficient way to estimate the state of sensors or systems, the derivation of the Kalman Filter (KF) algorithm is based on assumptions that the measurement model is a linear function of the state vector and the measurement noise has zero mean Gaussian (normal) distribution. For some applications which have time correlated noise and where measurement model is nonlinear, Kalman Filtering is not helpful and variants of Kalman filters such as Extended Kalman Filter (EKF) and Schmidt-Kalman Filter should be employed. EKF linearizes the nonlinear model and applies the conventional KF and generates an estimated state instead of working with the real state. However it does not guarantee the convergence because of propagating mean and covariance due to the linear

approximations of the nonlinear transformation. In addition, EKF cannot track signals around sharp turning points [67].

Furthermore, in Kalman Filtering, it is supposed that measurements errors are time uncorrelated. If correlation times are very short, measurement errors can be assumed to be white noise. For error sources over more than a minute, white noise approximation does not imitate the effects of these errors changing with time. The solution proposed to solve this problem is to use Schmidt-Kalman filter with uncertain parameters [68]. Schmidt-Kalman filter handles time-correlated noise which is observed frequently in inertial systems due to a loop filter or another estimation algorithm. However, it is reported that Schmidt-Kalman filter usually requires more computational power that Kalman Filter. In this thesis, it is assumed that there does not exist time correlated noise because the overall operation time is less than a minute. Therefore, it is not necessary to reformulate the state transition equation or to use Schmidt-Kalman filter.

There are also higher orders nonlinear filtering algorithms which do not linearize the error covariance propagation, that are known as sigma point Kalman Filters. The unscented Kalman Filter (UKF) is based on the unscented transformation approximation of a probability distribution by deterministic sample. It uses a set of sigma points which are calculated by moment matching method to come close to the nonlinear distribution in the Kalman filter framework and the flaw of Extended Kalman Filter is eliminated, resulting in a theoretically better performance than EKF. In addition, the implementation of the UKF does not necessitate the calculation of Jacobian matrices, which results in a suitable approach for real-time applications. However, there is known drawbacks of UKF, which are [70]

UKF preserves the linear update structure of the Kalman filter which is optimal only in linear Gaussian systems,
UKF uses second order moment which is valid only for Gaussian distributions,
The number of sigma points is small and may not be sufficient to represent complicated distributions.

The comparative study between the UKF and second order EKF indicates that the estimation accuracy of the UKF is better than that of the EKF and UKF algorithm takes longer because it has to handle all the sigma points using the unscented transformation [65][66]. Therefore, UKF should be used instead of the EKF in virtually all nonlinear estimation problems if the running time of the UKF is comparable with EKF. Although, the UKF algorithm takes a bit longer than the EKF in our problem, UKF will be used because the unscented transformation (UT) provides sufficient accuracy to be applied in many highly nonlinear filtering and control applications such as navigation, public transformation and high speed road vehicles.

Apart from the aforementioned variants of Kalman Filter, innovation based adaptive estimation (IAE) and multiple model adaptive estimation (MMAE) is available as adaptive filter when the system noise variance is not known in advance. However, these techniques are more computationally intensive due to the usage of several Kalman Filter processes [68]. In addition, these algorithms require estimation made over larger data to achieve reliable covariance measurement [69]. Therefore, utilization of these filters in real-time environment is problematic because of the high computation requirement and large windows of data input.

To summarize, there are several filtering algorithm for the estimation of the state of the sensor, however, a high portion of them either require intensive

computation for real time application or make several assumptions which are not applicable in real life. For example, the non recursive estimation algorithms require extensive processing power and Kalman Filtering assumes that the measurement model is a linear function of the state of vector. Therefore, it is important to utilize an algorithm which does not need intensive calculation, yet, estimates the states of sensor accurately. Therefore, within the balance of this thesis work, UKF is evaluated as a reasonable approach to estimate the sensor states because the filtering algorithm that will be used should not impose large delay while it estimates the actual state with a minimum error even though there is a sharp change in the measurement. In addition, it should not require extensive processing power. However, using very small noise covariance matrix in the UKF algorithm decreases the range that rate sensor can measure and imposes a delay as the analog filters do, while noise free measurement are obtained. Therefore, such matrix should be selected properly in accordance with the test results conducted by the manufacturer. As a last comment, the number of sigma points should be selected as small as possible; however, sigma points must represent the actual distributions.

CHAPTER 3

EARLY TRIALS

In Chapter 2, it is mentioned that each control technique proposed for line of sight stabilization deals with a particular problem and handles only a subset of the performance metrics. This problem can be solved by incorporating other control algorithm to tackle deficiencies of the original algorithm. In literature, various types of nonlinear controllers such as sliding mode control, fuzzy logic and neural network have been augmented to control a nonlinear dynamical system [71][72].

In our early trials, in order to comparatively evaluate approaches, Adaptive Neural Network Sliding Mode Controller (ANNSMC) and Fuzzy Logic Controller were applied to line of stabilization of a two axis gimbal system before introducing our final proposed architecture, proxy based sliding mode control. The advantages and disadvantages of the early trials will be overviewed and discussed throughout the Chapter 3.

3.1 Mathematical Model and Simulation

Mathematical model of the two axis gimbal system needs to be derived in order to design and justify operation of stabilization module in a simulation environment prior to its tests on the physical hardware system. The nonlinear

gimbal dynamics equations are derived using the Lagrangian dynamics [73][74].

The gimbal is a pivoted support which allows the rotation of the imaging system about the elevation and the azimuth axes (Figure 3.1).

φ is the azimuth angle and θ is the elevation angle of the payload with respect to base and these angles are controlled with a two axis gimbal mechanism.

The equation of motion of such system can be derived directly from the Lagrangian,

$$L = T - V \tag{3.1}$$

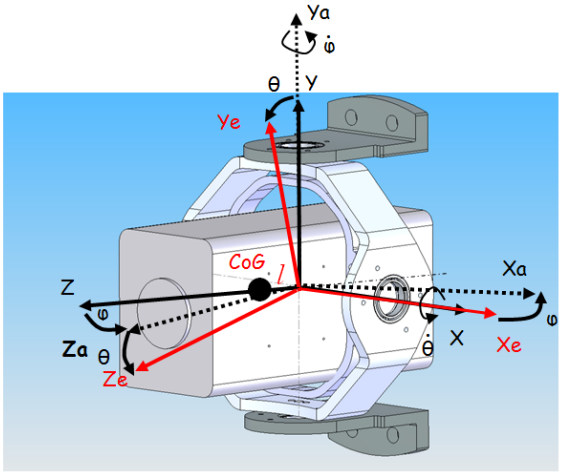

Figure 3.1 : Typical two axis gimbal system

The kinetic (T) and the potential (V) energies of the system are respectively:

$$T = \frac{1}{2}\left[(J_{Px} + J_{Ix})\dot{\theta}^2 + (J_{Pz} + J_{Iz})\dot{\phi}^2 \sin^2(\theta)\right.$$

$$+(J_{Py}+J_{Iy})\dot{\phi}^2\cos^2(\theta)+(J_{Oy})\dot{\phi}^2\Big] \tag{3.2}$$

and

$$V=-mgl\cos(\theta) \tag{3.3}$$

Here, the moment of inertia of the inner gimbal about the *X*, *Y* and *Z* axes are denoted as J_{Ix}, J_{Iy} and J_{Iz}. The moment of inertia of the payload about the *X*, *Y* and *Z* axes are represented as J_{Px}, J_{Py} and J_{Pz} respectively. J_{Oz} represents the moment of inertia of the outer gimbal about the *Z* axis. In addition, *m* is the total mass of payload + inner gimbal and *l* is eccentricity.

The corresponding Lagrange equations of the system are found as,

$$N_\phi=\frac{d}{dt}\left(\frac{\partial L}{\partial\dot{\phi}}\right)-\frac{\partial L}{\partial\phi} \tag{3.4}$$

$$\begin{aligned}N_\phi&=(J_{Pz}+J_{Iz})(\ddot{\phi}\ \sin^2(\theta)+2\dot{\phi}\,\dot{\theta}\ \sin(\theta)\cos(\theta))\\&+(J_{Py}+J_{Iy})(\ddot{\phi}\ \cos^2(\theta)-2\dot{\phi}\dot{\theta}\ \sin(\theta)\cos(\theta))+J_{Oy}\ddot{\phi}\end{aligned} \tag{3.5}$$

$$N_\theta=\frac{d}{dt}\left(\frac{\partial L}{\partial\dot{\theta}}\right)-\frac{\partial L}{\partial\theta} \tag{3.6}$$

$$\begin{aligned}N_\theta&=(J_{Px}+J_{Ix})\ddot{\theta}+(J_{Py}+J_{Iy}-J_{Pz}-J_{Iz})\dot{\phi}^2\cos(\theta)\sin(\theta)\\&+\frac{1}{2}mg\cos(\theta)\end{aligned} \tag{3.7}$$

where N_θ and N_φ are the corresponding generalized forces, which in this case turn out to be torques.

Experimental setup includes a MEMS rate sensor which has significant bias and random error values due to the limitation of the manufacturing technology, therefore, Unscented Kalman Filter (UKF) algorithm is used in rate sensor filtering in order to reduce the effect of uncertainty in the sensor state.

Unscented Kalman Filter (UKF) algorithm used for estimating the states of the rate sensor in our system consists of sampling particles, prediction equations and updating equations. The sampling principle assumes that the state of the rate sensor has Gaussian distribution and sampling particles is calculated by fully matching the mean and covariance of the state variable if two moments of a random variable are available [66]. The prediction part of UKF computes the mean and covariance of the sigma points of the state by propagating them through the dynamic model and adds the process noise covariance to state covariance. The design of noise covariance matrix has proven to play an important role in improving the stability of the algorithm as also stated in [75] Update algorithm of the UKF forms sigma points of the predicted state as in [76] and uses computation rules of Gaussian distributions for conditioning the joint distribution to the measurement after unscented transformation of the joint distribution of predicted state and measurement.

The overall simulation model of the system depicted in Figure 3.3 and Figure 3.4 consisting of three parts which are two axis gimbal system, designed controller and MEMS rate sensor. These blocks consist of m-files or block diagrams and any readily available toolbox is not used in simulations.

In order to give further information, this section is divided into three parts, namely;

- Two axis gimbal system including friction compensation and motor dynamics,
- Controller designed,
- MEMS rate sensor.

3.1.1 Two-Axis Gimbal Dynamics Block

The modeling of nonlinear gimbal dynamics is derived using the analytical mechanics explained briefly in previous section by assuming the inertia of gimbal rings do not change with the rotation of the inner and outer gimbal.

The mass properties such as mass unbalance, moment of inertias of the gimbals are taken from the 3D CAD model designed using CATIA®.

The friction observer summarized in Chapter 2, is incorporated in gimbal dynamics block.

Kollmorgen LAT 0802-A Limited Angle Brushed Direct Drive DC is selected for the gimbal system and required parameters for the simulation shown in Table 3.1 are used.

3.1.2 MEMS Rate Sensor Block

This block depicted in Figure 3.2 includes the filtering algorithm (UKF) to estimate the state of the rate sensor which is required for accurate operation. As a rate sensor, Systron Donner QRS28-00200-100 Quartz Dual Axis Rate Sensor is used because QRS28 is a small, lightweight, two-axis MEMS rate

sensor offering exceptional performance at a very attractive price. The sensor provides a simple DC-DC operation using two of Systron Donner Inertial's quartz rate sensors [94].The summary specification of the QRS28 is depicted in Table 3.2.

Table 3.1 : Direct Drive DC Motor Properties [93]

Size Constants	**Units**	**Value**
Peak Torque Rating - Tp	mN-m	91.8
	oz-in	13
Motor Constant - Km	mN-m/$\sqrt{\text{Watt}}$	13.35
	oz-in/$\sqrt{\text{Watt}}$	1.89
Excursion Angle	degrees	±35
Static Friction (Max.) - Tf	mN-m	2.83
	oz-in	0.40
Maximum Winding Temperature	°C	155
Temperature Rise per Watt-TPR	°C/Watt	15.7
Number of Poles		2
Rotor Inertia - Jm	g-cm^2	28.2
	oz-in-s^2	4.0 x 10^{-4}
Motor Weight	g	85
	oz	3.0

In this block, the sensor behavior is simulated by adding white noise whose noise power is the noise variance times sample time. Then, the filtering algorithm tries to estimate the actual value of the angular velocity.

As a note, the required parameters are taken from the test data conducted by the manufacturer instead of the datasheets published on their website.

Table 3.2 : QRS 28 Specifications [94]

PARAMETER	SUMMARY SPECIFICATIONS		
Part Number	QRS28-00100-100	QRS28-00200-100	QRS28-00400-100
Power Requirements			
Input Voltage (Dual Supply)	Plus and minus 4.75 to 5.35 Vdc		
Input Current	< 50 mA each supply		
Performance			
Standard Range Full Scale	100 °/sec	200 °/sec	400 °/sec
Full-Scale Output (Nominal)	± 3.50 V (Analog DC Voltage)		
Over-Range Capability	> 110% of Full Scale		
Scale Factor	0.035 V/°/sec	0.0175 V/°/sec	0.00875 V/°/sec
Scale Factor Accuracy	± 2% (factory set)		
Zero Rate Output (Bias)	< 33 mV@25°C		
Linearity Error	< 0.05% of Full Range		
Turn On Time	< 1.0 sec		
Random Noise (1-101 Hz)	< 0.005 °/sec./√Hz.	< 0.005 °/sec./√Hz	< 0.007 °/sec./√Hz
Bandwidth (-90° Phase Shift)	110 Hz ±10 Hz		
Input Axis Alignment	< 31 mrad, uncompensated**		
Environmental			
Operating Temperature	-55°C to +85°C		
Storage Temperature	-55°C to +105°C		
Shock	300 g's, ½ sine, 5 mSec		
G-Sensitivity	<0.02°/sec/g		
Weight	20 grams (0.71 oz)		

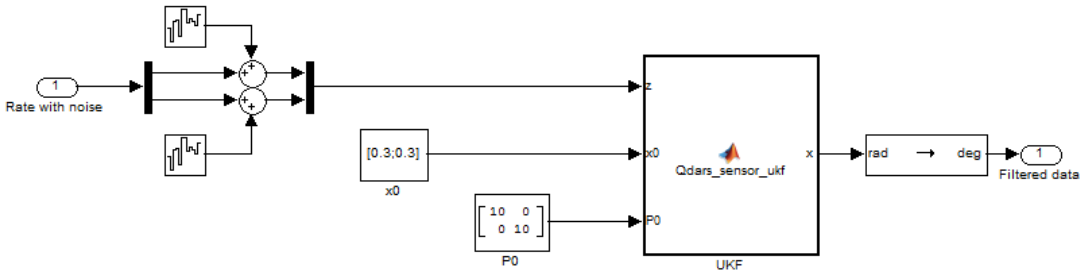

Figure 3.2 : Rate sensor filtering subsystem

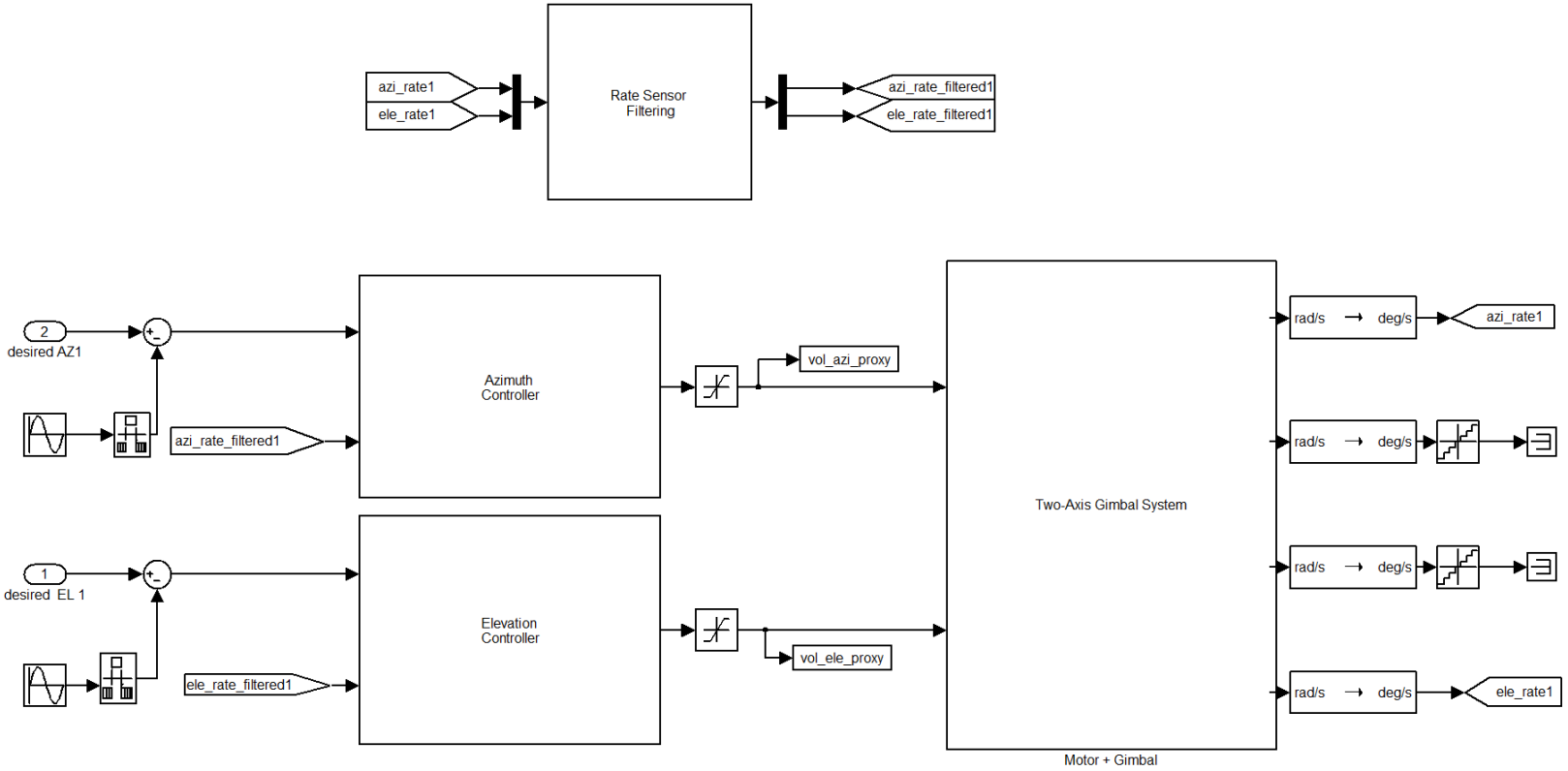

Figure 3.3 : Simulation Model of the Two-axis Gimbal System

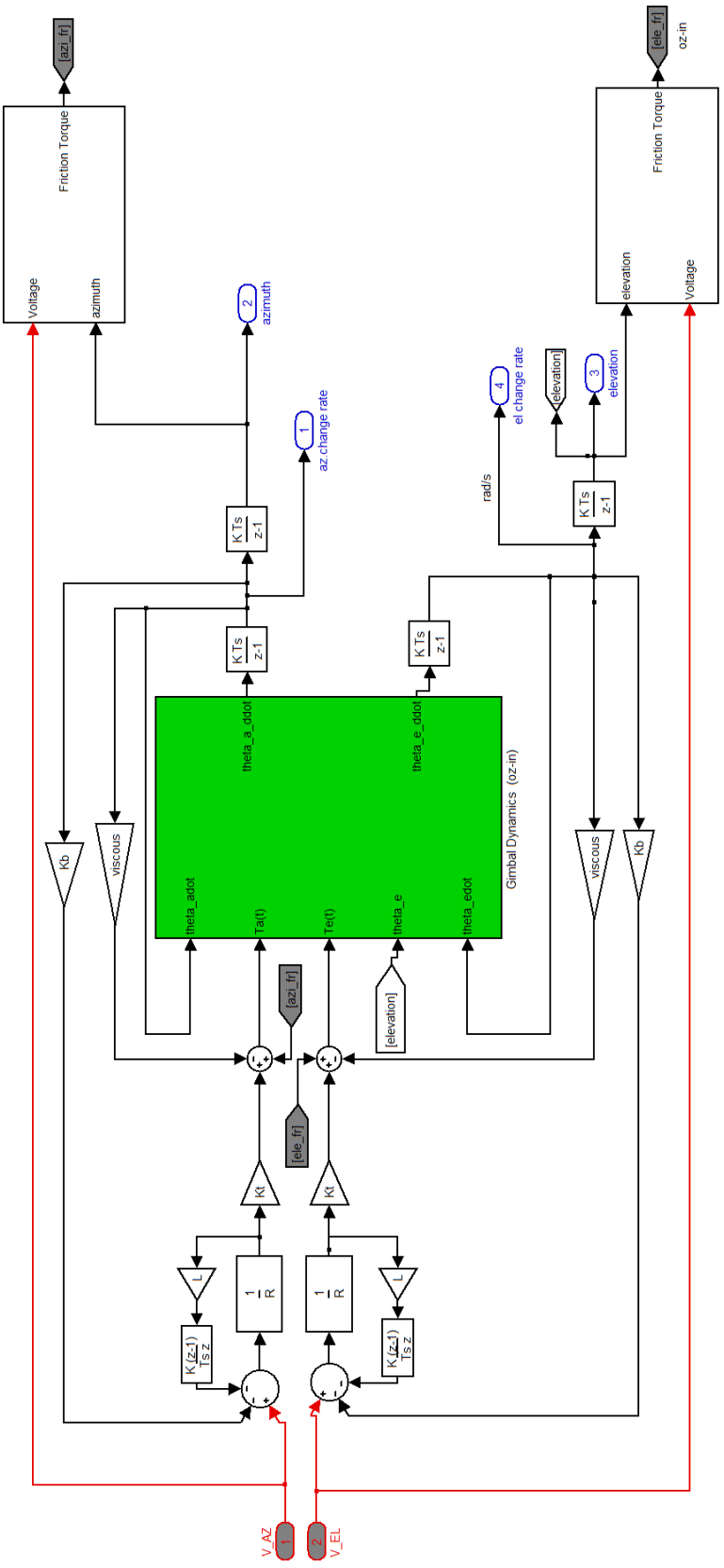

Figure 3.4 : Direct Drive DC Motor and Gimbal Dynamics Block

3.1.3 Controller Block

The controller developed for the stabilization is employed in controller block to prevent ambiguity. It usually takes the velocity error and generates an output which can be voltage as in sliding mode controller or corrected velocity error like in fuzzy controller. This block is not a generic block because different controller requires different input. Figure 3.5 and Figure 3.6 illustrates designed controllers which performance assessment to be done.

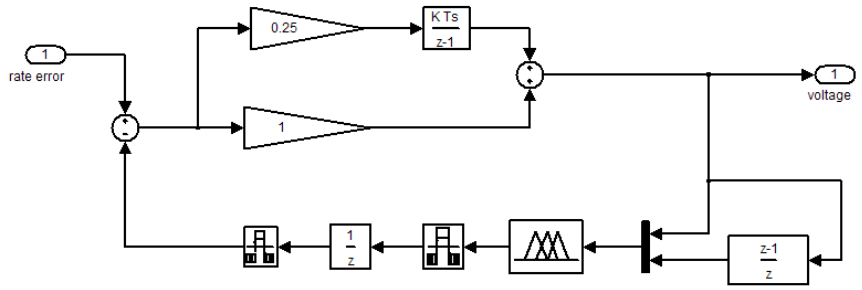

Figure 3.5 : PI Fuzzy Logic Controller

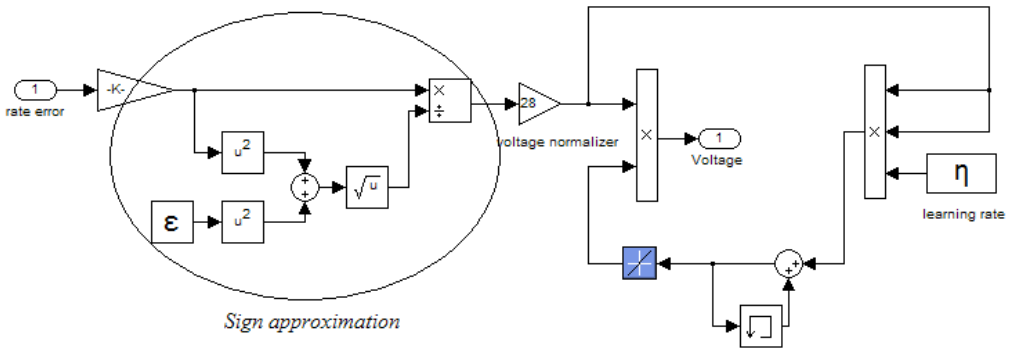

Figure 3.6 : Adaptive Neural Network Sliding Mode Controller (ANNSMC)

3.2 Adaptive Neural Network Sliding Mode Controller

Adaptive linear networks are very simple and fast learning artificial neural network that contains just one neuron with a few inputs and additional unit signal and they can solve only linearly separable problem. However, it is shown that they can approximate the nonlinear functions accurately if enough number of neurons is utilized [77]. The learning algorithm for adaptive linear network which is known as delta rule, is not only extremely simple but also linear, which makes learning fast and easy therefore and ADALINE has become a powerful tool in signal processing with its limited modeling capability [78].

The most popular learning method used with ADALINE is simple LMS (Least Mean Square) algorithm. The LMS algorithm is based on an approximate steepest descent procedure, which, minimizes the mean square error and thus moves the decision boundaries as far as it can from the training patterns [82].

The following assumption has been made for the adaptive linear neural network controller:

- Pitch and yaw channel are not coupled,
- Inertias of the inner and outer gimbals do not change,
- Friction is only viscous friction.

The sliding mode control law for each channel with is found by the following equations:

$$u = \hat{u}_{eq} + \hat{\rho}.sign(\sigma) \tag{3.8}$$

$$\hat{u}_{eq} = c*(\ddot{y}_d + d\dot{e} + \frac{1}{c} - \frac{a}{c}x_1 - \frac{b}{c}x_2) \tag{3.9}$$

where

$$\hat{\rho} \geq \frac{(\frac{L}{b_{\min}} + \rho)}{1-\alpha}, \tag{3.10}$$

$$\rho \geq \frac{2\sqrt{V(0)}}{t_{set}\sqrt{2b_{\min}}}, \tag{3.11}$$

$$L, \alpha \geq 0. \tag{3.12}$$

Here, the sliding manifold, σ, is in the form of

$$\sigma = \hat{x}_2 + \frac{4}{t_{set}}\hat{x}_1 \tag{3.13}$$

with desired and actual output of the each state

$$\begin{aligned} e &= y_d - y \\ \hat{x}_1 &= x_{1d} - x_1 \\ \hat{x}_2 &= x_{2d} - x_2 \end{aligned} \quad . \tag{3.14}$$

The *a,b* and *c* terms defined as with DC Motor parameters

$$a = B\frac{R}{k_t} + k_b \tag{3.15}$$

$$b = \frac{L}{k_t} B + J \frac{R}{k_t} \tag{3.16}$$

$$c = \frac{LJ}{k_t} \tag{3.17}$$

In addition, V is a positive definite Lyapunov function and derivative of the Lyapunov function shows that the origin of the system is asymptotically stable if the system reaches the sliding surface in a finite time. Positive definite Lyapunov function can be selected as

$$V = \frac{1}{2}(\frac{1}{c})^{-1}\sigma^2. \tag{3.18}$$

Then, each channel with sliding mode controller is;

$$\begin{aligned} \dot{x}_1 &= x_2 \\ \dot{x}_2 &= \frac{\hat{u}_{eq} + \hat{\rho}.sign(\sigma)}{c} - \frac{a}{c}x_1 - \frac{b}{c}x_2 . \\ y &= x_1 \end{aligned} \tag{3.19}$$

However, repetition of delayed switching on the sliding surface causes high-frequency oscillations when sliding mode control is directly implemented as a real time discrete controller. The chattering can be removed by introducing a boundary layer about the sliding surface. In this case, the system will not stay on the sliding surface but in some neighborhood about the sliding surface. However, the cost of the introduction a boundary layer about surface is loss in robustness in control system [6]. To eliminate the chattering of the following function approximations can be utilized.

$$sign(\sigma) \approx \frac{\sigma}{\sqrt{\sigma^2 + \varepsilon^2}} \tag{3.20}$$

$$sign(\sigma) \approx \tanh(kx) \tag{3.21}$$

Then, the adaptive neural network sliding mode controller is,

$$\begin{aligned} u_{smc\_nn} &= u_{smc} * f(\sum(w(k) + \eta u^2{}_{smc})) \\ w(k+1) &= w(k) + \eta u^2{}_{smc} \end{aligned} \tag{3.22}$$

3.3 Fuzzy Logic Controller

In deductive logic, it is always assumed that every proposition is either true or false. However, in real life, there are concrete situations which do not fit into such a simple scheme. In other words, it is quite possible that certain situations might have values other than falsehood and truth. Therefore, for the treatment of situations where it is not possible to ascribe values either true or false, techniques beyond those employed in ordinary logic must be developed. The first step in this direction was made by Zadeh who has proposed a so-called "fuzzy set" theory dealing with events and situations having subjectively ascribed attributes [84]. As a summary, fuzzy logic is an extension of Boolean logic based on Zadeh's fuzzy set theory in which the usual binary truth values (0 and 1) are extended to include any degree of membership in the closed interval of real numbers (0, 1) [83].

The first and the most important step in the design of a fuzzy controller is to generate a knowledge base for the system to lead an initial set of rules. To

develop a fuzzy rule base, there are different methods available. Simulating the closed loop system through its mathematical model, interviewing an operator who has had many years of experience controlling the system are some example methods to generate the set of rules. In our case, simulating the closed loop system with mathematical model is used to generate the knowledge base.

In general, there are two types of structure of the fuzzy logic controller which are position type fuzzy controller and velocity type fuzzy controller have been studied so far irrelevant to the application area. The velocity type fuzzy logic controller (FLC) generates the incremental control output error $u(k)$ from error $\omega(k)$ and error rate $\Delta\omega(k)$. The rules of the logic controller usually designed with the following basic ideas [87]

"If the response approaches given set value with large control input then take out the accumulated control input appropriately".

Actually the rules of the fuzzy controller designed with a phase plane in mind, where the fuzzy controller drive the system into sliding mode as the variable structure does.

The structure of the controller designed for elevation axis of the stabilization control of two axis gimbal mechanism is shown Figure 3.7. There are two inputs which are $\omega(k)$ and $\Delta\omega(k)$ and one output $u(k)$. Angular velocity error e is calculated with comparison between the reference command c and feedback signal y. $\omega(k)$ is the corrected angular velocity error after PI controller.

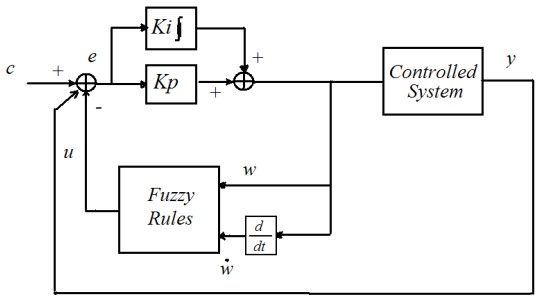

Figure 3.7 : Structure of the fuzzy logic controller

The universes of both input variables are divided into five fuzzy sets: "*Negative Big (NB)*", "*Negative Small (NS)*", "*Zero Error (ZE)*", "*Positive Small (PS)*", "*Positive Big (PB)*" and, while the universe of output is divided into 7 fuzzy sets: "*Negative Big (NB)*", "*Negative Medium (NM)"* , "*Negative Small (NS)*", "*Zero Error (ZE)*", "*Positive Small (PS)*", "*Positive Medium (PM)*", "*Positive Big (PB)*", as illustrated in Figure 3.8 and Figure 3.9 and if-then rules that fuzzy inference used is shown in Table 3.1. The output variable is obtained by using centroid fuzzifier.

Table 3.3 : Fuzzy linguistic rule table

w(k)	*Δw(k)*				
	NB	NS	ZE	PS	PB
NB	PB	PB	PM	PS	ZE
NS	PB	PM	PS	ZE	NS
ZE	PM	PS	ZE	NS	NM
PS	PS	ZE	NS	NM	NB
PB	ZE	NS	NM	NB	NB

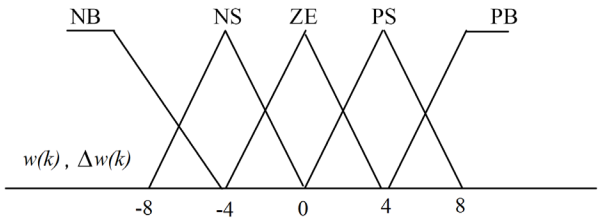

Figure 3.8 : The input membership functions

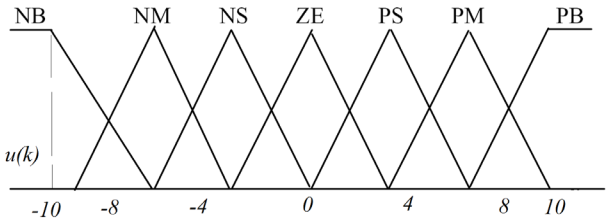

Figure 3.9 : The output membership functions

The output of the fuzzy controller can be plotted with respect to its inputs as in Figure 3.10, which can be considered as a look-up table for the controller.

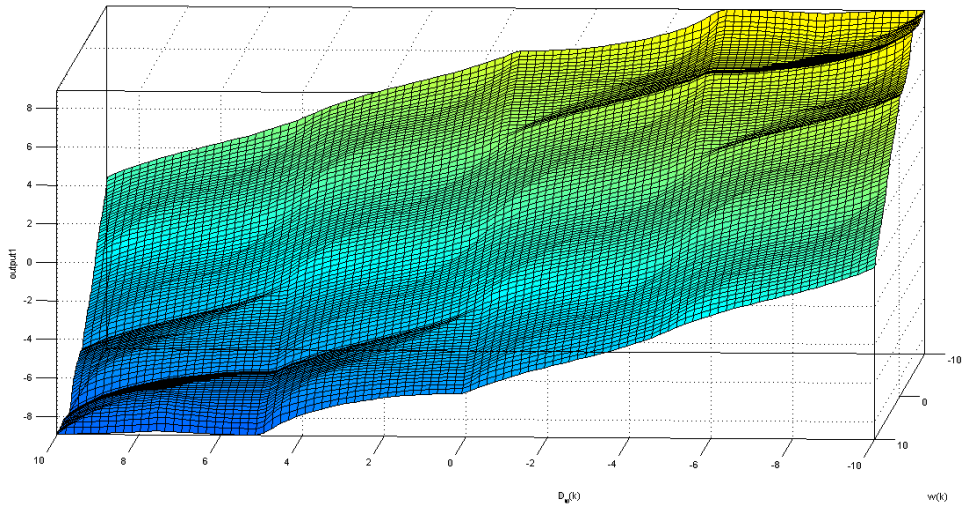

Figure 3.10 : Output surface of fuzzy logic controller

3.4 Comparative Analyses and Conclusive Remarks

In the first part, the behaviors of ANNSMC and FLC under large angular velocity error are compared against desired outputs. Both the exact and estimated angular velocities are used to show the effect of the uncertainty in the measured angular velocity.

In the second part, disturbance compensation capability of the ANNSMC and FLC are compared by exciting to the base with a sinusoidal angular velocity disturbance with variable amplitude and frequency.

3.4.1 Set Point Tracking

The MEMS rate sensor is installed on the electro optical payload. Initially the platform is stable, however, when the missile or the platform move up and down, the image is fuzzy and blurred. MEMS rate sensor sense the difference in the angular velocity and sends the change in the angular velocity required for the guidance system. Finally, the required command for the stabilization controller is generated and sent to controller. This controller analyzes and processes all the data collected than extracts the required parameter for the motion and compensate every frame from the camera and stable, clear image sequences are output on the screen. Therefore, 25 frames/sec commands are sent to the controller to evaluate the performance. In addition, this gimbal system is designed for the anti tank missile, therefore, the magnitude of the command sent to controller will not be so large because of the slow moving target. Therefore, random commands with a sample time 0.04 sec are sent to controller to evaluate the performance.

- **Ideal case with viscous friction**

In this section, the closed loop performance of the designed controller in Chapter 3 is evaluated. In these simulations, first, it is assumed that the actual angular velocities are measured precisely; the friction force is only viscous friction and no mass unbalance exists. The performances of the controllers are illustrated from Figure 3.11 to Figure 3.16.

Comparing the Figure 3.13 and Figure 3.15 clearly indicate that the performance of the ANNSMC increases over time. However, ANNSMC cannot track the desired trajectory at the beginning because of the low learning coefficient even though there is not any chattering problem in the response of the ANNSMC. Increasing the learning coefficient is not recommended because high learning coefficient degrades the stability by resulting chattering.

FLC has more smooth tracking response than ANNSMC, however, ANNSMC outperforms the FLC as the simulation time increases because as the time passes, ANNSMC begins to produce less tracking error with a small overshoot and it exhibits smaller delay in elevation axis represented in Figure 3.15.

In addition, Figure 3.12 and Figure 3.14 show the control command to the gimbaled platform generated by ANNSMC and FLC. Although, initial control command generated by FLC is satisfactory, in long term, ANNSMC incorporates more optimal control command with respect to FLC without producing high-frequency chattering.

In general, PI fuzzy control provides better controller performance because of the rigid response, however, the performance of the both controller with sensor noise and friction must be investigated.

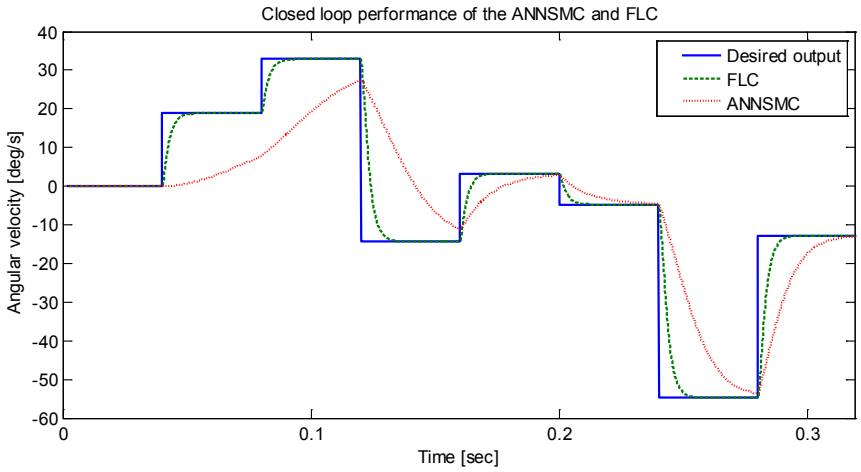

Figure 3.11 : Closed loop controller performance of ANSMC and FLC, elevation axis, ideal case

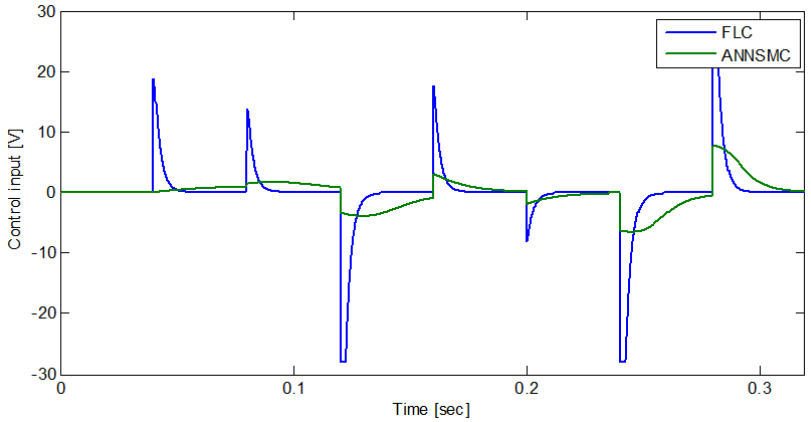

Figure 3.12 : Control commanded to plant, generated by ANSMC and FLC, elevation axis, ideal case

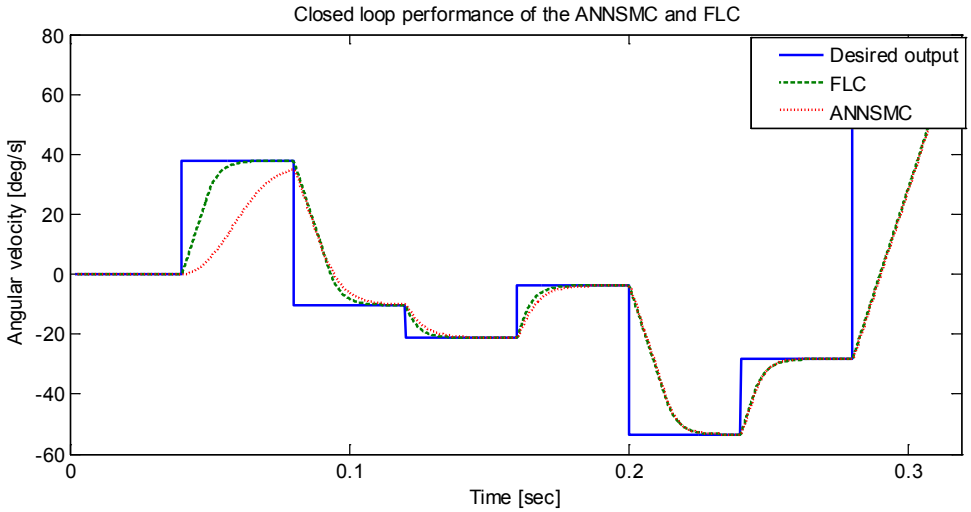

Figure 3.13 : Closed loop controller performance of ANSMC and FLC, azimuth axis, ideal case

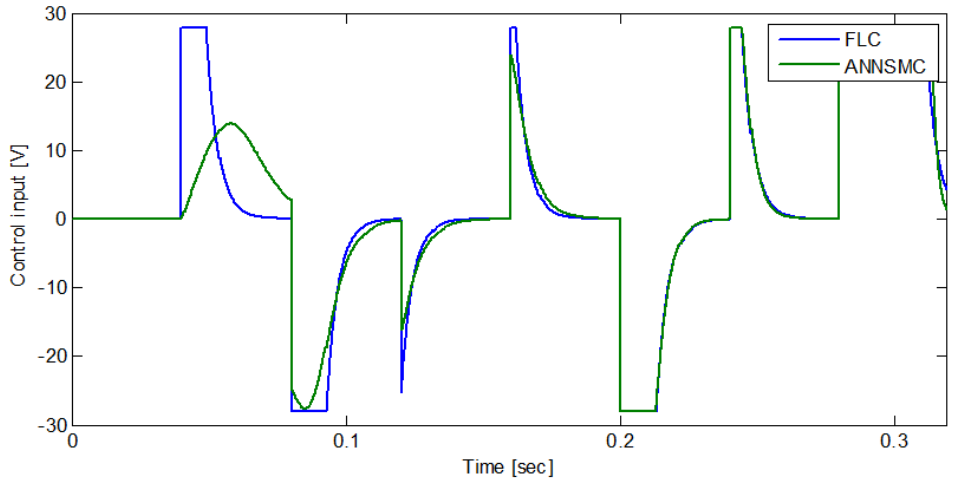

Figure 3.14 : Control commanded to plant, generated by ANSMC and FLC, elevation axis, ideal case

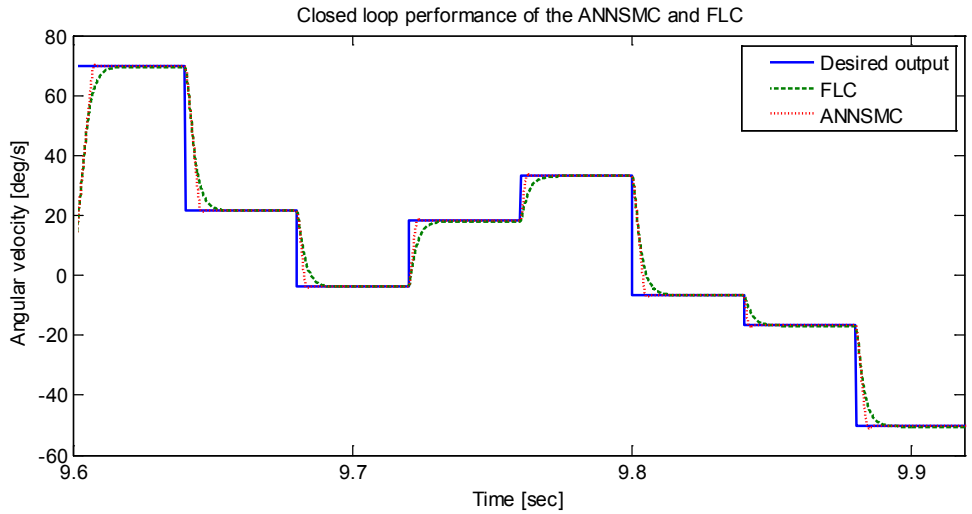

Figure 3.15 : Closed loop controller performance of ANSMC and FLC, elevation axis, ideal case

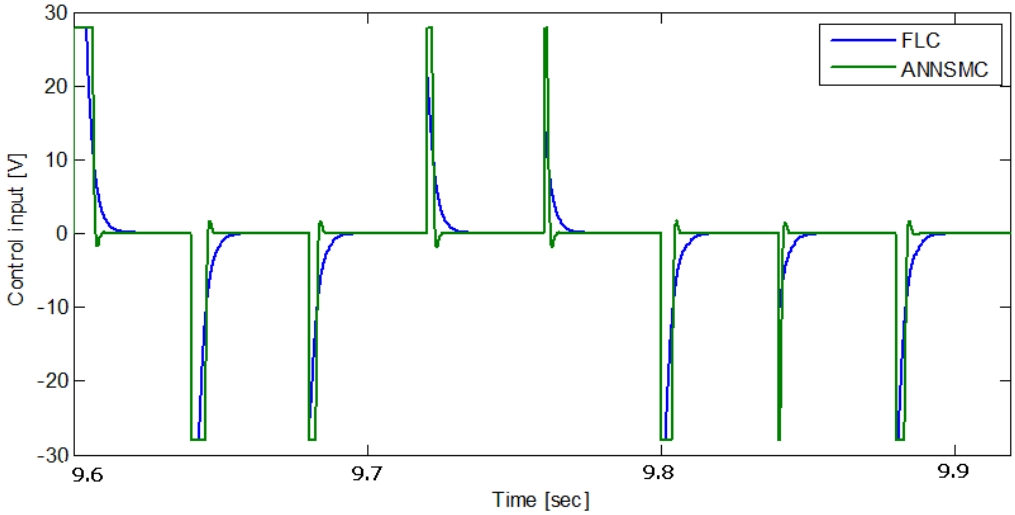

Figure 3.16 : Control commanded to plant, generated by ANSMC and FLC, azimuth axis, ideal case

- **Sensor noise with viscous friction**

In previous section it is assumed that the actual angular velocities are measured precisely. In this section, the states of the rate sensor are estimated with UKF, and the estimated angular velocities are fed back to controller.

The simulation result shown in Figure 3.17 indicates that ANNSMC responds to the given input slowly due the low value of learning rate again, however, in long run, the effect of the adaptive part of the sliding mode control does not work and it behaves like a pure sliding mode control according to control commanded to plant also as illustrated in Figure 3.17. The updating of the learning rate can solve this problem; yet, this is not the only problem in the ANNSMC. Due to the nature of the sliding mode, ANNSMC has high frequent switching, which can harm the controller electronics and can trigger the unmodeled dynamics. Therefore, it is not an intelligent solution to use pure sliding mode with boundary layer and adaptive neural network. To reduce the high frequency switching, the higher order sliding mode can be selected, however, the designed controller becomes very sensitive to unmodeled dynamics. In addition, such type of controller cannot be used as an outer loop feedback in a multi loop controller if the stabilization loop is designed as an outer loop.

3.4.2 Disturbance Rejection Capability

In this part, a sinusoidal angular velocity disturbance with amplitude of 10 deg/s and a frequency of 5 Hz is applied while the desired angular velocity of the elevation axis is zero. This disturbance are feed in to controller as a measurement error to the MEMS rate sensor output.

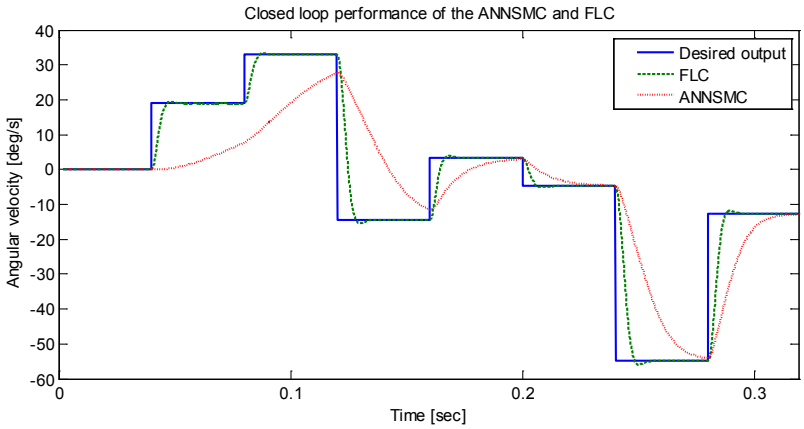

Figure 3.17 : Closed loop controller performance of ANSMC and FLC, elevation axis, with sensor noise

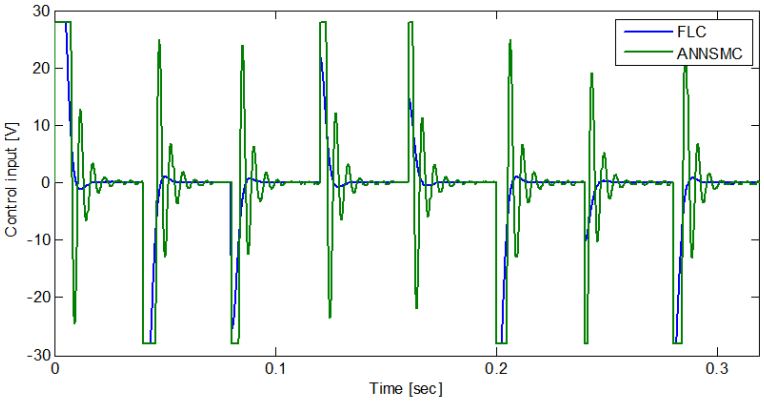

Figure 3.18 : Control commanded to plant, generated by ANSMC and FLC, elevation axis, with sensor noise

Figure 3.19 and Figure 3.20 show the comparison in performance between ANNSMC and FLC. These figures indicate clear superiority of the FLC in disturbance rejection capability. However, it cannot be considered that FLC method has perfect control performance because of the derivation of the control rules. In addition, it is difficult to select the membership function to

have a higher precision and perfect control performance. Therefore, it is required to utilize other control algorithms which can cope with any worst-case scenario resulting from interval bounded parametric perturbations, external disturbances and slip-stick friction.

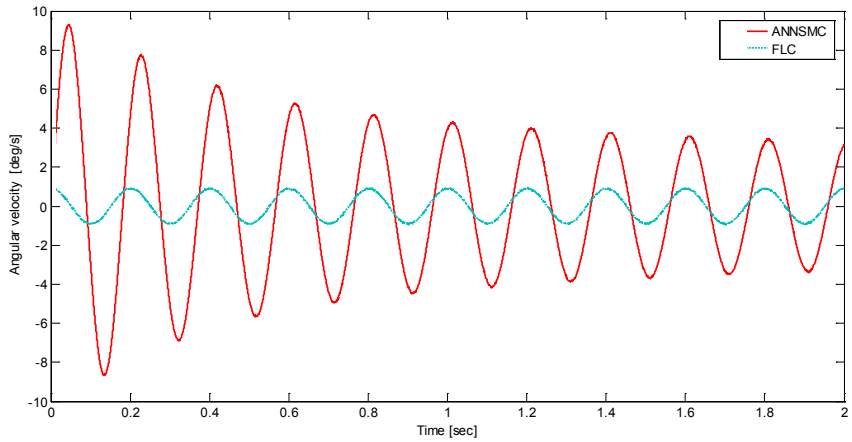

Figure 3.19 : Disturbance rejection capability of the ANSMC and FLC, elevation axis,

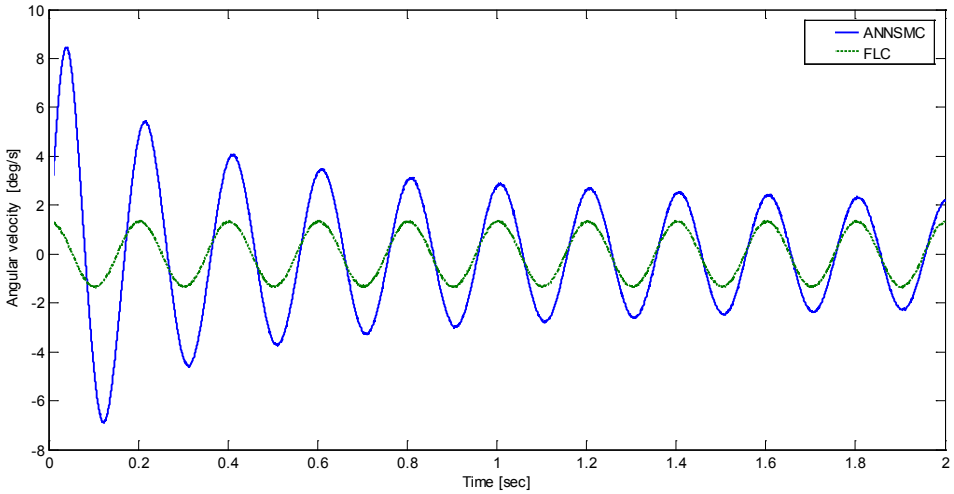

Figure 3.20 : Disturbance rejection capability of the ANNSMC and FLC, azimuth axis, ideal case

CHAPTER 4

PROXY BASED SLIDING MODE CONTROL

Proxy-Based Sliding Mode Control is a new control scheme first introduced by Kikuuwe and Fujimoto in [88]. The idea behind the Proxy-Based Sliding Mode Control is to attach a virtual object referred as a proxy through a virtual coupling controlled object. The virtual coupling can perform PID type control action to maintain its length as zero. In this thesis, this method is adopted and implemented for the inner and outer gimbals and is illustrated in 2D using inner gimbal only for ease of comprehension in Figure 4.1.

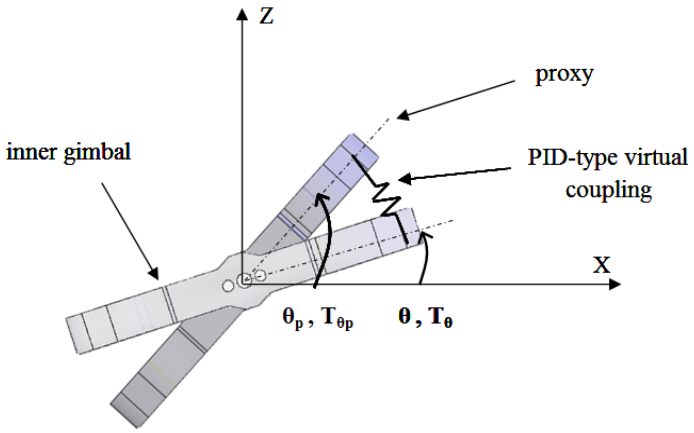

Figure 4.1 : Principle of PBSMC

Here, the proxy depicted as constrained virtual surfaces is a mass connected to the inner gimbal by a PID type virtual coupling.

The position of the proxy is controlled via sliding mode control that exerts a control torque $T_{\theta p}$. The proxy also accepts forces from a PID-type virtual coupling that causes a counter torque T_{θ} between proxy and inner gimbal.

The classically known sliding mode control law to control the proxy is used and formulated as,

$$T_{\theta p} = U \operatorname{sgn}(S) \tag{4.1}$$

Here, U is the control gain that varies at each step k and S is the sliding surface, which uses the dynamic approach error vector:

$$S = (q_d - q_p) + \lambda(\dot{q}_d - \dot{q}_p) \tag{4.2}$$

where q_p and $\dot{q_p}$ are position and velocity of the proxy and q_d and $\dot{q_d}$ are the desired position and velocity of the inner gimbal, respectively.

The error dynamics of the proxy is chosen to decay to zero based on a positive rate constant λ towards the sliding surface and is determined by,

$$\dot{q}_e + \frac{1}{\lambda} q_e = 0 \tag{4.3}$$

where

$$q_d - q_p = q_e. \tag{4.4}$$

On the other hand, torque T_θ is produced by the PID-type virtual coupling in a conventional way:

$$T_\theta = K_p(q_p - q) + K_d(\dot{q}_p - \dot{q}) + K_i\int(q_p - q)dt \tag{4.5}$$

where K_p , K_d and K_i are positive real numbers, which represent the proportional, derivative and integral gains. These parameters should be chosen appropriately so that the position of the inner gimbal q is controlled to follow the desired position of the proxy q_p in an accurate way. The block diagram of the proxy based sliding mode control is illustrated in Figure 4.2.

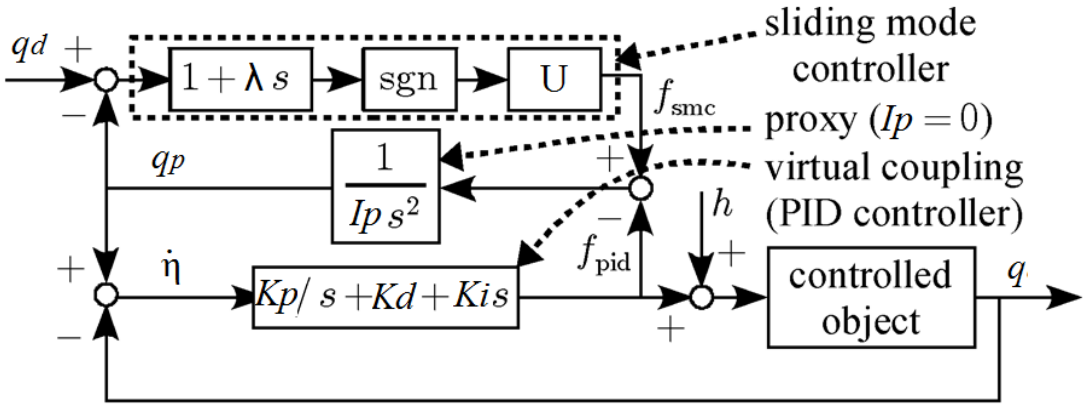

Figure 4.2 : Block diagram of PBSMC (Adapted from [88])

If inertia of the proxy is I_p, then the equation of the motion of the proxy is;

$$I_p\ddot{q}_p = T_{\theta p} - T_\theta. \tag{4.6}$$

Similar to [88][89][90], the inertia of the proxy is set to zero to simulate the controller. Therefore, by introducing

$$\eta = \int (q_p - q)dt \tag{4.7}$$

and using (4.1), (4.2) ,(4.5) and (4.6); the following set of equations representing the continuous time state space of proxy based sliding mode controller is obtained:

$$T = K_p\dot{\eta} + K_d\ddot{\eta} + K_i\eta \tag{4.8}$$

$$K_p\dot{\eta} + K_d\ddot{\eta} + K_i\eta - U\,\mathrm{sgn}(S - \dot{\eta} + \lambda\ddot{\eta}) = 0 \tag{4.9}$$

$$S = (q_d - q\ ) + \lambda(\dot{q}_d - \dot{q}\ ) \tag{4.10}$$

To implement PBSMC into real time environment, equation (4.8), (4.9) and (4.10) must be approximated by a suitable discrete time representation. Forward Euler discretization is difficult because $\ddot{\eta}$ is computed within a precedent time step. Therefore, PBSMC is then turned into a digital controller by a discrete time representation of equations (4.8), (4.9) and (4.10) using backward difference to approximate derivatives and the value of *U* at time step *k* is calculated as:

$$S(k) = (q_d(k) - q\ (k)) + \lambda(\dot{q}_d(k) - \dot{q}\ (k)) \tag{4.11}$$

$$U^*(k) = \frac{K_pT + K_d + K_iT^2}{\lambda + T} S(k) + K_i\eta(k-1)$$
$$+ \frac{(K_p + K_iT)\lambda - K_d}{(\lambda + T)T} \Delta\eta(k-1) \tag{4.12}$$

$$U(k) = \begin{cases} U^*(k) & if \quad \left\| U^*(k) \right\| \le V \\ VU^*(k) / \left\| U^*(k) \right\| & if \quad \left\| U^*(k) \right\| > V \end{cases} \tag{4.13}$$

$$a(k) = \frac{1}{K_p T + K_d + K_i T^2} \{ (K_p T + K_d) \eta(k-1) + K_d \Delta \eta(k-1) + T^2 F(k) \} \tag{4.14}$$

Here, T is the sampling rate, V is the torque limit and Δ is the backward difference operator.

The advantage of the proxy-based sliding mode control over PID control and classical sliding mode control is the separation of dynamics that carry large positional errors which in our case is the large amount of change in the desired angle in θ or φ, from the dynamics which responds to small errors between desired and the actual output governed by virtual couplings.

PBSMC was introduced for the position control of industrial robots because conventional high gain PID position control causes some abnormal events such as unexpected environment contacts and temporal power failures. Moreover, it is not straightforward to have both accuracy during normal operation and the safety in the case of abnormal events with conventional PID because excessive actuator force can results in unexpected environment contact. Therefore, an overdampad motion is required to prevent excessive speed and overshoots. Although, sliding mode control is capable of achieving both accuracy and safety with the design of a proper sliding surfaces, the chattering phenomena occurs when sliding mode control is directly implemented as a discrete time controller. On the other hand, in [88], PBSMC has provided smooth, overdampad recovering motion after abnormal events

without sacrificing accurate, responsive tracking capability during normal operation.

In the literature, PBSMC is declared as an alternative approximation of conventional continuous-time sliding mode control (SMC), and also as an extension of PID control. Therefore, in the following section, the performance of the conventional PID control and PBSMC as applied to our system is compared for the sake of completeness.

PBSMC can be applied to gimbal stabilization problem because it provides overdampad but as fast as possible motion and it offers to adjust the behavior of the controller with respect to the magnitude of the error. Actually, there are two controllers inside of the PBSMC; sliding mode controller and PID controller; the automatic switching mechanism inside in the PBSMC provides smooth, overdampad recovering motion and the utilization of the PBSMC in stabilization problem in this thesis work is a novelty.

4.1 PBSMC: An Extension of PID Control

The behaviors of PID Controller and PBSMC under large angular velocity error are compared against desired outputs. In all results of this subsection, the gimbaled platform is excited every 0.04 seconds. Table 4.1 shows the parameters used in simulation in this subsection.

The performance of PBSMC and conventional PID controller in elevation and azimuth axes are illustrated in Figure 4.3 and Figure 4.4, respectively. Figure 4.3 also shows the response obtained by the classical sliding mode controller.

Table 4.1: Simulation conditions

Subsystem	**Conditions**		
Motor + Gimbal	*mass unbalance*	*0.006 m*	
	payload	*0.7 kg*	
	static friction	*0.0003 Nm*	
	coulomb friction	*0.0036*	
	viscous friction	*0.03 Nm/rad/s*	
	cable stiffness	*0.09 Nm/rad*	
Controller	***Azimuth axis***	***PBSMC***	***PID***
	P	*3.6*	*3.6*
	I	*0.0435*	*0.0435*
	D	*0.0290*	*0.0290*
	F	*200000*	-
	λ	*4*	-
	sample time	*0.00005 s*	*0.00005 s*
	Elevation axis	***PBSMC***	***PID***
	P	*8*	*8*
	I	*0.0435*	*0.0435*
	D	*0.0290*	*0.0290*
	F	*1000000*	-
	λ	*10*	-
	sample time	*0.00005 s*	*0.00005 s*
Rate Sensor (for each axis)	*scale factor*	*17.488 mV*	
	bias	*-0.0074 VDC*	
	bandwidth	*111 Hz (@ -90° phase shift)*	
	damping ratio	*0.66*	
	noise	*0.0029 °/s/ rt Hz*	

in the form given in equation (4.1) with *U=20* as a reference. The green signal represents the desired tracking command. Although, the settling time of classical sliding mode controller is lower than that of PID, there is an undamped oscillation in the response of the classical sliding mode controller.

If a lower gain ($U=5$) is used, the settling time increased while the oscillations amplitude decreases. Therefore, it is almost impossible to get a response like that of PBSMC by using classical sliding mode controller.

For ease of comparison, the gains used in the PBSMC are taken as the same as of those in the PID controller. The simulation results given separately Figure 4.3 and Figure 4.4, indicate in both axes that PID controller has a much larger rise time that creates accumulation error in shorter pulse durations. On the other hand, PBSMC gives more accurate response than PID controller. In addition, the most important property of PBSMC is that a smooth response close to critically damped is observed rather than highly overdamped PID responses. PID controller exhibits larger delay in azimuth axis than in elevation, while PBSMC perform swiftly with very low rise time in both axes.

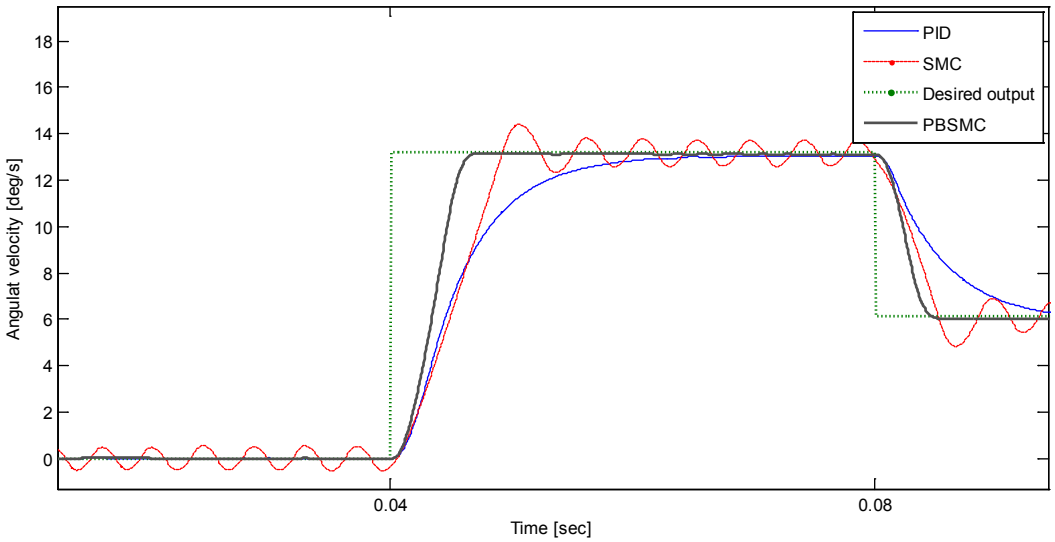

Figure 4.3 : Closed loop performance of PBSMC and PID, elevation axis

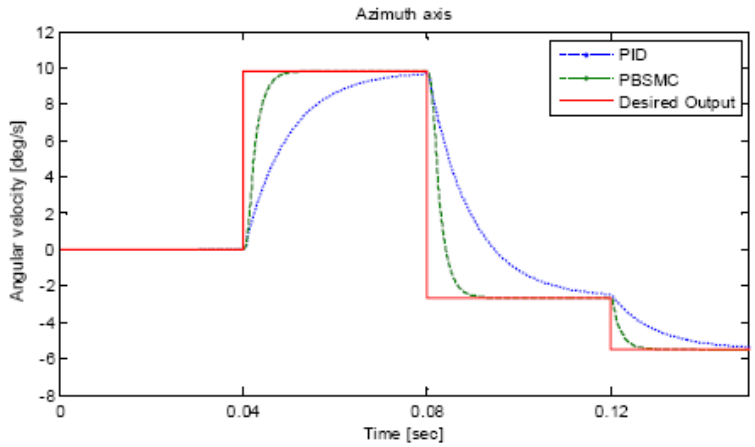

Figure 4.4 : Closed loop performance of the PBSMC and PID, azimuth axis

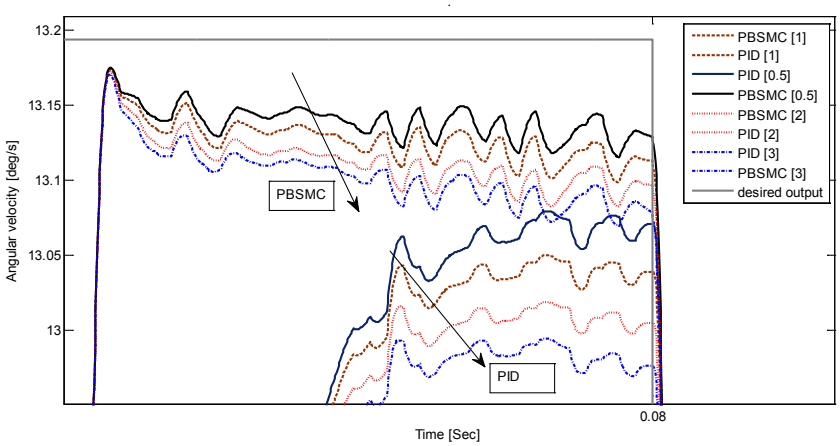

Figure 4.5 : Effect of the change in the stiffness to controller responses, elevation axis

In addition, the comparison in performance between PID and PBSMC stabilization controllers is shown while the inertia of the payload (Figure 4.7 and Figure 4.8), viscous friction on bearings (Figure 4.6), and the cable stiffness (Figure 4.5) on the gimbaled platform change. In these figures, the number in the brackets in the legend represents for the relevant changing

parameter, the multiplier of its original value given in Table 4.1. Although, increasing the stiffness and the viscous friction deteriorate the performance of both controllers, PBSMC can tolerate these changes at higher levels of angular velocities and the degradation of velocity amplitudes are much less than those for PID since PID controller accumulates larger errors owing to large delays in large values of rise time.

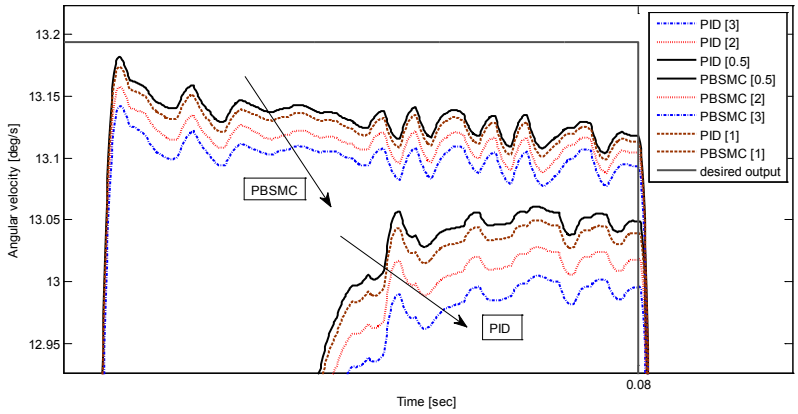

Figure 4.6 : Effect of the change in the viscous friction

Comparing changes in from Figure 4.5 to Figure 4.8, it is concluded that highest sensitivity is to the change in the inertia of the payload in the elevation axis (Figure 4.7). Changing the inertia of the payload does not affect much the accuracy of the PBSMC while large deterioration in the steady state settling time of the PID exists. Increasing the inertia further than a level [here level A shown by an arrow in Figure 4.8] results in an overshoot in the response of PBSMC. Since increasing the inertia represents a decrease in the damping ratio in linearized system, gimbaled system becomes an underdamped system resulting in overshoot in the responses of PBSMC.

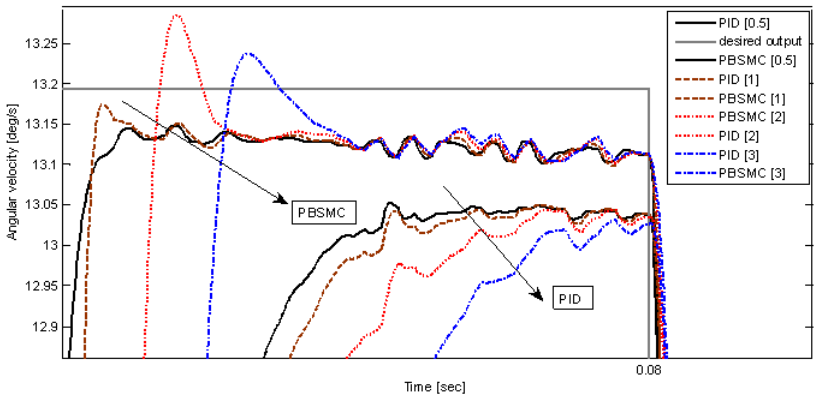

Figure 4.7 : Effect of the change in the inertia of the payload to controller responses

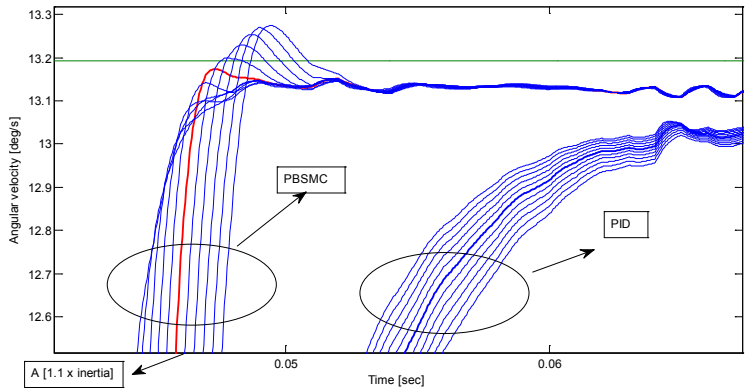

Figure 4.8 : Effect of the change in the inertia of the payload to controller responses

In general, an increase in inertia, when inertia becomes greater than 0.0022 kg-m^2 in our example, leads to deterioration in transient stability which is mainly governed by the damping factor. Therefore, it is important to investigate the change in the inertia while the gimbal is moving. The moment of the inertia of the payload and inner gimbal are known along rotation axes prior to assembly and the moment of inertia of the inner gimbal with payload can be calculated with the following formulas [91]:

$$k_1 = \frac{(I_x - I_z)}{2} \tag{4.15}$$

$$k_2 = \frac{(I_x + I_z)}{2} \tag{4.16}$$

$$I_x = k_2 + k_1 \cos(2\theta) + I_{xz} \sin(2\theta) \tag{4.17}$$

$$I_z = k_2 - k_1 \cos(2\theta) - I_{xz} \sin(2\theta) \tag{4.18}$$

$$I_y = I_y \tag{4.19}$$

However, the inertia of the inner gimbal with payload is measured inside CAD model. Original inertia of the inner gimbal with payload and inertia of the inner gimbal with payload after 20 degree rotation in elevation axis are illustrated in Table 4.2.

Table 4.2: Change of inertia of the inner gimbal with payload

Original inertia		
I_{xx}=0.00146633	I_{xy}=-0.00000591	I_{xz}=0.00007367
I_{yx}=-0.00000591	I_{yy}=0.00177605	I_{yz}=-0.00002099
I_{zx}=0.00007367	I_{zy}=-0.00002099	I_{zz}=0.00079820
Inertia after rotation (20 deg)		
I_{xx} = 0.00144687	I_{xy} = 0.00002921	I_{xz} = 0.00006254
I_{yx} = 0.00002921	I_{yy} = 0.00166062	I_{yz} = 0.00028685
I_{zx} = 0.00006254	I_{zy} = 0.00028685	I_{zz} = 0.00089213

According to Table 4.2, 10% increase in the inertia is not possible in principle axes, therefore, overshoots in the response of PBSMC will not be observed. However, a delay due to higher rise time is seen in both controllers if the inertia of the payload is increased. Furthermore, Figure 4.9 shows the control command to the gimbaled platform generated by PID and PBSMC. PBSMC incorporates an optimization based on the proxy coupling and does not generate high-frequency chattering. PID control, on the other hand, cannot generate any optimization without sacrificing its performance.

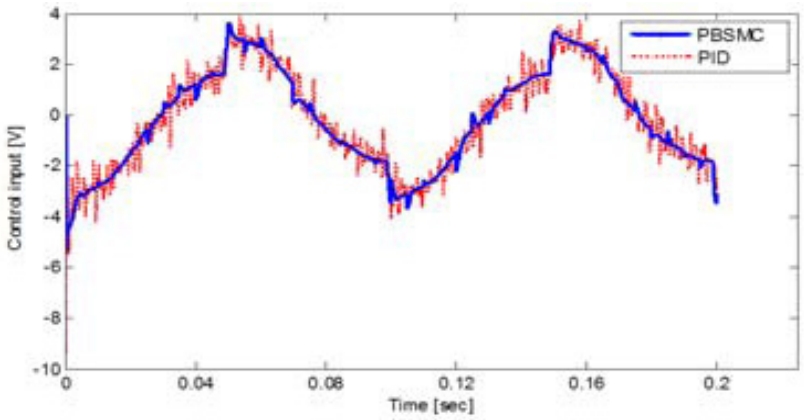

Figure 4.9 : Control commanded to plant, generated by PBSMC and PID

As a result of simulation run with equal gains for PID and PBSMC, it is decided to compare PBSMC with perfectly tuned PID. Figure 4.10 and Figure 4.11 show the set point tracking performance and disturbance rejection capability of both controllers: PBSMC and tuned PID, respectively.

Although, the rise time and steady state accuracy of the PID controller has been greatly improved, PBSMC is still found to be superior to tuned PID in both tracking performance and disturbance rejection capability. This is why

the PBSMC has been permanently adopted for stabilization in experimental setup.

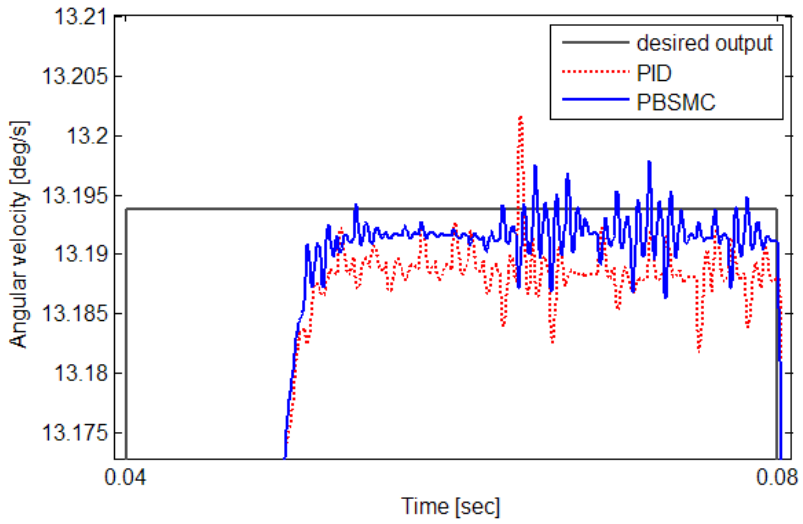

Figure 4.10 : Simulation result of the performance of PBSMC and PID with K=200 I=2 D=0.2 F=500000 and λ=2, elevation axis.

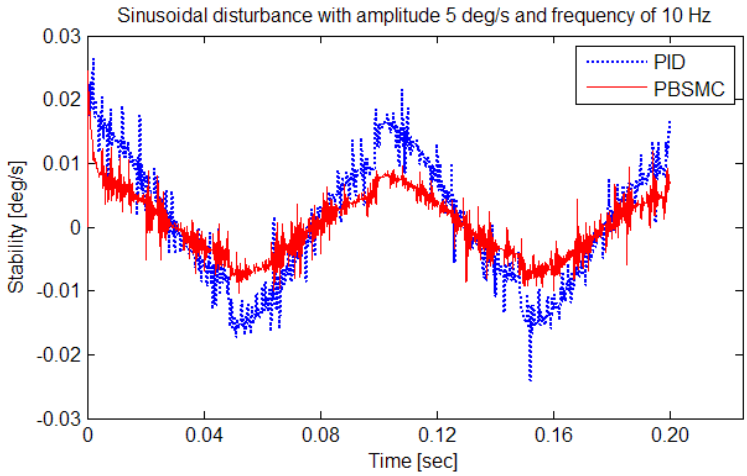

Figure 4.11 : Simulation results (disturbance rejection) of PBSMC and PID with K=200 I=2 D=0.2 F=500000 and λ=2, elevation axis.

4.2 Simulation Results of Disturbance Rejection Capability of PBSMC

In the previous subsection, the gains used in the simulation are for the comparison purpose only. After the tuning of the controller using the simulation model, the following gains are obtained. Table 4.3 shows the controller parameters used in simulation in accordance with our hardware, so that, unless otherwise noted, the gains values listed here are used in both simulations and in hardware experiments.

To measure the stabilization accuracy, the base of the platform is excited with four different sinusoidal disturbance profiles. Table 4.4 gives the set of sinusoidal disturbances that are going to be applied to the base of gimbaled platform.

It is very important that these disturbance profiles should act on the center of the rotation of the corresponding axes not to have translational acceleration which is not modeled. Therefore, in simulations, it is assumed that the yaw disturbances act around rotation of azimuth axis whereas pitch disturbances affect around rotation of elevation axis.

In simulation model, the 6 DOF motion simulator or hexapod is not modeled and these disturbance are feed as a measurement error to the MEMS rate sensor output. This approach will not give an incorrect stabilization accuracy result because the amplitude of the excited motion decreases through the azimuth and elevation axis joints.

Table 4.3 : Controller parameters used in simulations and experiments

Controller	***Azimuth axis***	***PBSMC***
	P	*800*
	I	*10*
	D	*0.15*
	F	*100000*
	λ	*0.15*
	sample time	*0.0001 s*
	Elevation axis	***PBSMC***
	P	***200***
	I	*2*
	D	***0.2***
	F	*100000*
	λ	*2*
	sample time	*0.0001 s*

Table 4.4 : Sinusoidal disturbance profiles applied to the base of the gimbal platform in simulations

Frequency	Amplitude (peak to peak)
1 Hz	8°
2 Hz	4°
5 Hz	2°
10 Hz	1°

According to test result obtained from four different disturbance profiles, the following table can be formed. Table 4.5 shows the standard deviation stabilization errors achieved elevation and azimuth axis under different disturbances profiles.

Table 4.5 : Stabilization accuracy values obtained with simulations

Disturbance Profile (sin wave)	Stabilization accuracy	
	Azimuth axis (μrad)	Elevation axis (μrad)
1 Hz - 8° (peak to peak)	17	29
2 Hz - 4° (peak to peak)	20	33
5 Hz - 2° (peak to peak)	24	41
10 Hz - 1° (peak to peak)	32	49

CHAPTER 5

EXPERIMENTAL STUDY

This chapter explains the mechanical setup, its sensors and actuators used in the experimental implementation of the approach developed together with its electronics and processors used in the control and data acquisition. Properties of the Stewart platform where the gimbaled system mounted upon used in the tests to simulate the disturbance profiles are also given. Figure 5.1 shows the schematic representation of the whole hardware experimental setup illustrated in Figure 5.2 which is mainly composed of four parts: the plant representing our two axis gimbaled platform of Figure 5.3, the controller, the rate sensor filtering and Stewart Platform represented in Figure 5.4 and Figure 5.10.

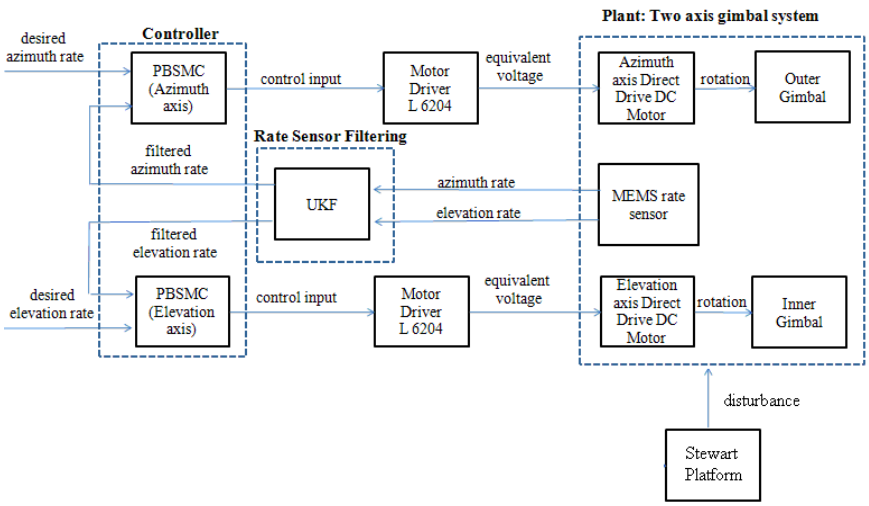

Figure 5.1 : Schematic representation of the hardware experimental setup

5.1 Experimental Setup

To assess the proposed control scheme in real time environment, an experimental setup is constructed in the Control System Laboratory of Tactical Missile Systems Division in ROKETSAN. This experimental setup consists of a designed two axis gimbal system with mechanical interface for connection actuators and sensors, motor drivers, data acquisition electronics, control and monitoring computer and cable connections. Stewart platform or hexapod is a part of this experimental setup to apply the disturbance profiles to the base of the gimbal platform. The properties of these elements are explained in detail in the following subsections.

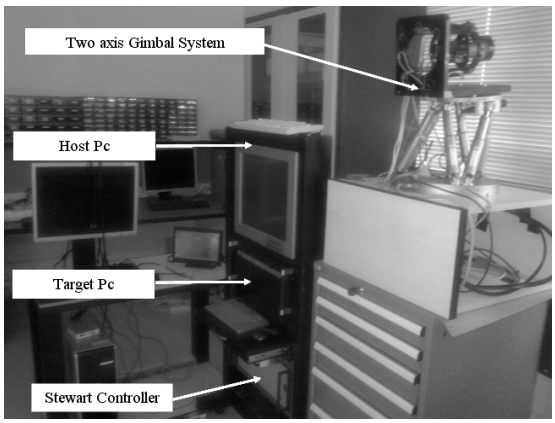

Figure 5.2 : Experimental hardware

5.1.1 Two-Axis Gimbal Mechanics

The two axis gimbal is designed is shown in Figure 5.3. This gimbal is a two-degrees of freedom system which is driven with limited angle brushless direct drive motors where each of their shafts is equipped with a 17-bit absolute encoder for measuring angular displacement. In addition, this setup has a two

axis MEMS rate sensor mounted on the inner gimbal to sense the disturbance about the LOS. The position and the velocity of gimbals are measured with incremental encoders and two axis MEMS rate sensor, respectively.

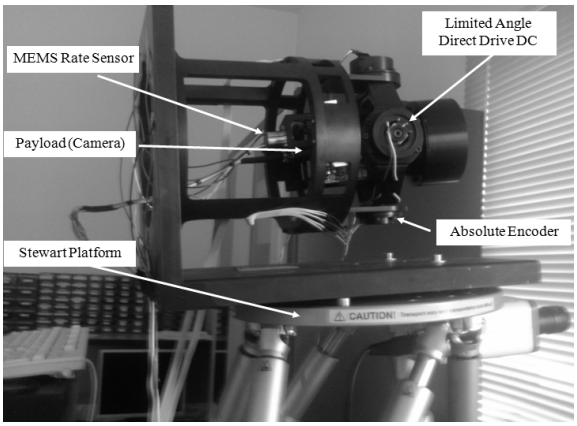

Figure 5.3 : Two axis gimbal system

5.1.2 Actuators

A limited angle brushless direct drive DC torque motors is used in both axes since a limited angle of rotation is requested. With the use of such motors, the needs for gearboxes or spindle drives are removed. In addition, backlash is eliminated. In both axes of the gimbal system, Kollmorgen LA-802-A type motor with a peak motor current 2.36A and peak motor torque 0.1 Nm is used. It has an excursion angle of 35 degrees and theorical operation curve is shown in Figure 5.5.

5.1.3 Motor Drivers

Dual Full Bridge Driver which was developed by ROKETSAN for a semi-active laser guided missile project is used as motor driver. This motor driver is

very low profile and can supply a peak current 5Amps at a DC voltage as high as 32 Volts at each channel, which is adequate for both motors of the gimbal.

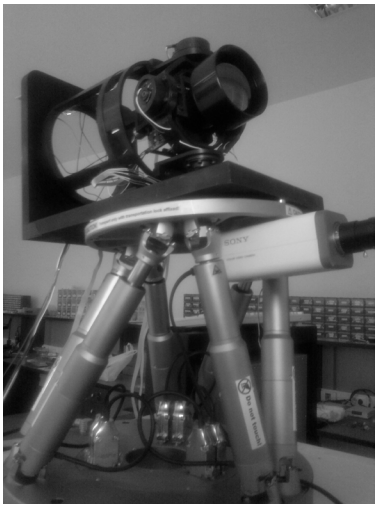

Figure 5.4 : Stewart platform and gimbal system

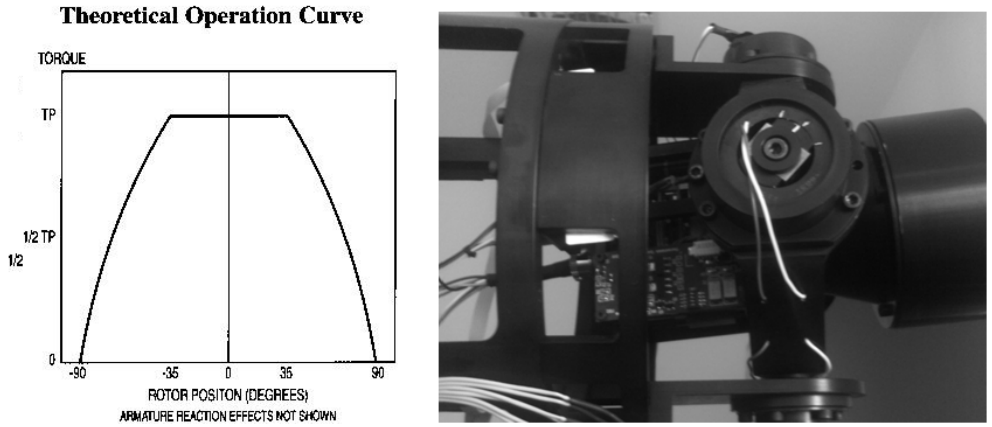

Figure 5.5 : Limited angle direct drive and theoretical operation curve [93]

5.1.4 Absolute Encoders

To measure the angular position on the gimbal rings, Netzer DS 25-16 high resolution absolute encoders are used in both axes (Figure 5.6). This absolute

encoder can count 131072 steps in a single revolution. In addition, this encoder offers several advantages:

- Low profile (7 mm)
- Hollow, floating, shaft
- No bearings or other contacting elements
- High precision
- High tolerance to temperature, shock, moisture, EMI, RFI and magnetic fields

These angular position signals make it possible to control the gimbal with high precision in many applications. However, in our gimbal stabilization problem, this high resolution sensor is not used for stabilization because stabilization requires controlling the angular rate relative to inertial frame.

Figure 5.6 : Netzer DS 25-16 17 bit absolute encoder 0

5.1.5 Rate Sensor

Tactical grade two axis MEMS rate sensor, QRS28 is used. QRS28, depicted in Figure 5.7 is a small, lightweight, two-axis MEMS rate sensor offering exceptional performance at a very attractive price. The sensor provides a simple DC-DC operation using two of Systron Donner Inertial's quartz rate

sensors. It is especially suited for demanding applications, which require reliable performance, such as missile seeker gimbal stabilization, where small size and low power consumption is required, while in a low cost design that is also ideally suited for high volume commercial applications. However, output of the rate sensor is degraded rapidly while being carried over a wire and QRS28 has significant bias and random error values due to the limitation of the manufacturing technology, therefore, an appropriate filtering algorithm is used order to reduce the effect of uncertainty in the sensor state.

Figure 5.7 : QDARS two axis MEMS rate sensor [94]

5.1.6 DAQ Hardware: Digital/Analog I/O Card

National Instruments' PCI 6289 DAQ (Figure 5.8) is used for the rate sensor and absolute angle measurement. This card is multifunction data acquisition card with 16 differential or 32 single-ended analog inputs (18 bit). In addition, it has 4 analog outputs (16 bit), 48 digital outputs and two 32-bit, 80 MHz counters. In our gimbal stabilization application, 4 differential and 2 single ended analog inputs and 2 digital outputs are used.

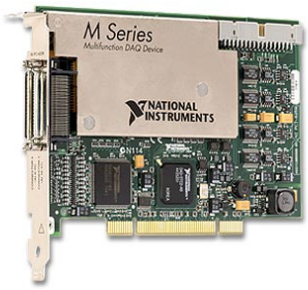

Figure 5.8 : PCI 6289 DAQ card [96]

5.1.7 DAQ Hardware: Counter Timer

To produce the PWM signal to control the gimbaled platform, National Instruments' PCI-6602 Counter/Timer card is used (Figure 5.9). This card has 8 up/down, 32-bit counter/timers with 80 MHz maximum source frequency. In addition, it is capable of performing three simultaneous high-speed DMA transfers. . In our gimbal stabilization application, 2 up/down counter/timers, one for elevation axis and one for azimuth axis, are used.

Figure 5.9 : NI PCI 6602 Counter/Timer Card [96]

5.1.8 Real Time Control and Monitoring Hardware and Software

A PC with E2160 dual core 1.8 Ghz processor and 2 GB RAM, running under Microsoft Windows XP operation system for host PC and a PC with E8400

dual core 3 Ghz processor and 2 GB RAM, running under Microsoft Windows XP operation system for target PC are used.

Matlab/Simulink version 2009A with XPc Target Toolbox is used for real time controller development and tuning. The controller is implemented in Simulink environment.
Each axis is controlled using the control law of equation (4.12), (4.13), (4.14) and tested separately. Proxy based sliding mode controller runs on target PC in real-time with sampling rates of 10 kHz. Direct access to the controller model for parameter changing and signal monitoring is possible in this environment with the host PC. This capability enables rapid development and tuning of different controllers in a relatively short amount of time.

5.1.9 Stewart Platform

Since the stabilization controller is designed for steady guidance of missile to be launched from the platform, the base of the gimbaled platform must be actuated in both axes to induce the required disturbance at the base of the gimbaled platform in a way similar to real life flight applications. For this purpose, a hexapod is used. This hexapod which can also be seen in Figure 5.10, emulates any motion of a platform within its position, speed and acceleration limits.

The M-840.5PD Hexapod, with direct-drive actuators, can move loads of up to 10 kg in horizontal and up to 3 kg in random orientation at up to 50 mm/s and 600 mrad/s with micron accuracy.

The desired motion is created by six linear direct drive actuators which are all connected to a real time motion control computer which calculates the

required motion of the individual actuators with sophisticated controller using vector algorithms. Therefore, the operator of the hexapod only defined the motion profile to be created.

In addition, this hexapod has an open controller architecture. Control of the hexapod is facilitated by the controller's open interface architecture, which provides a variety of high-level commands and includes a macro language for programming and storing command sequences.

Figure 5.10 : Physik Instrumente (PI) M-840.5PD hexapod [97]

5.2 Experimental Procedure

Our proposed method is introduced and tested in simulations in Chapter 4 is also experimentally tested on our two axis gimbaled hardware system illustrated in Figure 5.1. The purpose of the experimental setup is to measure the stabilization performance of the proposed controller architecture with

varying disturbance levels on an actual setup for ROKETSAN company needs. The disturbance level mentioned here is the amplitude and the frequency of the motion applied to the base of the gimbaled platform. With this setup, the level of the disturbance rejection can be measured by looking at the angular deviation from the intended angular position or velocity. In the disturbance rejection test, the desired angular position of the gimbal is selected to be zero.

Four different disturbance profiles are applied to the base of the gimbal which is rigidly fixed onto the Stewart Platform. Although, applying the disturbance to the both axis at the same time is possible, each axis is tested separately to obtain more reliable and accurate results. However, it is important to intersect the center of the rotation of the azimuth and elevation gimbals and center of the rotation of the disturbance motion. In our experimental setup, the base platform of the gimbal is mounted onto the top of the Stewart Platform so that the axis of the rotation of the Stewart Platform is as close to the axis of the rotation of the corresponding gimbals to reduce the induced translational motion. Translational motion especially the acceleration results in unbalance moment on the azimuth and elevation gimbal. Although some precautions are taken, it is not possible to eliminate such translation motion because it is very difficult to mount the two axis gimbal system on the Stewart Platform.

Since our experimental setup has a MEMS rate sensor with significant bias error, there is a bias removal process before the experiment is started. During 5 seconds without the power the actuators and the absolute encoder, the output is MEMS rate sensor is collected. The mean of the output is defined as a gyro bias which is different for each axis. In our experiments, data collecting time is not selected too much because large time values for the gyro bias removal process induces time correlated noise which moves us beyond the

aforementioned assumption we carried out in this thesis work. In addition, the mechanical parts are checked for loose connections and cabling to avoid any interaction to moving parts. At last, power supplies and the connectors are confirmed to have a consistent experimental setup.

Before the experiment, the azimuth and elevation gimbal is brought to its zero angular position and rate sensor outputs are monitored as previously explained before. After 5 seconds required for the bias removal process, the azimuth and elevation gimbal are stabilized. Then, Stewart Platform comes into play at 10 seconds by applying the disturbance of the gimbal base. While being stabilized in spite of the base disturbance, angular velocity readings are logged for 10 seconds.

After the experiment is conducted, the logged data are analyzed and the stabilization performance indexes are calculated. Whole of the angular rate outputs gives the deviation of the gimbal from the desired position while exposed to the base disturbances. The standard deviation of calculated data over time reflects stabilization performance. Although, perfect stabilization is not possible because of the rate sensor noise, unbalance, control electronics and manufacturing; this value is a measure of how good the platform is being stabilized, where the smaller the error the better is the stabilization performance.

The proposed controller is tested for each axis separately under four different sinusoidal disturbance profile frequency covering a frequency range starting form 1 Hz and ending at 10 Hz. The amplitute range of the disturbance profile starts from 1 deg to 10 deg. The amplitude and the frequency of the disturbance profile for each axis is tabulated in Table 5.1

Table 5.1 : Four different sinusoidal disturbance profiles

Frequency	Amplitude (peak to peak)
1 Hz	8°
2 Hz	4°
5 Hz	2°
10 Hz	1°

In the following section, the results of these 8 experiments will be presented and discussed.

5.3 Experimental Results

5.3.1 Elevation Axis

Our proposed controller is tested in the elevation axis under 4 different disturbance profiles. Friction moments caused by the relative motion of the base of the platform and the elevation gimbal, cable connections and unbalance of the payload are the main disturbance sources to be rejected.

The acting point of the disturbance to the base of the gimbaled platform is important to have a reliable stabilization performance measure. To be clear, pitch axis disturbances should operate around the center of the rotation of the elevation axis while the yaw disturbances should act the center of the rotation of azimuth axis to have a translational motion free operation because the rate sensor cannot measure such motions.

Although, the base platform of the gimbal is located onto the top of the Stewart platform so that center of rotation of the platform motion and gimbal axes center of rotation coincide with the center of rotation of gimbal axes, there is, in general, quite a big distance between the center of the top of the hexapod and the center of the rotation of the elevation axis. This distance leads to translational accelerations which cause dynamic unbalance torques acting on elevation axis since the COG of this axis is located above the center of rotation.

The proxy based sliding mode controller offers quite impressive stabilization accuracies although the experimental setup has not a superior mechanical assembly, cable connection, high quality sensors and actuators.

The stabilization plots and results given in this subsection indicate that the sudden change of the direction of the disturbance causes an instantaneous big angular position error against which the controller must react. However, the controller cannot decrease the error to zero until a new request comes. Therefore, the controller can reject only some portion of the given disturbance profile with high frequency.

Case 1: A sinusoidal angular position disturbance with amplitude of 8 deg and a frequency of 1 Hz is applied while the desired angular velocity of the elevation axis is zero. To measure the stabilization performance, the standard deviation of the integral of the controller errors is calculated as 50 μrad. Figure 5.11 shows a 3-second measured angular velocity. The given disturbance results in sinusoidal angular velocity disturbance with amplitude of 50 deg/s and amplitude of the measured velocity is around 0.02 deg/s.

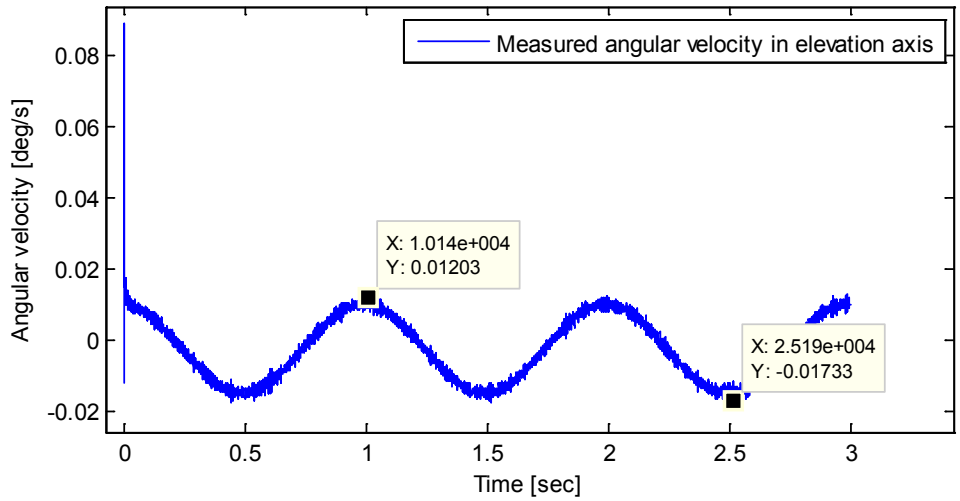

Figure 5.11 : Measured angular velocity, disturbance amplitude of 8 deg and a frequency of 1 Hz, elevation axis

Case 2: A sinusoidal angular position disturbance with amplitude of 4 deg and a frequency of 2 Hz is applied while the desired angular velocity of the elevation axis is zero. To measure the stabilization performance, the standard deviation of the integral of the controller errors is calculated as 43 µrad. Figure 5.12 shows a 3-second measured angular velocity. The given disturbance also results in sinusoidal angular velocity disturbance with amplitude of 50 deg/s; however, amplitude of the measured velocity is almost the same as with the Case 1.

Case 3: A sinusoidal angular position disturbance with amplitude of 2 deg and a frequency of 5 Hz is applied while the desired angular velocity of the elevation axis is zero. To measure the stabilization performance, the standard deviation of the integral of the controller errors is calculated as 65 µrad. Figure 5.13 shows a 3-second measured angular velocity. The given disturbance, in this case, results in sinusoidal angular velocity disturbance with amplitude of 60 deg/s and amplitude of the measured velocity is 0.05 deg/s

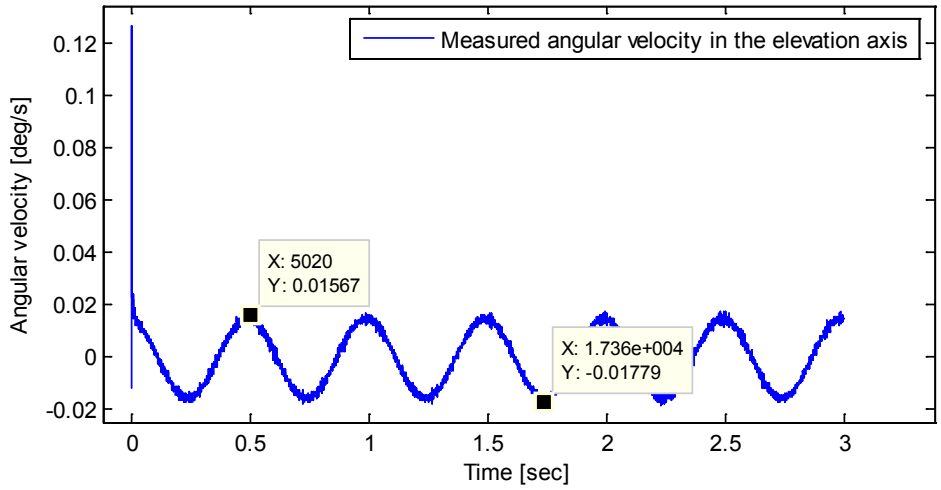

Figure 5.12 : Measured angular velocity, disturbance amplitude of 4 deg and a frequency of 2 Hz, elevation axis

Case 4: A sinusoidal angular position disturbance with amplitude of 1 deg and a frequency of 10 Hz is applied while the desired angular velocity of the elevation axis is zero. To measure the stabilization performance, the standard deviation of the integral of the controller errors is calculated as 74 μrad. Figure 5.14 shows a 3-second measured angular velocity. The given disturbance, in this case, results in sinusoidal angular velocity disturbance with amplitude of 60 deg/s and amplitude of the measured velocity is 0.1 deg/s.

5.3.2 Azimuth Axis

The proposed controller is also tested in the azimuth axis under 4 different disturbance profiles. In this axis, the friction moments caused by the relative motion of the base and the azimuth gimbal and cable connections are the main disturbance source to be rejected.

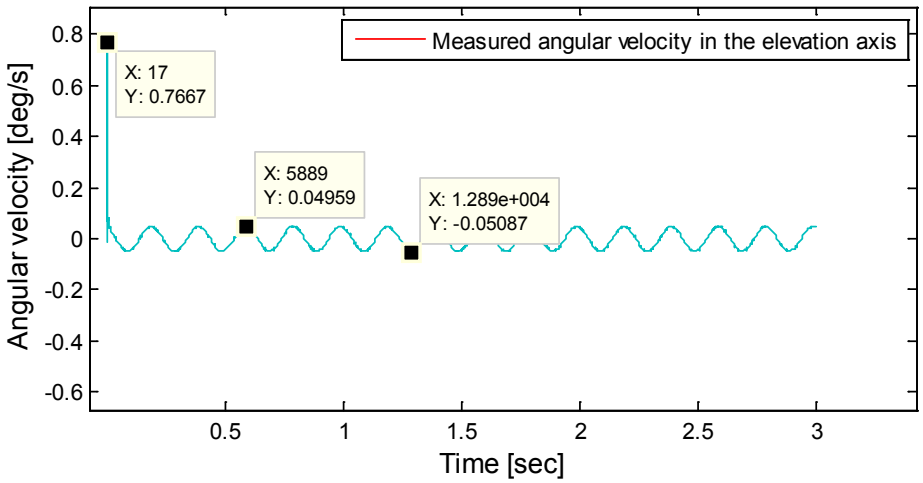

Figure 5.13 : Measured angular velocity, disturbance amplitude of 2 deg and a frequency of 5 Hz, elevation axis

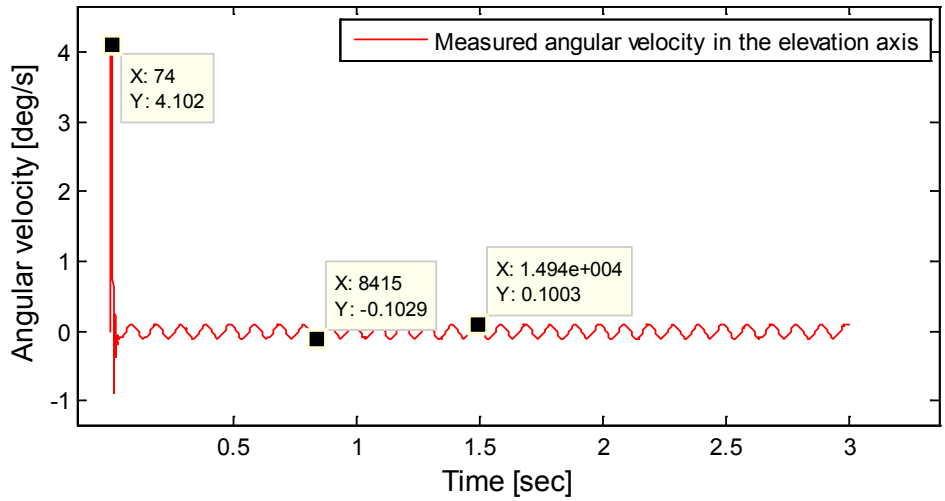

Figure 5.14 : Measured angular velocity, disturbance amplitude of 1 deg and a frequency of 10 Hz, elevation axis

Although, there exists translational motion in elevation axis due to the distance between the center of the top of the hexapod and the center of the rotation of the elevation axis, this distance quite small for the azimuth axis. Therefore, the level of the dynamic unbalance torques acting on azimuth axis is small. However, using the same type actuator in azimuth and elevation, the azimuth controller can respond slowly with respect to the elevation controller because azimuth actuator is responsible to rotate outer gimbal and the inner gimbal also. Therefore, it is expected that the performance of the azimuth controller is inferior to the elevation controller. However, there is a passive stabilization technique by using high inherent inertia, which helps to the system to be less susceptible to the exposed disturbances.

Case 1: A sinusoidal angular position disturbance with amplitude of 8 deg and a frequency of 1 Hz is applied while the desired angular velocity of the elevation axis is zero. To measure the stabilization performance, the standard deviation of the integral of the controller errors is calculated as 24 μrad. Figure 5.15 shows a 3-second measured angular velocity. The given disturbance results in sinusoidal angular velocity disturbance with amplitude of 50 deg/s and amplitude of the measured velocity is around 0.02 deg/s.

Case 2: A sinusoidal angular position disturbance with amplitude of 4 deg and a frequency of 2 Hz is applied while the desired angular velocity of the elevation axis is zero. To measure the stabilization performance, the standard deviation of the integral of the controller errors is calculated as 26 μrad. Figure 5.16 shows a 3-second measured angular velocity. The given disturbance results in sinusoidal angular velocity disturbance with amplitude of 50 deg/s and amplitude of the measured velocity is around 0.03 deg/s.

Case 3: A sinusoidal angular position disturbance with amplitude of 2 deg and a frequency of 5 Hz is applied while the desired angular velocity of the elevation axis is zero. To measure the stabilization performance, the standard deviation of the integral of the controller errors are calculated as 30 μrad . Figure 5.17 shows a 3-second measured angular velocity. The given disturbance results in sinusoidal angular velocity disturbance with amplitude of 60 deg/s and amplitude of the measured velocity is 0.08 deg/s.

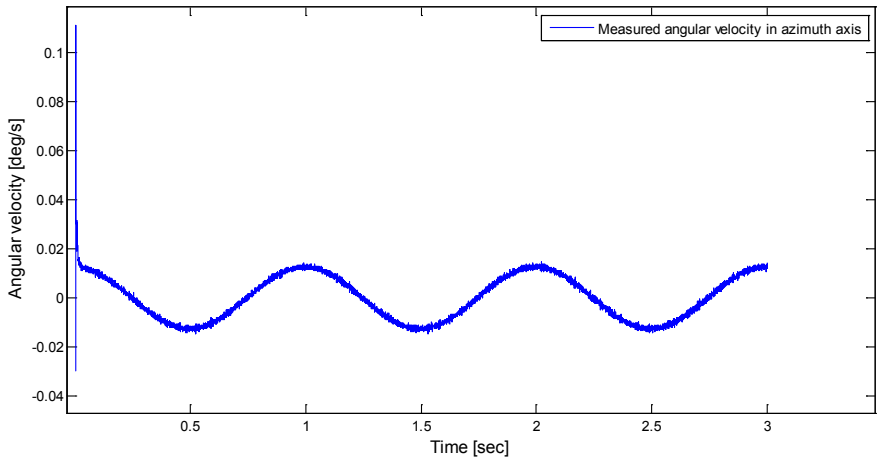

Figure 5.15 : Measured angular velocity, disturbance amplitude of 8 deg and a frequency of 1 Hz, azimuth axis

Case 4: A sinusoidal angular position disturbance with amplitude of 1 deg and a frequency of 10 Hz is applied while the desired angular velocity of the elevation axis is zero. To measure the stabilization performance, the standard deviation of the integral of the controller errors is calculated as 39 μrad. Figure 5.18 shows a 3-second measured angular velocity. The given disturbance results in sinusoidal angular velocity disturbance with amplitude of 60 deg/s and amplitude of the measured velocity is 0.18 deg/s.

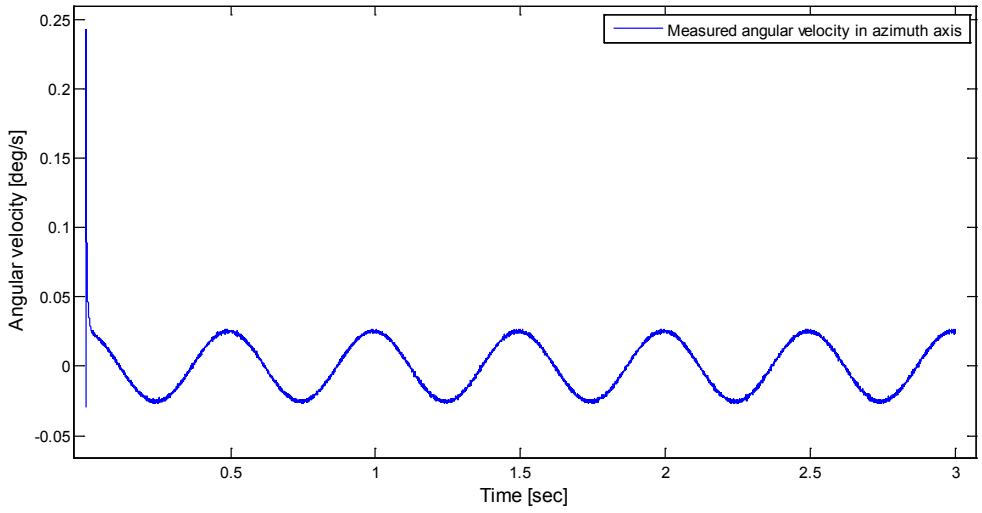

Figure 5.16 : Measured angular velocity, disturbance amplitude of 4 deg and a frequency of 2 Hz, azimuth axis

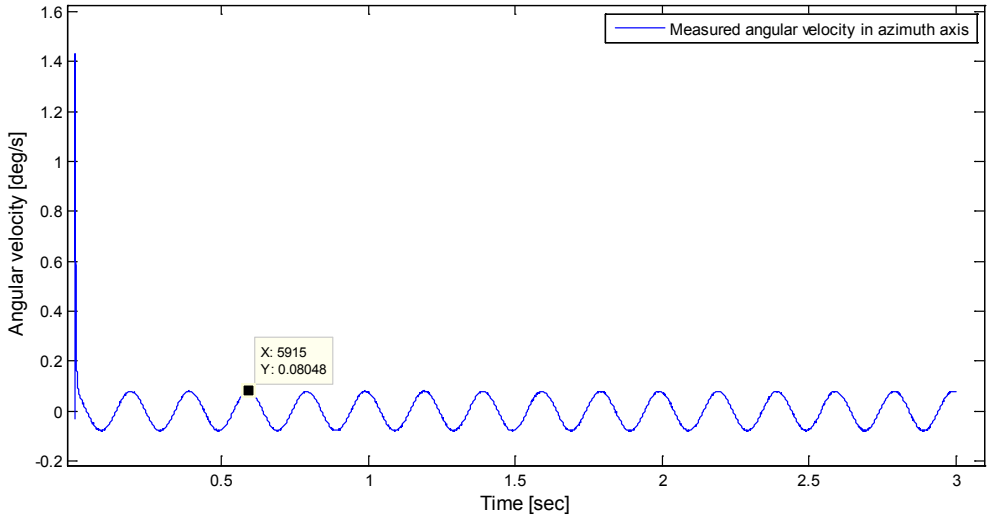

Figure 5.17 : Measured angular velocity, disturbance amplitude of 2 deg and a frequency of 5 Hz, azimuth axis

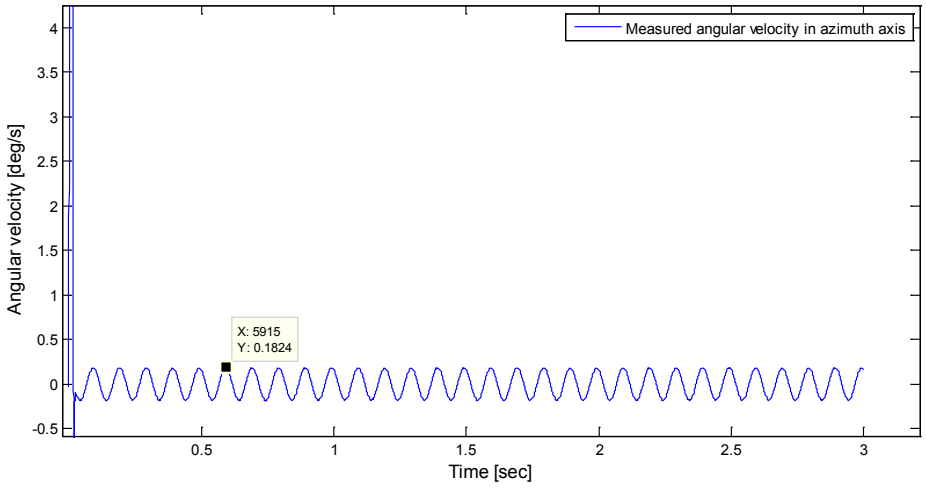

Figure 5.18 : Measured angular velocity, disturbance amplitude of 1 deg and a frequency of 10 Hz, azimuth axis

5.4 Comparative Discussions and General Conclusive Remarks

According to test result obtained from four different disturbance profiles, the following table can be formed. Table 5.2 shows the standard deviation stabilization errors achieved elevation and azimuth axis under different disturbances profiles.

Experimental results show that the standard deviation stabilization errors in azimuth axis are smaller than those of elevation axis. This case is valid for all frequency range. In addition, there are instantaneous high angular velocity measurements in both axes. Although, before the experiment, the Stewart platforms is tried to bring out its zero position, there exists some deviation from the initial position because the weight of the gimbaled platform. When Stewart Platform comes into play, it goes to its zero or initial position and it begins to apply disturbance to the gimbaled platform. This initialization

process induces an instantaneous angular acceleration therefore there exists some high velocity measurements. If this portion is omitted, the stabilization accuracy values improve in both axes. Moreover, the assumption that center of the rotation of payload and hexapod are coincident is not valid and the unmeasured linear acceleration can results in more stabilization errors in elevation axis with respect to azimuth axis.

In general, the measurements in both axes are similar but the stabilization accuracies are different. For instance, when Figure 5.11 and Figure 5.15 are compared, the amplitude and the frequency of the measured angular velocities seem to be same. However, the stabilization accuracy values are totally different. This is due to the existing bias around zero angular velocity in Figure 5.11 and such deviation from the zero changes heavily the stabilization accuracy behavior.

Table 5.2: Summary of experimental result

Disturbance Profile (sin wave)	Stabilization accuracy	
	Azimuth axis (μrad)	Elevation axis (μrad)
1 Hz - 8° (peak to peak)	24	50
2 Hz - 4° (peak to peak)	26	43
5 Hz - 2° (peak to peak)	30	65
10 Hz - 1° (peak to peak)	39	74

It is clear that the inertia of the azimuth axis is larger than inertia of the elevation axis. This high inherent inertia results in a passive stabilization because of the low friction to inertia ratio.

There is a similar result in low frequency disturbance for both axes. The reason of such behavior can be the stiction on the joints. In these frequencies, the resuming smooth motion is requested which leads to lower stabilization errors.

CHAPTER 6

SENSITIVITY ANALYSIS

In this section, the sensitivity of the proposed control architecture to sensor noises, viscous friction, eccentricity and changing inertia will be examined. Then, the performance of the proposed controller architecture will be explored using the mathematical model of the gimbaled system. The critical parameters of the system, which can be changed in practice, namely the Columb friction, disturbance characteristics and inertia, are made to vary slightly during simulations and the performance of the controller is analyzed using the results of these simulations.

6.1 Sensitivity Analysis of the PBSMC for Sensor Noise

In computer simulations performed in previous chapters, the effect of the sensor noise is included. However, sensor manufacturers usually specify a measurement noise bound other than giving an exact value for the sensor noise. Although, the test data conducted in the manufacturer's site provides a value to determine noise characteristics, this value only helps us to guess the degree of the sensor noise because the test conditions and equipments in the manufacturer's site are not identical with the environment that the sensor will be located.

In this analysis, the sensor noise will be increased from zero to the upper bound given for the MEMS rate sensor mounted on the inner gimbal with

steps of 0.001 deg/s/√Hz . The measurement noise of the MEMS rate sensor used in the experimental setup is maximum 0.005 deg/s/√Hz in the frequency interval from 1 Hz to 100 Hz.

In reference [79], the RMS accelerometer noises are approximated as,

$$Rms\_noise = Noise\_density * \sqrt{Bandwidth * 1.6} \quad (6.1)$$

Using same approach, sensor noise is increased from zero to upper bound indicated in the datasheet which is tabulated in Table 6.1 , the resulting tracking response is illustrated throughout Figure 6.1 and Figure 6.4.

Table 6.1 : MEMS rate sensor noises used in simulation

	Measurement noise (deg/s/√Hz)	Rms noise acc. to [79]	White noise power used in simulation
Case 1	0	0	0
Case 2	0,001	0,013266499	1,76E-08
Case 3	0,002	0,026532998	7,04E-08
Case 4	0,003	0,039799497	1,584E-07
Case 5	0,004	0,053065997	2,816E-07
Case 6	0,005	0,066332496	0,00000044

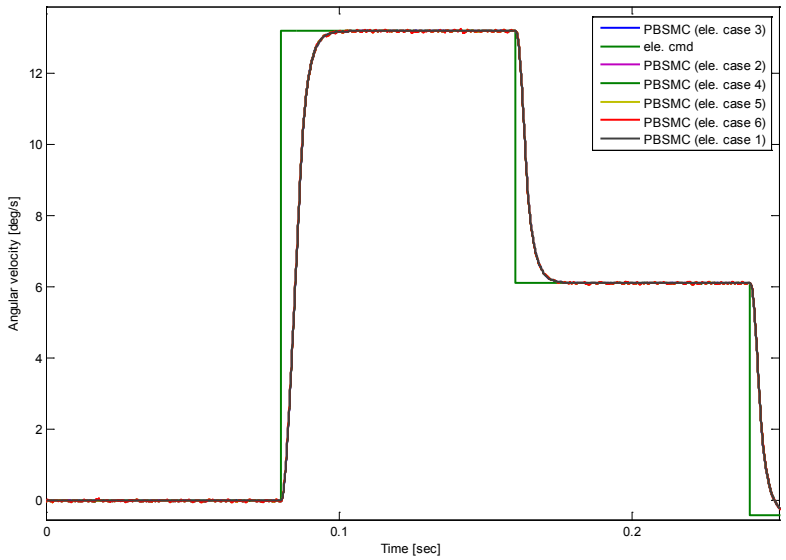

Figure 6.1 : Set point tracking result with varying rate sensor noise, elevation axis

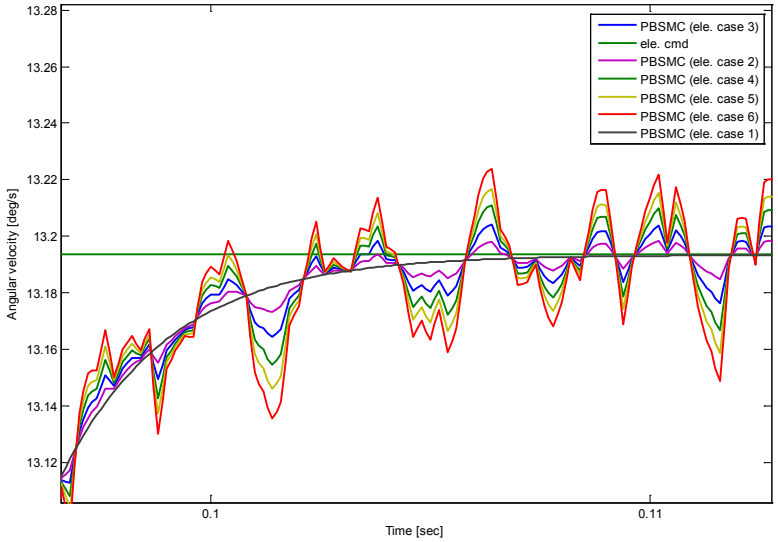

Figure 6.2 : Set point tracking result with varying rate sensor noise, elevation axis

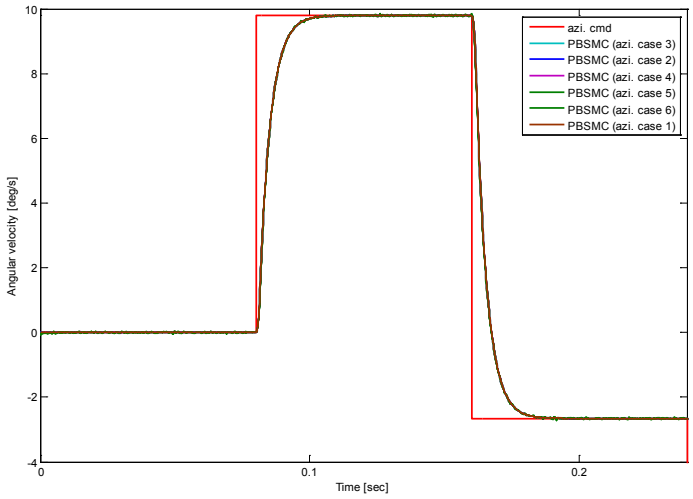

Figure 6.3 : Set point tracking result with varying rate sensor noise, azimuth axis

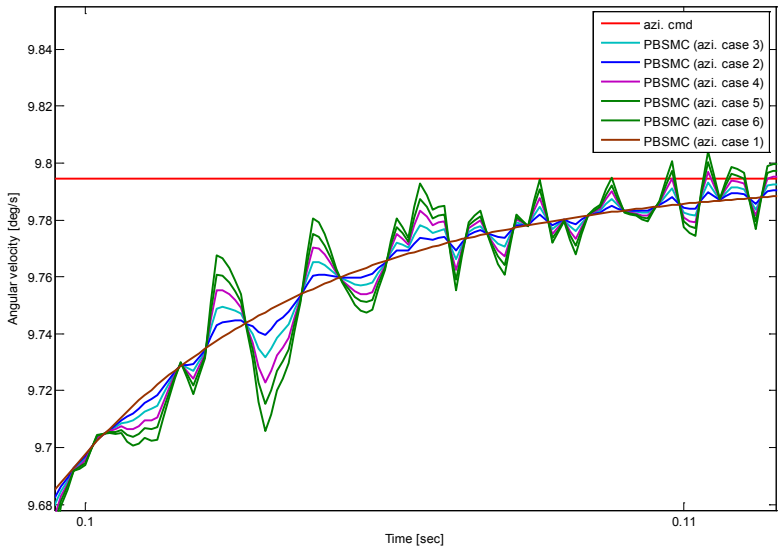

Figure 6.4 : Set point tracking result with varying rate sensor noise, azimuth axis.

Comparing Figure 6.1 till Figure 6.4, it is concluded that the measurement noise in the MEMS rate sensor output has a similar effect on the both axis,

however, elevation axis is more susceptible to sensor noises because there exist large chattering in the response of the elevation axis as depicted in Figure 6.2 although the controller output converge to the desired angular velocity. Small deviations from the desired position result in an unwanted decrease in the stabilization accuracy of the gimbaled platform. Moreover, the elevation axis is more important than the azimuth axis because of the missile motion and the limited target motion in yaw plane, the filtering the sensor noises or utilization of the high grade rate sensors apart from MEMS based technology such as DTG (Dynamically Tuned Gyroscope) or FOG (Fiber Optic Gyroscope) in elevation axis is very important to have success in mission.

6.2.1 Sensitivity of the Proposed Controller to Parameters of the Mathematical Model

In this section, the set point tracking performance of the proposed controller methodology is analyzed by performing computer simulations with the mathematical model.

The performance analysis of the proposed control architecture is conducted in into two parts:
varying plant dynamics with mathematical model,
varying frictional characteristics with mathematical model.

The performance of the proposed control algorithm is analyzed using the mathematical model of the gimbaled system. First, the viscous friction of the system is changed incrementally. The similar analysis is repeated by changing the inertia of the inner gimbal. In these simulations, it is assumed that the angular rate measurement is perfect.

Initially, the viscous friction on the gimbaled system is increased incrementally from the 0.5 oz-in/rad/s to 2.5 oz-in/rad/s by 5 steps. Figure 6.5 and Figure 6.6 clearly show that increasing the viscous friction results in more damped motion and this causes the more frictional energy consumption. Therefore, the controller cannot track the given angular trajectory precisely. For instance, according to Figure 6.5, increasing to coulomb friction from 0.5 oz-in/rad/s to 1 oz-in/rad/s, results in a 0.014 deg/s error accumulation. Although, this value is very small, if the coulomb friction is 2.5 oz-in/rad/s, the resulting error is 0.036 deg/s. In addition, the increase in the viscous friction from the 1.5 oz-in/rad/s to 2.5 oz-in/rad/s in azimuth axis causes the settling time to increase %1. In elevation axis, the percentage change of the settling time is twice of that in azimuth axis. In general, friction affects the steady state behavior of the controlled system rather than transient behavior, and zero steady state aim is reached only a satisfactory friction identification and compensation. Moreover, changes in the settling time and deviations from the desired position result in a decrease in bandwidth of the controller because of the accumulated steady state error.

The inertia of the inner gimbal with payload changes in time during the flight relative to the frame which the moment of inertia calculated from. Therefore, now, the inertia of the payload in elevation and azimuth axis is increased incrementally from 0.00114 $kg.m^2$ to 0.00341 $kg.m^2$ with 5 steps in elevation axis and 0.016 $kg.m^2$ to 0.048 $kg.m^2$ with 5 steps in azimuth axis. The resulting set point tracking performance is illustrated in Figure 6.7 and Figure 6.8. In elevation axis, increasing to inertia 25% from its original value causes 1.7% increase in the settling time. The increase in the settling time is 3.5% if the inertia is selected as 0.00341 $kg.m^2$ in elevation axis. The decrease in the inertia results in a lower settling time, however, the percentage of change is

not same as those resulting from the increase in the inertia in elevation axis. In azimuth axis, the effect of the change of the inertia is not so important because 50% decrease or increase in the inertia leads only to 0.5% change in the settling time. Although, increasing the inertia results in a less damped motion, it does not seem to create any overshoot in the response of the controller. However, increasing the inertia of the payload in elevation axis from 0.0227 kg.m^2, which, is the original value measured with the CAD software, to 0.0341 kg.m^{2,} the settling time increased 1.6 ms in elevation axis as already mentioned. In missile seekers, the settling time of the line of sight stabilized control is generally in milliseconds and 1.6 ms increase in the settling time is not so bad because % 50 increase in the elevation axis during flight is not possible.

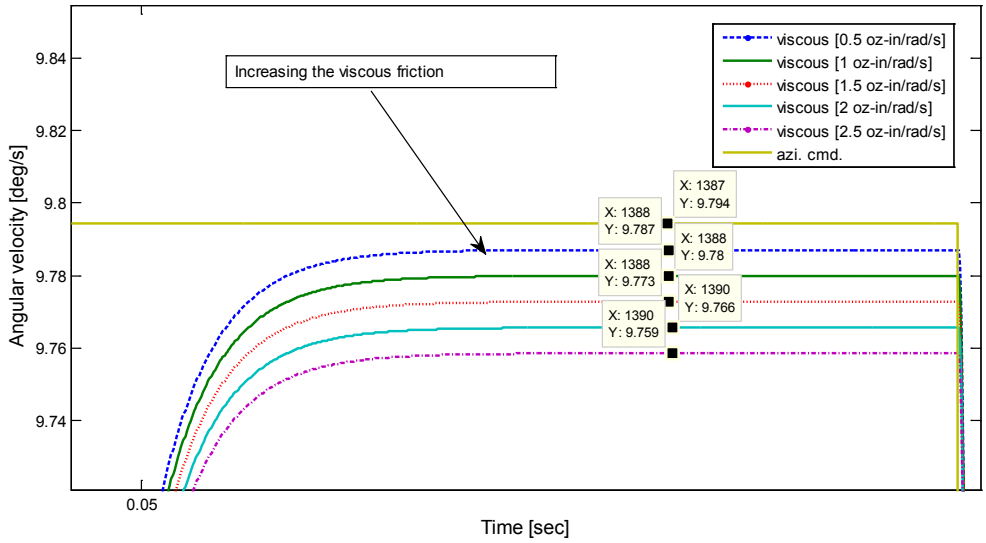

Figure 6.5 : Set point tracking result of the varying coulomb friction, azimuth axis.

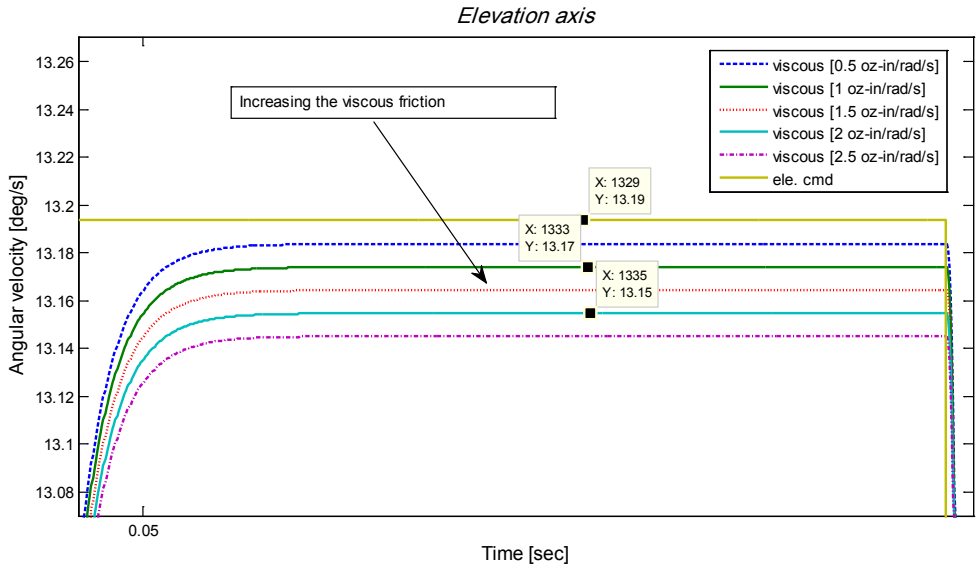

Figure 6.6 : Set point tracking result of the varying coulomb friction, elevation axis.

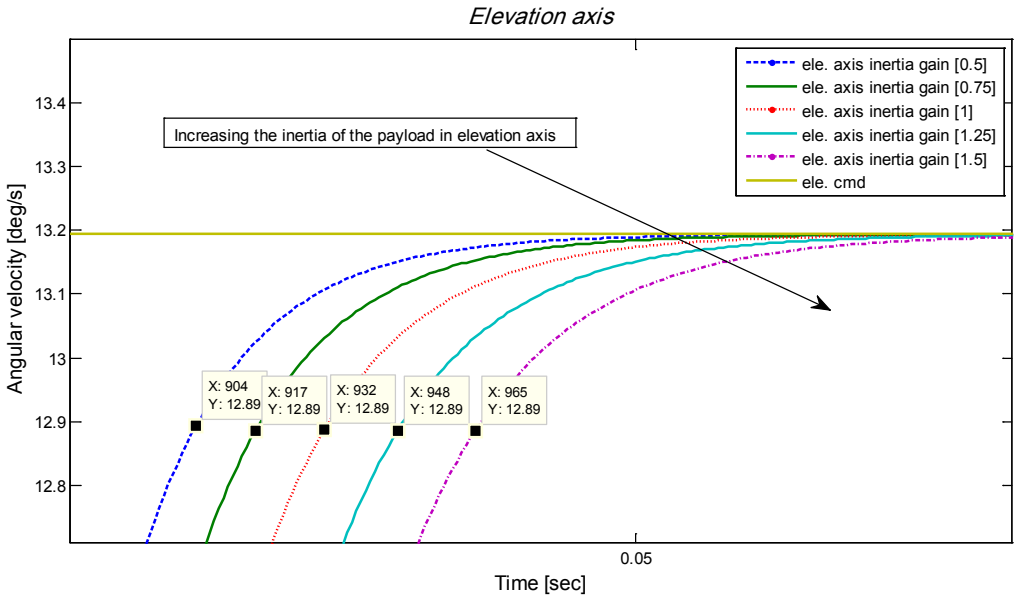

Figure 6.7 : Set point tracking result of the varying inertia, elevation axis.

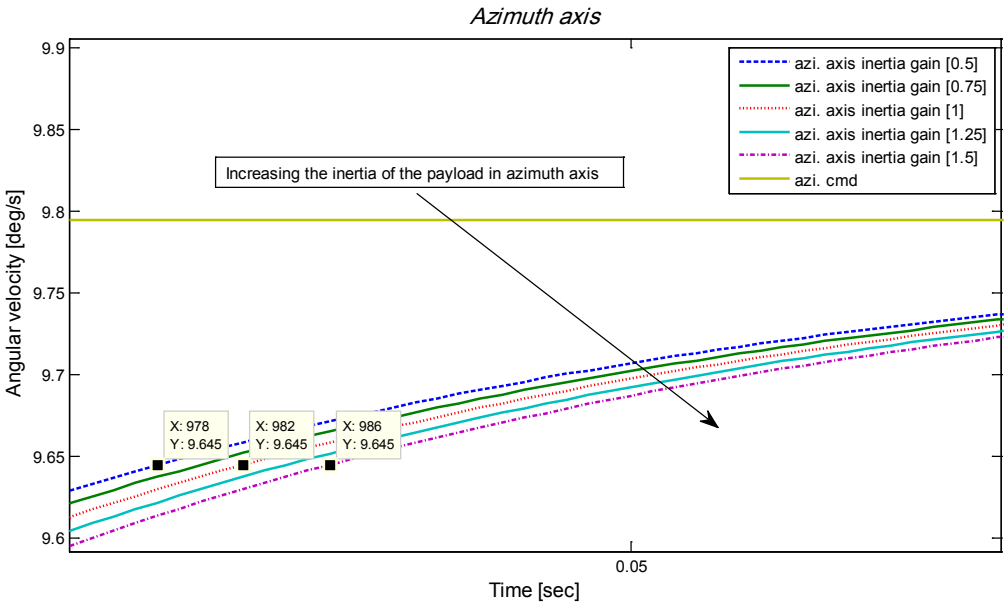

Figure 6.8 : Set point tracking result of the varying inertia, azimuth axis.

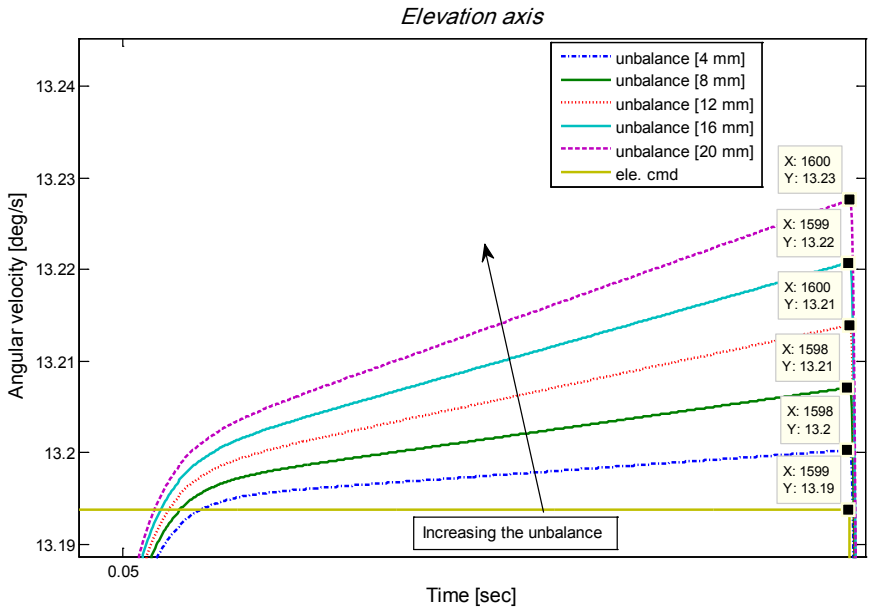

Figure 6.9 : Set point tracking result of the varying unbalance, elevation axis

The final analysis with the simulation model in this section is changing the unbalance value in the elevation axis of the two axis gimbal system. Unbalance is increased incrementally from 4 mm to 20 mm with 5 steps. Figure 6.9 and Figure 6.10 depict the tracking response of the proposed controller in elevation axis with different set point. Note that positive angular change is towards to gravity according to model given in Chapter 3.

According to Figure 6.9, a positive unbalance leads to an extra torque that the controller cannot compensate completely when the desired angular velocity is positive. As an example, increasing the unbalance value to 20 mm results in a 0.4 deg/s overshoot. In general, every 4 mm unbalance caused 0.15 deg/s total steady state error. When the desired motion is towards to gravity, settling time increases %0.5 percent for each 4 mm unbalance, while, the motion is opposite to gravity, the settling time decrease, settling time increases about %0.5 percent for each 4 mm unbalance, which, changes the behavior of the controlled plant completely. Moreover, if the desired angular rate is negative or the requested motion is opposite the gravity, the controller cannot pass the desired angular rate.

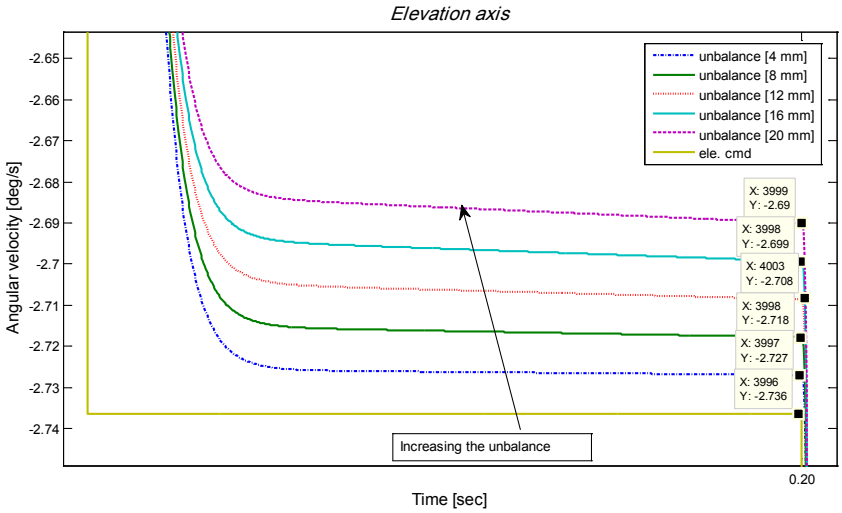

Figure 6.10 : Set point tracking result of the varying unbalance, elevation axis

6.2 Disturbance Rejection Capability Analysis of the Proposed Controller

In this section, the disturbance rejection capability of the proposed controller methodology is analyzed by performing computer simulations with the mathematical model.

The disturbance rejection capability analysis of the proposed control architecture is conducted in into three parts:
varying disturbance characteristics and varying plant dynamics with mathematical model,
varying frictional characteristics with mathematical model.

The stabilization performance the proposed controller is measured with the following performance indices.

Stabilization accuracy

According to International Test Operations Procedure (ITOP), stabilization accuracy can be calculated as the standard deviation of the integral of the controller errors. If the controller error is defined as ϵ, then, the stabilization accuracy is,

$$Stab\_acc = st.dev\left(\int_0^t (\varepsilon)dt\right) \tag{6.2}$$

ISE

Integral of the square of error is defined as

$$ISE = \int_0^t (\varepsilon^2)dt. \tag{6.3}$$

The upper limit t is a finite time chosen as settling time. ϵ is the error between the desired system output and the actual system output at time t.

IAE

Integral of absolute magnitude of error is defined as

$$IAE = \int_0^t |\varepsilon|dt. \tag{6.4}$$

ITAE

Integral of time multiplied by absolute error is defined as

$$ITAE = \int_0^t t|\varepsilon|dt. \tag{6.5}$$

6.3.1 Disturbance Rejection Analysis of the Proposed Control Methodology with Simulation Model

The disturbance rejection capability of the proposed controller is measured with the varying amplitude and varying frequency using the simulation model. First, the disturbance characteristics are changed while the plant dynamics are kept unchanged. Then, the inertia of the payload in elevation and azimuth axis is increased incrementally. The similar analysis is also performed with the unbalance and viscous friction.

Initially, the disturbance rejection capability for different amplitude and different frequency values is analyzed. MEMS rate sensor noise in elevation axis and azimuth axis are taken as 0.0028 deg/s/√Hz and 0.0023 deg/s/√Hz respectively. The resulting performance indexes are tabulated in Table 6.2 and Table 6.3.

In Table 6.2 , all stabilization performance indexes except ITAE when the disturbance frequency is 10 Hz, increases with the increasing disturbance amplitude. If the disturbance frequency increased, the stabilization indexes listed here generally increased. However, there exists some inconsistency in the values in Table 6.2 and Table 6.3. Although the stabilization accuracy when the disturbance amplitude is 25 deg/s is equal for the frequency of 5 Hz and 10 Hz, the other values in these regions are totally different. In addition, values for the ISE are almost same in Table 6.2 and Table 6.3. Therefore, it seems that stabilization accuracy and ITAE values can be used for the evaluation of the performance of the controller. However, in this subsection, values of the all performance indexes are illustrated.

Table 6.2 : Disturbance rejection capability for different amplitude and frequency, elevation axis

			Disturbance Amplitude [deg/s]				
		Performance Index [mrad]	**5**	**10**	**15**	**20**	**25**
Disturbance frequency	**1 Hz**	*Stab. Acc.*	5,0	7,1	9,7	12,6	15,6
		IAE	515,5	521,9	532,8	547,9	567,2
		ITAE	10,8	11,4	12,0	12,5	12,9
		ISE	0,1	0,2	0,2	0,2	0,2
	2 Hz	*Stab. Acc.*	5,5	7,7	10,5	13,4	16,4
		IAE	523,3	550,2	593,4	650,8	720,3
		ITAE	11,0	11,3	11,6	12,1	12,8
		ISE	0,2	0,2	0,2	0,2	0,3
	5 Hz	*Stab. Acc.*	6,0	8,3	11,0	14,0	17,1
		IAE	571,2	721,2	931,2	1172,8	1429,9
		ITAE	12,3	13,7	15,8	18,6	21,8
		ISE	0,2	0,3	0,4	0,7	0,9
	10 Hz	*Stab. Acc.*	5,2	7,1	10,0	13,4	17,1
		IAE	726,2	1183,2	1713,0	2276,7	2866,4
		ITAE	10,2	8,3	7,3	10,1	13,1
		ISE	0,3	0,7	1,3	2,4	3,8

Comparing all changes in Table 6.2 and Table 6.3, it is clear that the stabilization accuracy in elevation axis is always better than the stabilization accuracy in azimuth axis. This behavior results from the use of the identical DC motor for the both axes even though the inertia of the azimuth gimbal is bigger than the inertia of the elevation gimbal. In addition, the amplitude of the disturbance is more important than the frequency of the applied disturbance because there is not a slight change in the stabilization accuracy if the disturbance frequency is increased while the disturbance amplitude is the same. For example, in the elevation axis, increasing the disturbance frequency from 1 Hz to 10 Hz results in 9.6 % increase in the stabilization accuracy if the

disturbance amplitude is 25 deg/s. This increase is only 4% if the disturbance amplitude is lower than 10 deg/s. However, increasing the disturbance amplitude while keeping the disturbance frequency same, cause about %200 increase in the stabilization accuracy. This behavior is valid for all frequency values.

Table 6.3 : Disturbance rejection capability for different amplitude and frequency, azimuth axis

			Disturbance Amplitude [deg/s]				
		Performance Index [mrad/s]	**5**	**10**	**15**	**20**	**25**
Disturbance frequency	**1 Hz**	*Stab. Acc.*	20,0	22,9	25,6	28,6	30,9
		IAE	803,7	811,4	824,6	842,5	861,7
		ITAE	-58,3	-64,7	-65,3	-66,5	-66,0
		ISE	0,4	0,4	0,4	0,4	0,4
	2 Hz	*Stab. Acc.*	22,6	22,4	22,9	25,3	27,8
		IAE	804,9	826,7	862,2	914,8	976,1
		ITAE	-70,6	-65,3	-60,8	-61,6	-61,1
		ISE	0,4	0,4	0,4	0,5	0,5
	5 Hz	*Stab. Acc.*	22,4	25,6	29,2	28,0	28,2
		IAE	857,9	998,3	1210,5	1441,6	1710,3
		ITAE	-67,2	-72,3	-80,5	-69,6	-60,9
		ISE	0,4	0,5	0,8	1,0	1,4
	10 Hz	*Stab. Acc.*	14,1	10,0	12,4	16,4	21,6
		IAE	967,7	1393,8	1953,2	2541,6	3186,5
		ITAE	-47,8	-17,7	5,7	25,0	61,0
		ISE	0,5	1,0	1,8	2,9	4,6

In azimuth axis, there exists totally different behavior. Although, increase in the disturbance amplitude leads increased stabilization accuracy, increasing the disturbance frequency increases the stabilization performance. Moreover, increasing the disturbance amplitude while keeping the disturbance frequency same cause at most %100 increase in the stabilization accuracy which is the

half of the change in the elevation axis. These behaviors are due to high inherent inertia in the azimuth axis as high inertia is less susceptible to the exposed disturbance. Note that the smaller the stabilization accuracy value, the better is the stabilization performance.

Table 6.4 : Effect of the inertia change on the stabilization accuracy, azimuth axis.

			Disturbance Amplitude [deg/s]								
			5			10			15		
		Performance Indices [mrad/s]	50% decrease in inertia	Original inertia	50% increase in inertia	50% decrease in inertia	Original inertia	50% increase in inertia	50% decrease in inertia	Original inertia	50% increase in inertia
Disturbance frequency	1 Hz	*Stab. Acc.*	3.9	5.0	5.0	4.0	7.1	9.2	6.1	9.7	13.5
		IAE	674.3	515.5	491.0	677.9	521.9	505.4	680.0	532.8	528.4
		ITAE	4.5	10.8	2.5	8.2	11.4	3.1	3.8	12.0	3.7
		ISE	0.3	0.1	0.1	0.3	0.2	0.1	0.3	0.2	0.2
	5 Hz	*Stab. Acc.*	4.6	6.0	4.9	6.2	8.3	9.2	7.7	11.0	13.7
		IAE	696.2	571.2	595.7	745.7	721.2	864.2	824.2	931.2	1202.3
		ITAE	6.4	12.3	5.0	7.1	13.7	8.7	6.5	15.8	12.7
		ISE	0.3	0.2	0.2	0.3	0.3	0.4	0.4	0.4	0.7
	10 Hz	*Stab. Acc.*	5.3	5.2	4.8	5.9	7.1	9.3	8.1	10.0	14.1
		IAE	740.9	726.2	870.1	928.4	1183.2	1576.5	1202.5	1713.0	2351.8
		ITAE	-4.7	10.2	3.0	-3.1	8.3	4.8	-4.6	7.3	8.8
		ISE	0.3	0.3	0.4	0.5	0.7	1.1	0.8	1.3	2.4

Table 6.5 : Effect of the inertia change on the stabilization accuracy, elevation axis.

			Disturbance Amplitude [deg/s]								
			5			10			15		
		Performance Indices [mrad/s]	50% decrease in inertia	Original inertia	50% increase in inertia	50% decrease in inertia	Original inertia	50% increase in inertia	50% decrease in inertia	Original inertia	50% increase in inertia
Disturbance frequency	1 Hz	*Stab. Acc.*	11.1	20.0	14.0	12.8	22.9	16.0	28.6	25.6	19.2
		IAE	912.7	803.7	739.8	922.5	811.4	747.4	924.7	824.6	759.6
		ITAE	-21.8	-58.3	-49.3	-29.8	-64.7	-46.7	-72.3	-65.3	-45.6
		ISE	0.5	0.4	0.3	0.5	0.4	0.3	0.5	0.4	0.3
	5 Hz	*Stab. Acc.*	13.3	22.4	15.6	19.6	25.6	18.4	22.7	29.2	20.4
		IAE	944.4	857.9	803.8	1033.7	998.3	989.4	1181.4	1210.5	1248.6
		ITAE	-29.2	-67.2	-52.4	-50.3	-72.3	-54.8	-64.5	-80.5	-52.7
		ISE	0.5	0.4	0.4	0.6	0.5	0.5	0.8	0.8	0.8
	10 Hz	*Stab. Acc.*	18.9	14.1	9.0	24.9	10.0	10.2	19.3	12.4	13.6
		IAE	1040.5	967.7	941.8	1366.2	1393.8	1463.6	1811.7	1953.2	2106.0
		ITAE	-41.4	-47.8	-31.9	-66.9	-17.7	-13.0	-31.1	5.7	1.7
		ISE	0.6	0.5	0.5	1.0	1.0	1.0	1.6	1.8	2.0

Table 6.6 : Effect of the unbalance on the stabilization accuracy, elevation axis.

			Disturbance Amplitude [deg/s]					
			1		5		10	
		Performance Indices [mrad/s]	10 mm unbalance	20 mm unbalance	10 mm unbalance	20 mm unbalance	10 mm unbalance	20 mm unbalance
Disturbance frequency	1 Hz	*Stab. Acc.*	7.3	15.7	17.5	35.1	28.0	54.5
		IAE	517.5	521.2	530.7	546.3	553.1	587.1
		ITAE	-19.6	-50.0	-49.2	-109.9	-78.8	-169.9
		ISE	0.1	0.2	0.2	0.2	0.2	0.2
	5 Hz	*Stab. Acc.*	4.8	4.9	7.1	7.5	10.1	11.8
		IAE	572.8	574.4	726.7	732.3	941.3	951.6
		ITAE	6.1	0.0	1.4	-10.8	-2.6	-21.0
		ISE	0.2	0.2	0.3	0.3	0.4	0.4
	10 Hz	*Stab. Acc.*	4.7	4.9	6.8	7.0	10.2	11.1
		IAE	727.5	728.9	1186.9	1190.6	1719.0	1725.0
		ITAE	7.1	4.0	2.1	-4.1	-2.2	-11.7
		ISE	0.3	0.3	0.7	0.7	1.3	1.4

In addition, Table 6.4 and Table 6.5 show the effect of the inertia change on the stabilization accuracy in azimuth and elevation axis respectively while Table 6.6 indicates the effect of the unbalance on stabilization performance.

According to Table 6.4, any increase in the azimuth axis usually leads to a decrease in the stabilization performance; however, there is not an exact relation between the inertia and the stabilization accuracy. In the case of elevation axis, the increase in the inertia usually increases the stabilization accuracy, however, increasing the inertia represents a decrease in the damping ratio and the system has a less damped motion which can result in overshoots if the linearized system equation of gimbal is considered. However, high inertia is less susceptible to the applied disturbance because the higher disturbance torque is required to move the high inertia. Therefore, the positive effect of the increasing inertia is more observable than the harmful effect of the increasing inertia.

The effect of the unbalance on stabilization accuracy in Table 6.6 clearly demonstrates the destructive consequences of the increasing unbalance in low disturbance frequency. For example, changing to unbalance value from 100 mm to 20 mm, stabilization accuracy increases %100 if the disturbance frequency is 1 Hz. However, in high frequency, there is not significant change in stabilization performance, therefore, it can be concluded that the effect of the unbalance diminishes with the increasing disturbance frequency.

CHAPTER 7

CONCLUSION AND FUTURE WORKS

The objective of this thesis is stated to develop a controller for the stabilization of a two axes gimbal of a roll stabilized missile under disturbance from uncertain base motion due to the inestimable missile motion and from the uncertainties and nonlinearities of the controlled system. In addition, very important criterion while developing the controller architecture is to ensure real-time implementation of the controller.

As discussed in Chapter 1, several controller algorithms are studied in order to improve the stabilization performance. However, most of them either use the conventional PID –based control or uses extra inertial sensors apart from the rate sensor mounted on the inner gimbal. Conventional controller cannot provide high speed, high accuracy and strong robustness. Angular acceleration assisted stabilization increases the stabilization accuracy but it increases the cost of the system and the complexity of the control algorithm.

Implementation of the more advanced controller such as fuzzy logic and neural networks are problematic because the derivation of the control rules in fuzzy logic is not straightforward and real-time recurrent learning in neural network requires high computational power. Therefore, a recently introduced control technique, proxy-based sliding mode control, is adopted for two-axis gimbal system.

The gimbal system that is used in experimental setup has a two-axis MEMS rate sensor with significant bias and random error therefore one of the biggest problem which affect the stabilization is the rate sensor noise. In this thesis, UKF is used for the estimation of the states of the MEMS rate sensor, because, UKF provides sufficient accuracy to be applied in many highly nonlinear filtering and control applications such as navigation. In addition, experiments show a drift-free motion of the gimbal, which is very important to have a high efficient target tracking. However one fundamental problem that is encountered in the experimental study is the forming of the noise covariance matrix in the UKF algorithm. If very small covariance matrix is used, UKF behaves as an analog filter by inducing a delay and in such a case, the measurement range of the rate sensor also decreases.

The gimbaled mechanics is designed so that the geometrical center of the payload coincides with the intersection of the gimbal axes. However, in the gimbaled platform, there is an uncertain unbalance because of manufacturing. In addition, the cable connection in the gimbal system that is used in experiment is not perfect and therefore a spring-like cabling stiffness produces a disturbance torque on the gimbal. Therefore, the harness design of the gimbal is important if very tight stabilization accuracy is necessary.

Gimbaled platform has identical limited angle direct drive motors which eliminates the backlash and increases the torsional stiffness between motor and the gimbal. However, the assembling of the inner and outer part of direct drive motors is very important because incorrect mounting of the direct motor induces friction and eccentricity on the system.

Although, these consequences lead to unpredictable disturbance sources in experiments on hardware, proxy based sliding mode control has a satisfactory

response with the help of augmented friction and sensor noise compensation techniques.

The performance assessment of the proposed controller is studied both using the mathematical model of the system and the experimental setup. Since changing the system dynamics such as the friction is difficult in experimental setup, this analysis is completed using the mathematical model of the two axis gimbal system. The inertia of the elevation axis, sensor noise, coulomb friction and unbalance is changed in order to visualize the effect of these changes in the response of proposed controller. The only changeable parameter with the experimental setup is the disturbance amplitude and the frequency.

The missile dynamics and the aerodynamic conditions cannot be precisely estimated. Hence, disturbance on the gimbal base is highly uncertain. Therefore, disturbance handling capability of the PBSMC is evaluated through more performance criteria other than variable sinusoidal disturbances at the base of the gimbaled platform. However, real-time experiments on gimbaled platform show that the proxy based sliding mode control can overcome a large range of disturbances with different amplitude patterns while preserving stability.

During experiments, there exist translational motion in both axes is observed while the gimbal is stabilized. This is due to distance between the center of the top of the hexapod and the center of the rotation of the elevation and azimuth axes. Although, distance in the azimuth axis is small compared to the elevation axis, there is still movement of the outer gimbal in pitch plane. Actually, while designing a system, designing of an experimental test setup for performance tests or inspection of the some physical properties such as unbalance or the location of center of mass are also important because using the Stewart

platform for the stabilization accuracy test does not seem a suitable technique. The gimbaled platform "as is" used in the experiments is a table prototype which will not be assembled in a missile therefore this type of test is for demonstration purposes only. If the gimbal is designed for a missile to be launched, the stabilization accuracy values are usually smaller than 150μrad. Therefore, performance test should be conducted on more sophisticated platform such as Flight Motion Simulator (FMS).

In modeling the two axis gimbal system, the inertia of the inner gimbal with payload is treated as constant although change of the inertia after the rotation is studied. Since the inertia changes with the relative motion of the inner gimbal, effect of this change should be investigated thoroughly.

One of the most important problems in two axis gimbal system is the harnessing design. The location of cable should be selected properly because cable bundle induces high disturbance with respect to cable connection like spider's web. The use of slip rings can decrease the cable compliance, however, it decreased the already limited space. Cables can be passed inside axis shaft, however, the assembling the encoder and DC motor is important in this case.

Missile seekers must operate in low and high temperature without losing the stabilization performance. Although, the gimbaled platform has elements which can operate in low and high temperature such as rate sensor and absolute encoder, stabilization performance in these conditions has not been investigated. Therefore, it is important to conduct this experimental study to prevent from a degradation in performance

REFERENCES

[1] Titterton D., Weston J., Strapdown. “Inertial Navigation Technology”, Second Edition.

[2] Wikipedia Organization, “Infrared Homing”, “en.wikipedia.org”, January 2011

[3] R. A. Decarlo, S. H. Zak, G. P. Matthews, “Variable Structure Control of Nonlinear Multivariable Systems: A Tutorial”, Proc. IEEE, Vol76, No. 3, pp 212-232, 1988.

[4] Carl Knospe, “PID Control”, IEEE Control Systems Magazine, pp. 30-32, February 2006

[5] Ho-Pyeong Lee; Inn-Eark Yoo; , "Robust Control Design for a Two-axis Gimbaled Stabilization System," Aerospace Conference, 2008 IEEE , vol., no., pp.1-7, 1-8 March 2008

[6] Smith, B.J.; Schrenk, W.J.; Gass, W.B.; Shtessel, Y.B.; , "Sliding mode control in a two-axis gimbal system," Aerospace Conference, 1999. Proceedings. 1999 IEEE , vol.5, no., pp.457-470 vol.5, 1999

[7] Yong-xiang Zhang, Wei-gong Zhang, Xiao-xu Zhao, Hui-mei Yuan, "Study on Electronic Image Stabilization System Based on MEMS Gyro," icect, pp.641-643, 2009 International Conference on Electronic Computer Technology, 2009.

[8] J. Piotrowski, W. Swiderski and D. Szabra, “Infrared homing head for rotating missiles”, Military Institute of Armament Technology

[9] Meir Iecovich, "Line-of-sight stabilization requirements for target tracking systems", Proc. SPIE 1304, 100 (1990)

[10] Raman K. Mehra; Ralph D. Ehrich; , "Air-to-air missile guidance for strapdown seekers," Decision and Control, 1984. The 23rd IEEE Conference on , vol.23, no., pp.1109-1115, Dec. 1984

[11] Se-Ah Jang; Chang-Kyung Ryoo; Keeyoung Choi; Min-Jea Tahk; , "Guidance algorithms for tactical missiles with strapdown seeker," SICE Annual Conference, 2008 , vol., no., pp.2616-2619, 20-22 Aug. 2008

[12] MIT Projects , “Smartpen”, “xenia.media.mit.edu”, Retrieved 27 March 2011

[13] Stabilized Gimbal Systems, www.southernresearch.org, Retrieved 20 January 201 1

[14] Dejun Sheng; Dapeng Fan; Hu Luo; Xutao Nie; , "Bond Graph Approach to the Modeling and Simulation of a Two-Axis Pointing and Tracking System," *Mechatronics and Automation, 2007. ICMA 2007. International Conference on* , vol., no., pp.2337-2341, 5-8 Aug. 2007

[15] George M. Siouris, “Missile guidance and control systems”, Springer-Verlag, 2004

[16] Yu Shuang, Zhao Yanzheng, A New Measurement Method for Unbalanced Moments in a Two-axis Gimbaled Seeker, Chinese Journal of Aeronautics, Volume 23, Issue 1, February 2010, Pages 117-122

[17] K. Rue, “Stabilization of precision electro-optical pointing and tracking systems,” IEEE Trans. Aerosp. Electron. Syst., vol. AES-5, pp.805–819, Sept. 1969

[18] Ambrose, H.; Qu, Z.; Johnson, R.; , "Nonlinear robust control for a passive line-of-sight stabilization system," Control Applications, 2001. (CCA '01). Proceedings of the 2001 IEEE International Conference on , vol., no., pp.942-947,

[19] Kennedy, P.J.; Kennedy, R.L.; , "Direct versus indirect line of sight (LOS) stabilization," *Control Systems Technology, IEEE Transactions on* , vol.11, no.1, pp. 3- 15, Jan 2003

[20] Yonggen Han; Yanhong Lu; Haitao Qiu; , "An Improved Control Scheme of Gyro Stabilization Electro-Optical Platform," Control and Automation, 2007. ICCA 2007. IEEE International Conference on , vol., no., pp.346-351, May 30 2007-June 1 2007

[21] Ki-Jun Seong; Ho-Gyun Kang; Bo-Yeon Yeo; Ho-Pyeong Lee; , "The Stabilization Loop Design for a Two-Axis Gimbal System Using LQG/LTR Controller," SICE-ICASE, 2006. International Joint Conference, vol., no., pp.755-759, 18-21 Oct. 2006

[22] J. C. Lozier, “A steady-state approach to the theory of saturable servo systems,” IRE Trans. Automat. Contr., pp. 19–39, May 195

[23] Wei Ji; Qi Li; Bo Xu; Jun-Jun Tu; De-An Zhao; , "Cascade servo control for LOS stabilization of opto-electronic tracking platform—design and self-tuning," Information and Automation, 2009. ICIA '09. International Conference on , vol., no., pp.1034-1039, 22-24 June 2009

[24] Stein, G.; Athans, M.; , "The LQG/LTR procedure for multivariable feedback control design," Automatic Control, IEEE Transactions on , vol.32, no.2, pp. 105- 114, Feb 1987

[25] Ray, L.R.; , "Stability robustness of uncertain LQG/LTR systems," Automatic Control, IEEE Transactions on , vol.38, no.2, pp.304-308, Feb 1993

[26] Xie, L.; Fu, M.; de Souza, C.E.; , "H_∞ control and quadratic stabilization of systems with parameter uncertainty via output feedback," Automatic Control, IEEE Transactions on , vol.37, no.8, pp.1253-1256, Aug 1992

[27] Abdullah I. Al-Odienat, Ayman A. Al-Lawama, "The Advantages of PID Fuzzy Controllers over the Conventional Types", American Journal of Applied Sciences 5 (6): 653-658, 2008

[28] Radu-Emil Precup, Stefan Preitl , "Stability and Sensitivity Analysis of Fuzzy Control Systems"

[29] Siew, B.C.; Chen, B.M.; Lee, T.H.; , "Design and implementation of a robust controller for a free gyro-stabilized mirror system," American Control Conference, 1998. Proceedings of the 1998 , vol.4, no., pp.2231-2235 vol.4, 21-26 Jun 1998

[30] Nie, J.; , "Fuzzy control of multivariable nonlinear servomechanisms with explicit decoupling scheme," Fuzzy Systems, IEEE Transactions on , vol.5, no.2, pp.304-311, May 1997

[31] Williams, R.J., Zipser, D. “Experimental analysis of the real-time recurrent learning algorithm”, Connection Science, vol.1, no. 1, pp. 87–111, 1989.

[32] Xiang, Z.; Bi, G.; , "Mixed gradient based fast learning algorithm for MLP with its applications to MQAM digital mobile radio receptions,"*Acoustics, Speech, and Signal Processing, 1993. ICASSP-93., 1993 IEEE International Conference on* , vol.1, no., pp.473-476 vol.1, 27-30 April 1993

[33] Yee-Ling Lu; Man-Wai Mak; Wan-Chi Siu; , "Application of a fast real time recurrent learning algorithm to text-to-phoneme conversion," Neural Networks, 1995. Proceedings., IEEE International Conference on , vol.5, no., pp.2853-2857 vol.5, Nov/Dec 1995

[34] Giles, C.L.; Dong Chen; Guo-Zheng Sun; Hsing-Hen Chen; Yee-Chung Lee; Goudreau, M.W.; , "Constructive learning of recurrent neural networks: limitations of recurrent cascade correlation and a simple solution," *Neural Networks, IEEE Transactions on* , vol.6, no.4, pp.829-836, Jul 1995

[35] Utkin, V.I., 1978. “Sliding Modes and their Application in Variable Structure Systems”, MIR Publishers, Moscow, pp: 9-38.

[36] Fujisawa, S. and K. Kawada, 2004. Speed Control of 3- mass System with Sliding mode control and CMAC. Proceeding of the IEEE Conference

on Systems, Man and Cybernetics, Oct. 10-13, IEEE Xplore Press, USA, pp: 4400- 4407.

[37] Chi-Ying Liang; Shun-Wen Tan; , "A New Approach to Chattering Reduction in the Sliding Mode Controls," Innovative Computing, Information and Control, 2007. ICICIC '07. Second International Conference on , vol., no., pp.334, 2007

[38] Kachroo, Pushkin and Tomizuka, Masayoshi, "Integral action for chattering reduction and error convergence in sliding mode control" (1992). Faculty Publications (ECE). Paper 76.

[39] Tan, K.C., Li, Y. "Performance-based control system design automation via evolutionary optimization", Engineering Applications of Artificial Intelligence, vol. 14, pp. 473–486, 2001.

[40] Meirovitch L. , "Methods of Analytical Dynamics" 1970.

[41] Gomonwattanapanich, O.; Pattanapukdee, A.; Mongkolwongrojn, M.; , "Compensation and Estimation of Friction by Using Extended Kalman Filter," SICE-ICASE, 2006. International Joint Conference, vol., no., pp.5032-5035, 18-21 Oct. 2006

[42] Lrinc Marton; Bla Lantos; , "Modeling, Identification, and Compensation of Stick-Slip Friction," Industrial Electronics, IEEE Transactions on , vol.54, no.1, pp.511-521, Feb. 2007

[43] Jyh-Ching Juang; Jeng-Shi Chen; , "On combining adaptive estimation and robust control for friction compensation," Intelligent Control and

Automation, 2004. WCICA 2004. Fifth World Congress on , vol.5, no., pp. 4396- 4400 Vol.5, 15-19 June 2004

[44] Ramasubramanian, A.; Ray, L.R.; , "Adaptive friction compensation using extended Kalman-Bucy filter friction estimation: a comparative study," American Control Conference, 2000. Proceedings of the 2000 , vol.4, no., pp.2588-2594 vol.4, 2000

[45] P.S.Maybeck , “Stochastic Models, Estimation, and Control: Vol. 3”, Academic Press.

[46] B. Armstrong-Hèlouvry, Control of Machines With Friction. Boston, MA: Kluwer, 1991.

[47] Armstrong-Helouvry, B., P. Dupont and C. Canudas deWit, ÒA Survey of Models, Analysis Tools andCompensation Methods for the Control of Machines with Friction,Ó Automatica, Vol. 30(7), 1994, pp. 1083-1138.

[48] Evangelos G. Papadopoulos and Georgios C. Chasparis, “Analysis and Model-based Control of Servomechanisms with Friction”, Proceedings of the International Conference on Intelligent Robots and Systems (IROS 2002), EPFL Lausanne, Switzerland

[49] P.R. Dahl. A solid friction model. The Aerospace Corporation. Technical report, 1968.

[50] Chi-haur Wu; Richard P. Paul; , "Manipulator compliance based on joint torque control," Decision and Control including the Symposium on

Adaptive Processes, 1980 19th IEEE Conference on , vol.19, no., pp.88-94, Dec. 1980

[51] V. van Geffen, “A study of friction models andfriction compensation” , Eindhoven, December, 2009

[52] Radcliffe, Clark J.; Southward, Steve C.;, "A Property of Stick-Slip Friction Models which Promotes Limit Cycle Generation," American Control Conference, 1990 , vol., no., pp.1198-1205, 23-25 May 1990

[53] Torben O. Andersen, Lasse Schmidt ”Friction Modelling And Parameter Estimation For Hydraulic Asymmetrical Cylinders”, Aalborg University, 2011

[54] Townsend, W.; Salisbury, J., Jr.; , "The Effect of coulomb friction and stiction on force control," Robotics and Automation Proceedings. 1987 IEEE International Conference on, vol.4, no., pp. 883- 889, Mar 1987

[55] Voda Alina, Laleh Ravanbod-Shirazi, “High Performance Position Tracking with Friction Compensation for an Electro-Pneumatical Actuator”, CEAI, Vol.6, No.2, pp.15-33, 2004.

[56] Ashok Ramasubramanian, Laura R. Ray “Comparison of EKBF-based and Classical Friction Compensation”

[57] Ray, L. R., Ramasubramanian, A., & Townsend, J. R. 1999. Adaptive Friction Compensation using Extended Kalman-Bucy filter friction estimation. Control Engineering Practice, 9, 457-479.

[58] Misovec, K.M.; Annaswamy, A.M.; , "Friction compensation using adaptive nonlinear control with persistent excitation," American Control Conference, 1998. Proceedings of the 1998 , vol.3, no., pp.1483-1487 vol.3, 21-26 Jun 1998

[59] J. Amin, B. Friedland, and A. Harnoy, 1997. Implementation of a Friction Estimation and Compensation Technique. IEEE Control Sys. Mag., pp. 71-76.

[60] Dong, L.; , "Adaptive Estimation and Control of a Z-axis MEMS Gyroscope with Time-varying Rotation Rates," *Autonomic and Autonomous Systems, 2006. ICAS '06. 2006 International Conference on* , vol., no., pp.18, 16-18 July 2006

[61] Liu Rui Hua; Liang Rongqiang; Zhang Lei; , "Filtering Algorithm Research on MEMS Gyroscope Data," Computer Science and Software Engineering, 2008 International Conference on , vol.4, no., pp.186-189, 12-14 Dec. 2008

[62] Xu Jianmao, Zhang Haipeng, Sun Junzhong, "Periodic Error Compensation for Quartz MEMS Gyroscope Drift of INS", Chinese Journal of Aeronautics, Volume 20, Issue 6, December 2007, Pages 539-545.

[63] P. A. Stubberud, A. R. Stubberud, "A signal processing technique for improving the accuracy of MEMS inertial sensors", ICSENG '08. 19th Int. Conf. Systems Engineering, pp. 13-18, Aug. 2008.

[64] V. I. Kortunov, I. Yu. Dybska, G. A. Proskura, "Integrated mini INS based on MEMS sensors for UAV control," IEEE Aerospace and Electronic Systems Magazine, vol. 24, pp.41-43, Jan. 2009.

[65] Walters-Williams, J.; Yan Li; , "Comparison of Extended and Unscented Kalman Filters applied to EEG signals," Complex Medical Engineering (CME), 2010 IEEE/ICME International Conference on , vol., no., pp.45-51, 13-15 July 2010

[66] Guanglin Li; Fuming Sun; Na Cheng; , "Performance Analysis of UKF for Nonlinear Problems," Intelligent Information Technology Application, 2009. IITA 2009. Third International Symposium on , vol.2, no., pp.209-212, 21-22 Nov. 2009

[67] R. Sameni, M.B. Shamsollahi, and C. Jutten, "Filtering Electrocardiogram Signals using the Extended Kalman Filter", Proceedings of the 27'h IEEE Engineering in Medicine and Biology (EMBS) Annual Coriference, 2005.

[68] Groves Paul D., “Principles of GNSS, Inertial and Multi Sensor Integrated Navigation Systems”, 2008

[69] M. Karasalo and X. Hu , "An Optimization Approach to Adaptive Kalman Filtering"

[70] Qi Cheng; Bondon, P.; , "A new unscented particle filter," Acoustics, Speech and Signal Processing, 2008. ICASSP 2008. IEEE International Conference on , vol., no., pp.3417-3420, March 31 2008-April 4 2008

[71] Nakanishi, H., Inoue, K., “Sliding mode controller by use of neural networks” Springer Wien, pp. 36-42, 2000

[72] Sadati, N.; Ghadami, R.; , "Adaptive Fuzzy Sliding Mode Control Using Multiple Models Approach," Engineering of Intelligent Systems, 2006 IEEE International Conference on , vol., no., pp.1-6

[73] L. Meirovitch. “Methods of Analytical Dynamics.” McGraw-Hill, New York, NY, 1970.

[74] Dejun Sheng; Dapeng Fan; Hu Luo; Xutao Nie; , "Bond Graph Approach to the Modeling and Simulation of a Two-Axis Pointing and Tracking System," Mechatronics and Automation, 2007. ICMA 2007. International Conference on , vol., no., pp.2337-2341, 5-8 Aug. 2007

[75] K. Xiong, H. Y. Zhang, and C. W. Chan, “Performance evaluation of UKF-based nonlinear filtering,” Automatica, vol.42, pp.261-270,2006

[76] Simo Särkkä, “Sigma Point and Particle Approximations of Stochastic Differential Equations in Optimal Filtering” Helsinki University of Technology , Nalco Company, May, 2008

[77] Hung, J.Y.; Gao, W.; Hung, J.C.; , "Variable structure control: a survey," Industrial Electronics, IEEE Transactions on , vol.40, no.1, pp.2-22, Feb 1993

[78] Hongmei Li; Xiao Ye; , "Sliding-mode PID control of DC-DC converter," Industrial Electronics and Applications (ICIEA), 2010 the 5th IEEE Conference on , vol., no., pp.730-734, 15-17 June 2010.

[79] Analog Devices, “Small, Low Power, 3-Axis ±3 g Accelerometer ADXL335”

[80] Fallahi M., Azadi S., “Adaptive Control of a DC Motor Using Neural Network Sliding Mode Control”, Proceedings of the International Multi Conference of Engineers and Computer Scientists 2009 Vol II IMECS 2009, March 18 - 20, 2009, Hong Kong.

[81] Zhiqiang Cheng; Chongsheng Hou; Xiaojin Wu; , "Global Sliding Mode Control for Brushless DC Motors by Neural Networks," Artificial Intelligence and Computational Intelligence, 2009. AICI '09. International Conference on , vol.4, no., pp.3-6, 7-8 Nov. 2009

[82] Matlab Neural Networks Toolbox User Manual, Mathworks Corp., USA, 2010.

[83] Gaines, B.R.; , "Stochastic and fuzzy logics," Electronics Letters , vol.11, no.9, pp.188-189, May 1 1975

[84] Marinos, P.N.; , "Fuzzy Logic and its Application to Switching Systems," Computers, IEEE Transactions on , vol.C-18, no.4, pp. 343-348, April 1969

[85] Passino, K. M. and Yurkovich, S., “Fuzzy Control”, Addison Wesley Longman Inc., 1998

[86] Nanayakkara T., Jamshidi M., Sahin F., “Intelligent Control Systems with an Introduction to System of Systems Engineering”, CRC Press, 2010

[87] Jihong Lee; , "On methods for improving performance of PI-type fuzzy logic controllers," Fuzzy Systems, IEEE Transactions on , vol.1, no.4, pp.298-301, Nov 1993

[88] Kikuuwe, R.; Fujimoto, H.; , "Proxy-based sliding mode control for accurate and safe position control," Robotics and Automation, 2006. ICRA 2006. Proceedings 2006 IEEE International Conference on , vol., no., pp.25-30, 15-19 May 2006.

[89] Kikuuwe, R.; Yamamoto, T.; Fujimoto, H.; , "Low-Force Kinesthetic Guidance for Accurate Positioning and Tracking," Haptic Interfaces for Virtual Environment and Teleoperator Systems, 2006 14th Symposium on , vol., no., pp. 491- 498, 25-26 March 2006.

[90] M. Van Damme, B. Vanderborght, B. Verrelst, R. Van Ham, F. Daerden, and D. Lefeber, “Proxy-based sliding mode control of a planar pneumatic manipulator,” Int. J. Robot. Res., vol. 28, no. 2, pp. 266–284, 2009.

[91] Waldmann, J.; , "Line-of-sight rate estimation and linearizing control of an imaging seeker in a tactical missile guided by proportional navigation," *Control Systems Technology, IEEE Transactions on* , vol.10, no.4, pp.556-567, Jul 2002

[92] Matlab Fuzzy Logic Toolbox User Manual, Mathworks Corp., USA, 2010.

[93] Frameless Direct Drive DC Motors Catalogue, Kollmorgen Corp., USA,

[94] QRS28 User Manual, Systron Donner Inertial, USA, 2010.

[95] “Rotary Absolute Position Encoders”, Netzer Precision Motion Sensors Ltd, www.netzerprecision.com, January 2011.

[96] “Products and Services”, National Instruments, www.ni.com, Retrieved 15 January 2011.

[97] “Hexapods”, Physik Instrumente (PI) GmbH, http://www.physikinstrumente.com, Retrieved 15 January 2011